HSD17BS IN STEROID AND LIPID METABOLISM AND LIPID DISORDERS

The role of HSD17B12 and HSD17B13

Hanna Heikelä

HSD17BS IN STEROID AND LIPID METABOLISM AND LIPID DISORDERS

The role of HSD17B12 and HSD17B13

Hanna Heikelä

University of Turku

Faculty of Medicine
Institute of Biomedicine
Physiology
Drug Research Doctoral Programme

Supervised by

Professor, Matti Poutanen
Faculty of Medicine
Institute of Biomedicine
Research Centre for Integrative
Physiology and Pharmacology
University of Turku
Finland

Docent, Leena Strauss
Faculty of Medicine
Institute of Biomedicine
Research Centre for Integrative
Physiology and Pharmacology
University of Turku
Finland

Reviewed by

Dr. Gabriele Möller
Institute of Diabetes and Cancer
Helmholtz Zentrum München
Germany

Adjunct Professor Katariina Öörni
Molecular and Integrative Biosciences
Research Programme
University of Helsinki
Finland

Opponent

Docent, Kaija Autio
Faculty of Biochemistry and Molecular
Medicine
University of Oulu
Finland

To my family and friends

ABSTRACT

Non-alcoholic fatty liver disease (NAFLD), characterized by the accumulation of fat within hepatocytes, has become the most common chronic liver disease in developed countries. NAFLD is associated with insulin resistance, obesity, and cardiovascular disease. In this work, the role of hydroxysteroid 17-beta dehydrogenase (HSD17B) type-12 and -13 in the development of fatty liver disease was investigated using knockout (KO) mouse models. Previous results have shown that HSD17B13 is mostly expressed in the liver on the surface of lipid droplets. In humans, certain HSD17B13 variants have been found to protect against NAFLD. HSD17B12, on the other hand, is highly expressed in metabolically active tissues, including the liver, and previous studies suggest that the enzyme is involved in lipid metabolism. However, the exact function of either enzyme in liver cells is still unclear. HSD17B13 deficiency led to fat accumulation in hepatocytes and hepatic inflammation in 9-month-old male mice. Inhibition of HSD17B12 enzyme activity in the whole body of adult mice led to the development of fatty liver, but also to very rapid weight loss. The observed weight loss in mice was associated with reduced food intake. Similar but slower changes were also observed in hepatocyte-specific HSD17B12cKO mice. The results indicate that the functions of HSD17B13 and HSD17B12 enzymes are related to cellular mechanisms that regulate the formation and growth of hepatic lipid droplets. The molecular mechanisms of both enzymes remain to be elucidated, but our results and those of others suggest that HSD17B13 and HSD17B12 are promising targets for the development of drug therapies for fatty liver disease.

KEYWORDS: Fatty liver, metabolism, inflammation, mouse model

TIIVISTELMÄ

Alkoholista riippumattomasta rasvamaksasta (NAFLD), jolle on ominaista rasvan kertyminen maksasoluihin, on tullut yleisin krooninen maksasairaus kehittyneissä maissa. NAFLD on yhteydessä insuliiniresistenssiin, liikalihavuuteen sekä sydän- ja verisuonisairauksiin. Työssä tutkittiin Hydroksisteroidi-17-beeta-dehydrogenaasi (HSD17B) tyyppi-12 ja -13 osuutta rasvamaksan kehityksessä poistogeenisten hiirimallien avulla. Aiemmat tulokset ovat osoittaneet, että HSD17B13 ilmentyy enimmäkseen maksassa lipidipisaroiden pinnalla. Ihmisellä tiettyjen HSD17B13-varianttien on havaittu suojaavan NAFLD:tä vastaan. HSD17B12 puolestaan ilmentyy voimakkaasti aineenvaihdunnallisesti aktiivisissa kudoksissa, mukaan lukien maksa, ja aiempien tutkimusten perusteella entsyymi toimii rasva-aineenvaihdunnassa. Kummankaan entsyymin tarkkaa tehtävää maksasoluissa ei kuitenkaan vielä tunneta. HSD17B13-entsyymin puutos johti rasvan kertymiseen maksasoluihin ja maksan tulehdukseen 9 kuukautta vanhoilla uroshiirillä. HSD17B12-entsyymin toiminnan esto aikuisella hiirellä koko elimistössä johti maksan rasvoittumiseen, mutta myös erittäin nopeaan painon putoamiseen. Havaittu painon lasku hiirissä liittyi ruokahaluttomuuteen. Saman suuntaiset, mutta hitaammin ilmenevät muutokset havaittiin myös hiirissä, joilla HSD17B12-entsyymin toiminta estettiin vain maksassa. Tulokset osoittavat, että HSD17B13- ja HSD17B12-entsyymien toiminnat liittyvät solutason mekanismeihin, joilla säädellään rasvapisaroiden muodostumista ja kasvua maksassa. Molempien entsyymien molekyylitason mekanismit ovat edelleen selvittämättä, mutta meidän ja muiden saamien tutkimustulosten perusteella HSD17B13- ja HSD17B12-entsyymit ovat lupaavia kohteita kehitettäessä lääkehoitoja rasvamaksasairauteen.

AVAINSANAT: Rasvamaksa, aineenvaihdunta, tulehdus, hiirimalli

Table of Contents

Abbreviations

AA	Arachidonic acid
ACC	Acetyl-CoA carboxylase
ACOX	Acyl-CoA oxidase
ALT	Alanine aminotransferase
ARK	Aldo-keto reductase family
AST	Aspartate transferase
AthD	Atherogenic diet
ATP	Adenosine triphosphate
CD36	Cluster of differentiation 36
CE	Cholesteryl ester
CER	Ceramide
ChREBP	Carbohydrate-responsive element-binding protein
CTRL	Control
CYP	Cytochromes P450 enzyme
DCER	Dihydroceramide
DEN	Diethylnitrosamine
DNL	De novo lipogenesis
ELOVL	FA elongase
ER	Endoplasmic reticulum
FABP	Fatty acid binding protein
FASN	Fatty acid synthase
FATP	Fatty acid transport protein
FA	Fatty acid
FFA	Free fatty acids
FXR	Farnesoid X receptor
GCKR	Glucokinase regulator
GH	Growth hormone
GWA	Genome-wide association
HCC	Hepatocellular carcinoma
HCV	Hepatitis C virus
HDL	High-density lipoprotein

HFD	High-fat diet
HSD17B	Hydroxysteroid 17-beta dehydrogenase
IFN-g	Interferon gamma
Il	Interleukin
IP-10	Interferon gamma-induced protein 10
IR	Insulin resistance
JVS	Juvenile visceral fat
KAR	Ketoacyl-CoA reductase
KC	Keratinocyte chemoattractant
KO	Knockout
LCFA	Long-chain fatty acid
LD	Lipid droplet
LDL	Low-density lipoprotein
LXR	Liver X receptor
MBOAT7	Membrane-bound O-acyltransferase
MTTP	Microsomal triglyceride transfer protein
MTP	Mitochondrial trifunctional protein
NAFLD	Non-alcoholic fatty liver disease
NADPH	Nicotinamide adenine dinucleotide phosphate
NASH	Non-alcoholic steatohepatitis
PC	Phosphatidylcholine
PE	Phosphatidylethanolamine
PEPCK	Phosphoenolpyruvate carboxykinase
PI	Phosphatidylinositol
PPAR	Peroxisome proliferator-activated receptor
SCD-1	Stearoyl-Coenzyme A desaturase 1
SD	Standard deviation
SDR	Short-chain dehydrogenases/reductase
SM	Sphingomyelin
SNP	Single nucleotide polymorphism
SREBP	Sterol regulatory element-binding protein
SUV	Standard uptake value
TAG	Triacylglycerol
Tam	Tamoxifen
TER	Trans-enoyl-CoA reductase
TM6SF2	Transmembrane 6 superfamily 2
TNFa	Tumor necrosis factor alpha
VLCFA	Very-long-chain fatty acid
VLDL	Very-low-density lipoprotein
WT	Wild type

List of Original Publications

This dissertation is based on the following original publications, which are referred to in the text by their Roman numerals:

I   Marion Adam*, **Hanna Heikelä***, Cyril Sobolewski, Dorothea Portius, Jenni Mäki-Jouppila, Arfa Mehmood, Prem Adhikari, Irene Esposito, Laura L. Elo, Fu-Ping Zhang, Suvi T. Ruohonen, Leena Strauss, Michelangelo Foti, Matti Poutanen. Hydroxysteroid (17beta) dehydrogenase 13 deficiency triggers hepatic steatosis and inflammation in mice. *FASEB journal*, 2018; 32:3434-3447. *equal contribution.

II   **Hanna Heikelä**, Suvi T Ruohonen, Marion Adam, Riikka Viitanen, Heidi Liljenbäck, Olli Eskola, Michael Gabriel, Laura Mairinoja, Alberto Pessia, Vidya Velagapudi, Anne Roivainen, Fu-Ping Zhang, Leena Strauss, Matti Poutanen. Hydroxysteroid (17β) dehydrogenase 12 is essential for metabolic homeostasis in adult mice. *American journal of physiology. Endocrinology and metabolism*, 2020; 319:E494-E508.

III   **Hanna Heikelä**, Laura Mairinoja, Suvi T. Ruohonen, Kalle Rytkönen, Simone de Brot, Asta Laiho, Satu Koskinen, Tomi Suomi, Laura Elo, Leena Strauss, Matti Poutanen. Disruption of *Hsd17b12* in mouse hepatocytes leads to defect in the lipid droplet expansion associated with microvesicular steatosis. *Manuscript*

The original publications have been reproduced with the permission of the copyright holders.

1   Introduction

Non-alcoholic fatty liver disease (NAFLD) is becoming a major health burden especially in the developed world. It is the most common cause for chronic liver disease and hallmark is the accumulation of lipid droplets (LD) inside hepatocytes in the absence of excessive alcohol consumption [1]. The lipid accumulation can be reversed, but it can also progress to non-alcoholic steatohepatitis (NASH), in which the liver is affected by inflammation. The progression of NAFLD into NASH increases the risk of hepatic cirrhosis or hepatocellular carcinoma (HCC). Cirrhosis and HCC are end-stages of liver disease. NAFLD is a multisystem disease, as it affects other organ systems and regulatory pathways outside the liver [2]. It is associated with insulin resistance (IR), obesity, cardiovascular disease, and chronic kidney disease. In addition, toxic substances and some infections can lead to fat accumulation in the liver. Furthermore, there are also some genetic variants that alter the risk of developing NAFLD. Most well-known genes with variants associated with NAFLD are the patatin-like phospholipase domain-containing protein 3 (PNPLA3), transmembrane 6 superfamily 2 (TM6SF2), glucokinase regulator (GCKR) and membrane-bound O-acyltransferase (MBOAT7) [3]. However, there is also evidence that some members of the hydroxysteroid 17-beta dehydrogenase (HSD17B) enzymes are involved in the liver lipid metabolism and that they could play a role in the development of NAFLD. Recently, there has been interest towards the enzymes HSD17B12 and HSD17B13 in the liver metabolism and fatty liver disease [4].

HSD17B enzymes are a heterogenous family of enzymes that are able to catalyze the conversion between inactive and active sex steroid hormones. Even though they share the same motifs, their sequence similarity is low. In addition, their tissue expression pattern and substrate specificity vary greatly. Some HSD17B enzymes prefer substrates other than steroids [5]. HSD17B12 is highly expressed in metabolically active tissues, including the liver [6]. It is proposed to be involved in the elongation of very long-chain fatty acids (VLCFA). Earlier animal studies have shown that HSD17B12 is essential for embryonic development because the gene disruption in embryonic stem cells leads to an embryonic lethal phenotype [7]. HSD17B13 could be described as a liver specific protein because its expression is

high in the liver and low in other tissues [8]. It has been characterized as a LD-associated protein with overexpression in mouse leading to hepatic steatosis [8,9]. In addition, certain HSD17B13 variants have been found to protect against NAFLD [10].

In this work, we developed knockout (KO) mouse models to study the function of HSD17B12 and HSD17B13 in lipid metabolism, with special focus on the liver. For HSD17B13, we obtained a conventional KO model that had been developed by homologous targeting. In the case of HSD17B12, we used the Cre-Lox recombination technique to bypass the embryonic lethality. We generated a floxed HSD17B12 mouse strain and crossbred that with three different Cre-expressing mouse strains to target the gene disruption spatially and temporally. The first Cre-strain was Rosa26-CreERT, in which the gene disruption was dependent on tamoxifen (Tam) induction. This allowed us to induce gene disruption in the tissues of adult animals, after a normal development (with intact *Hsd17b12* gene). The second Cre-strain targeted the gene disruption in adipose tissue of adult mice upon tamoxifen induction, while the HSD17B12 function remained intact in other tissues. Finally, we crossbred the floxed mouse strain with Albumin-Cre strain, which targeted the *Hsd17b12* disruption to hepatocytes, from early development on.

2 Review of the Literature

2.1 The structure and function of the liver

The liver is an organ located under the thorax right beneath the diaphragm on the right side of the body, and it is considered as a part of the gastro-intestinal tract. In humans, the liver is composed of four lobes and in mouse the liver is composed of five lobes [11]. Liver performs many essential metabolic, exocrine and endocrine functions. It produces and secretes bile and cholesterol, takes up and neutralizes toxic compounds and drugs, metabolizes hormones and stores vitamins as well as nutrients [12]. It stores glucose in the form of glycogen and maintains blood glucose levels between meals (by glycogenolysis and gluconeogenesis). Liver also regulates the levels of circulating plasma lipids by regulating the secretion of very-low-density lipoproteins (VLDL). In addition, liver produces circulating plasma proteins, such as albumin.

2.1.1 The microscopic structure of the liver

On microscopic level, the liver can be divided into lobules, the building blocks of the liver tissue. Each lobule is composed of one central vein in the center and the surrounding six portal triads in the periphery, giving the lobule a hexagonal shape [13]. Portal triads are composed of the hepatic artery, the portal vein, and the bile ductule (Fig. 1). Each lobule and acinus can be divided into three zones, numbered from 1 to 3. The zone closest to the portal triad is labeled zone 1, which receives highly oxygenated blood via the arterioles and nutrient rich blood from the portal vein, and therefore functions that require high oxygen are common in this zone. The blood from portal triad flows towards the central vein, creating a decreasing gradient of oxygen and nutrients through zone two and finally zone three next to the central vein [12].

Liver parenchyma is mainly composed of hepatocytes (80-90%), which are epithelial cells of polygonal shape and large centrally located nuclei. Hepatocytes with two nuclei are relatively common. Hepatocytes contain abundant mitochondria and a large network of endoplasmic reticulum (ER) and Golgi apparatus, due to their active metabolism [12]. Depending on the nutrient status, hepatocytes contain varying

amounts of stored energy, in the form of glycogen and lipids. Hepatocytes are arranged in cords that are a few cell layers thick. These cords are separated by channels called sinusoids, through which blood flows toward the hepatic vein. Sinusoids are lined by endothelial and Kupffer cells, as well as liver associated lymphocytes. Kupffer cells are resident macrophages and part of the phagocytotic monocyte-macrophage system, and they are important for clearing unwanted material, such as bacteria, virus particles and damaged erythrocytes from the blood stream [14]. Hepatocytes produce bile (composed of bile salts, phospholipids, bile pigments and proteins), which is transported along bile canaliculi, which drain into portal ductules, and finally bile is stored in the gall bladder until it is released into the intestines during digestion. Cholangiocytes are epithelial cells lining the bile duct network and their role is to modify the bile during its flow through the biliary tree [13]. Bile ducts often proliferate in response to liver injury [15].
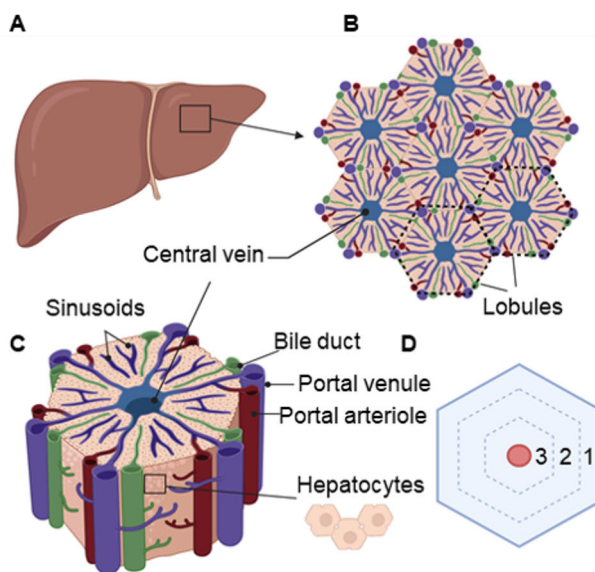
Figure 1. The liver is divided in lobes and lobules. A) Human liver is divided in four lobes, but only two lobes are visible in the anterior view. B) Each lobe contains thousands of hexagonally shaped lobules. C) A lobule consists of hepatocytes, arranged in outwards radiating rows from central vein. Between the rows are sinusoids. Portal triad includes a bile duct, portal venule and portal arteriole. D) The lobule can be divided into zones 1, 2 and 3 based on their metabolic function. Created with BioRender.com.

The perisinusoidal region between endothelial cells and hepatocytes is called the space of Disse. Hepatocyte cell membrane forms finger-like projections into the space of Disse, significantly increasing the surface area capable of absorption. The

space of Disse contains plasma, connective tissue, and Ito cells (stellate cells) [13]. Ito cells store vitamin A (retinol), regulate sinusoidal blood flow and produce extracellular matrix. Ito cells also participate in the repair process after injury.

Nutrients, including amino acids, monosaccharides, and fatty acids (FA) are transported to the liver via circulation and further processed for storage, or consumed as energy.

Hepatogenesis is conserved throughout evolution. The liver is formed from the endodermal progenitor cells of the digestive tract during fetal development [12,16]. At first the fetal liver is composed mainly of hematopoietic stem cells, however these cells disappear from the liver soon after birth, and the neonatal liver is metabolically in a transition state between the fetal and adult liver [16]. Newly specified hepatic cells in embryos are referred to as hepatoblasts. Hepatoblasts are bipotential; they can differentiate into either bile epithelial cells or into hepatocytes, depending on the location. Those residing next to portal veins become the intrahepatic bile ducts while most of the hepatoblasts in the parenchyma differentiate to hepatocytes [16].

2.1.2   Energy metabolism in the liver

The liver acts as a metabolic centre. It regulates energy metabolism and sustains whole-body homeostasis by combining information provided by signalling molecules, including hormones. The main energy pathways it regulates include the storage, synthesis and breakdown of glucose, FAs and amino acids. The liver is able to switch between different metabolic pathways and convert metabolites to another, i.e., carbohydrates to lipids, depending on the energy requirements and availability of the nutrients [12].

2.1.2.1   Carbohydrate metabolism

Hepatocytes take up glucose through glucose transporters located on the cell membrane. Once inside the cell, monosaccharides are phosphorylated by enzymes called hexokinases. These enzymes phosphorylate carbon at position 6 to form glucose-6-phosphate (G6P) or in the case of fructose and galactose, the carbon at position 1 to form fructose-1-phosphate or galactose-1-phosphate [17]. Fructose-1-phosphate is further converted into G6P while galactose-1-phosphate is used in other metabolic pathways, such as glycoprotein or glycolipid biosynthesis. Phosphorylated forms of monosaccharides are "trapped" inside hepatocytes (cannot be secreted into blood circulation) and used mainly in energy metabolism pathways [17]. These include glycogenesis, gluconeogenesis, glycogenolysis and glycolysis.

During a time of abundant glucose (after a meal), excess glucose is stored in the form of glycogen within hepatocytes. Glycogen is the most important form of

glucose storage and can make up to 7-10% of weight of a healthy, normal sized liver [12]. Glycogen is a multibranched polysaccharide of glucose, stored in the cytoplasm in the form of granules. The enzyme responsible for adding new glucose units to the chain is glycogen synthase. During fasting (between meals) glycogen is hydrolyzed into glucose in a process called glycogenolysis and released into blood circulation. This maintains a steady blood glucose level and allows other organs (such as brain) to use glucose as an energy source. Once the glycogen storage has been used up, the liver can synthesize glucose using noncarbohydrate substrates, such as lipids, amino acids, and lactate [12]. This is called gluconeogenesis. It starts from pyruvate and uses energy obtained from beta-oxidation of FAs. Gluconeogenesis is an important process for maintaining stable blood sugar levels and utilized a lot during fasting. It is stimulated by epinephrine and glucagon and inhibited by insulin. The rate limiting factors are not the enzymes of the gluconeogenesis pathways, but the availability of substrates. The most commonly used substrate is alanine (derived from the muscle tissue), but most amino acids are suitable for gluconeogenesis [18]. Hepatocytes can also break down glucose molecules into pyruvate in a process called glycolysis.

Carbohydrate metabolism is hormonally regulated, mainly by insulin and glucagon. Liver is sensitive to the insulin levels in circulation, and insulin stimulates glycogenesis and inhibits glycogenolysis and gluconeogenesis [18]. Glucagon, in turn, stimulates glycogenolysis and gluconeogenesis and therefore increases blood glucose levels. Farnesoid X receptor (FXR) also plays a role in carbohydrate metabolism by regulating the expression of the phosphoenolpyruvate carboxykinase (PEPCK) gene [19].

2.1.2.2   Fat metabolism

FAs are building blocks of the fat and they consist of a carboxyl group (C(=O)OH) attached to a straight chain of carbon atoms, with hydrogen atoms along the length. They are fat soluble. They can be saturated or unsaturated, depending on the presence of one or more double bonds. Unsaturated FAs are further divided into monounsaturated or polyunsaturated (one or more double bonds, respectively). The most common FAs in living organisms are 16 to 18 carbon atoms long [20]. Commonly, FAs with chain length of 18 to 20 are called long-chain FAs (LCFA) and FAs chain length of 22 or more carbon atoms are called very-long-chain fatty acids (VLCFA). FA structure is visualized in Figure 2.
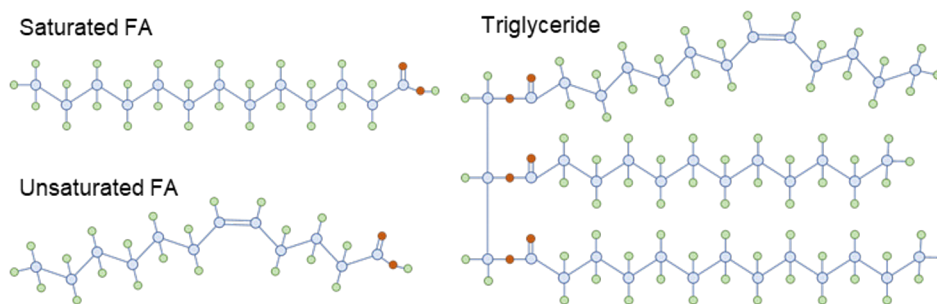
Figure 2. FA structure. FAs can be saturated or unsaturated, depending on the presence or absence of double bonds. Carbon atoms are represented by blue circles, hydrogen atoms are represented by green circles and oxygen atoms are represented by red circles are. Connecting lines represent covalent bonds between the atoms, double bonds are marked with double line.

FAs can be incorporated in phospholipids or triacylglycerol (TAG) or used in bile acid production, as well as used for energy production by oxidation reactions when glucose stores are depleted [20]. FAs are also precursors for eicosanoids, growth regulators and hormones. Hepatocytes can also convert glucose into FAs when glucose is abundant. Cellular lipid homeostasis is controlled by metabolic nuclear receptors. These include members of the NR superfamily and are key regulators in both cholesterol and FA metabolism, namely liver X receptors (LXRs), but also FXR, peroxisome proliferator-activated receptors (PPAR) and well-known transcription factors such as sterol regulatory element-binding proteins (SREBPs). LXRα and SREBP-1c play an important role in the development of NAFLD [21].

Bile salts assists the absorption of lipid particles from food by emulsifying large dietary fat particles into smaller particles, which helps their hydrolysis into free FA by digestive enzymes [22]. FAs are absorbed by enterocytes where they are esterified in TAG and incorporated in chylomicrons, which are phospholipid-covered particles that allow water insoluble lipids to be transported in the blood circulation to target tissues (adipose, cardiac, and skeletal muscle). Once target tissues have taken up most of the lipid load, the liver absorbs the remnants of chylomicrons [20].

The liver is able to absorb circulating FAs, esterify, oxidize and then export them to other parts of the body via blood circulation. Hepatocytes take up FAs from blood circulation in the form of chylomicrons and LDL. From chylomicrons the FAs are released mainly by lipoprotein lipase, which is regulated by hepatic cyclic AMP–responsive element–binding protein H [23]. FAs can be oxidized to provide energy. Hepatocytes exhibit a high turnover of FAs and esterify them into TAG and cholesteryl esters (CE) and can either store them in LD within hepatocytes or secrete them in VLDL particles [20]. Hepatic lipid metabolism is illustrated in Figure 3.
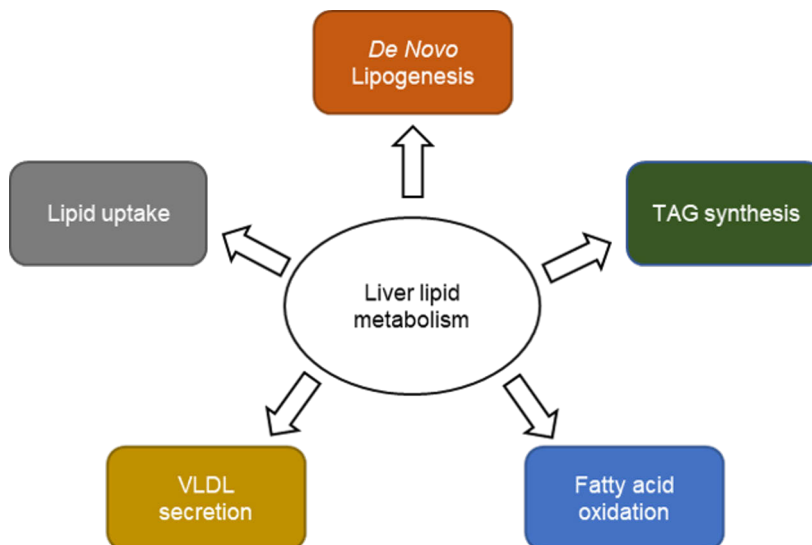
Figure 3. Liver lipid metabolism includes various anabolic and catabolic processes.

2.1.2.2.1 Fatty acid uptake

FAs circulating in the blood stream are mostly bound to albumin, from which it dissociates upon uptake by hepatocytes. Hepatocytes take up lipids from circulation via diffusion through the cell membrane and transport proteins located on the membrane. Most important transport proteins are the family of Scl27a FA transport proteins (FATP) and cluster of differentiation 36 (CD36) protein and plasma membrane FA-binding protein (FABPpm) and caveolin-1 [20]. The expression level of CD36 is low in hepatocytes under normal conditions, however, CD36 level has been observed to increase in some animal models of fatty liver and patients of NAFLD [24,25]. FABPpm expression increases in the hepatocyte membranes in animal models of obesity [26], but their role in lipid uptake under normal conditions is still unclear. FATPs are present on both plasma membrane and intracellular membranes, [27]. In the liver FATP2 [28] and FATP5 are the dominant forms [29]. Even though FATP2 is located mainly in the ER membrane, its overexpression has been associated with increased uptake of long-chain FAs [24]. FATP5 is located in the plasma membrane and seems to be important player in hepatic FA uptake [29]. Caveolins are integral membrane proteins that play a role in FA transport. They are the main structural proteins of membrane regions called caveolae, which are rich in cholesterol as well as sphingolipids, and involved in endocytosis by forming vesicles pinching off from the plasma membrane. Caveolins are regulated by PPAR [30]. After the transport across the cell membrane, the FAs are bound to intracellular carrier proteins and finally esterified to coenzyme A (CoA).

2.1.2.2.2 De novo lipogenesis

Hepatocytes can convert glucose into FAs when glucose is abundant. Liver is the main organ where *de novo* lipogenesis (DNL) takes place and the end product (FA chain linked to coenzyme A) can be either stored in LDs, incorporated into various lipid species or VLDL. Approximately 15-25% of hepatic FAs originate from DNL [31].

For DNL, glucose needs to be broken down by glycolysis and tricarboxylic acid (TCA) cycle to produce citrate [20]. Citrate is then converted to acetyl-CoA. Saturated FAs with chain length up to 16 carbon atoms are synthetized in cytoplasm. The process uses acetyl-CoA as substrate, which may originate from glycolysis or beta-oxidation and begins by a condensation step producing malonyl-CoA from acetyl-CoA precursor in the cytosol [20]. This step is catalyzed by acetyl-CoA carboxylase (ACC). Malonyl-CoA is then transferred to FA synthase (FASN), which will convert the substrate acyl chain into palmitate. Finally, the palmitate will produce complex FAs in elongation and desaturation reactions.

The elongation of VLCFA and LCFA occurs at the ER[32]. The process uses fatty acyl CoA, malonyl CoA, and NADPH as substrates and consists of four steps (Fig. 4). It begins with a condensation step of malonyl CoA with a fatty acyl-CoA precursor. This is followed by reductions steps by β-ketoacyl CoA reductase. During the third step, the FA is dehydrated by the dehydrase to an enoyl-CoA, and during the fourth step it is further reduced by the enoyl reductase [33]. The process leads to lengthening of the acyl chain by two carbon increments. SREBP1c is activated by insulin, translocates and activates genes of FA synthesis [34]. Increased glucose uptake by hepatocytes activates carbohydrate-responsive element-binding protein (ChREBP), which increases the expression of many FA synthesis genes, but also pyruvate kinase [35], which also promotes FA synthesis by increasing the availability of citrate. ACC represents the target of specific modulators, such as the metabolic intermediate citrate. A minor FA elongation pathway occurs in mitochondria [36].
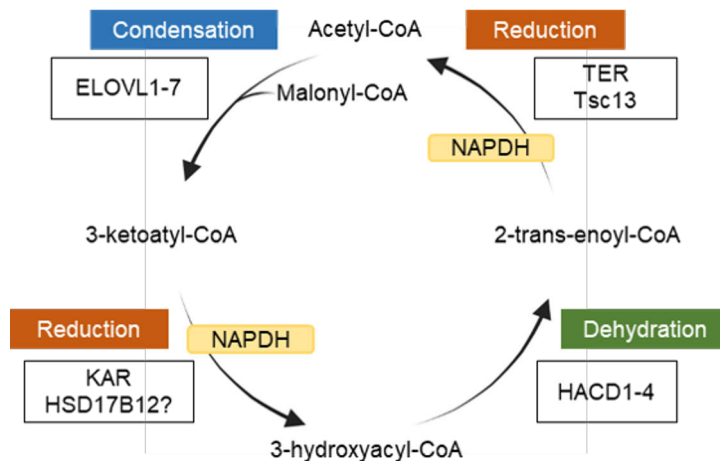
Figure 4. Long-chain fatty acid (LCFA) elongation happens in four steps. The first step is condensation, where Acetyl-CoA and Malonyl-CoA form 3-ketoacyl-CoA. This step is catalyzed mostly by the FA elongases (ELOVL). The second step is reduction, where the 3-ketoacyl-CoA is reduced to 3-hydrozyacyl-CoA. 3-Ketoacyl-CoA reductase (KAR) enzymes catalyze this step, and HSD17B12 is thought to be involved in this step in the elongation of LCFAs. The first reduction is followed by a dehydration step, by 3-Hydroxyacyl-CoA dehydratases (HACD), to produce 2-trans-enoyl-CoA. This product undergoes the last step, the second reduction by 2,3-Trans-enoyl-CoA reductase (TER) enzymes. After each cycle, the fatty acid is elongated by two carbon atoms. The reduction steps require NAPDH. Created with BioRender.com. Modified from [32].

2.1.2.2.3 Fatty acid oxidation

The rate of FA oxidation is normally low under the fed state. During oxidation, FAs are broken down into acetyl-CoA, which can be used for adenosine triphosphate (ATP) production, for synthesis of new fatty acid or for production of ketone bodies. The FA oxidizing enzymes are regulated at the transcription level by PPARs [20]. FA oxidation takes place in mitochondria (short-to medium-chain FAs) and peroxisomes (very-long-chain FAs) [20]. For mitochondrial beta-oxidation, FAs are activated on the outer mitochondrial membrane before FAs are transferred in the mitochondrial matrix for oxidation. The acyl-residue of acyl-CoA is transferred to carnitine before it can cross the mitochondrial membrane. This is catalyzed by carnitine palmitoyltransferase I and this is the rate limiting step of mitochondrial beta-oxidation [37]. For peroxisomal beta-oxidation, the first step is catalyzed by acyl-CoA oxidase (ACOX), and the product of peroxisomal oxidation is H_2O_2 instead of ATP.

2.1.2.2.4 Fatty acid esterification

FA esterification is the process in which FAs are combined with glycerol (alcohol) to produce monoglycerides, diglycerides TAG or phospholipids, as well as with

cholesterol to form CE. TAGs are the most stable and common form of dietary fats. It is also the most common form of storage and transport of FAs. Triacylglycerols (TAG) consist of a glycerol backbone to which three (often saturated) FA chains are esterified. Before the esterification can take place, the glycerol molecule needs to be phosphorylated. The process can be carried out in (1) mitochondria and ER or (2) ER and peroxisomes. In the first case, the initial step is catalyzed by glycerol-3-phosphate acyltransferase (GPAT3), and it consists of esterifying FA to a (reduced) glycerol molecule (producing a monoglyceride phosphate (called lysophosphatidic acid). The expression of GPAT is regulated by ChREBP [20]. In the second case the first step of the reaction is catalyzed by DHAP acyltransferase. The FAs need to be activated by acyl-CoA synthetase before they can be incorporated into glycerol.

2.1.2.2.5   The lipid droplet

LDs are dynamic organelles and belong to a system that packs and redistributes lipids in the cell and is involved in cellular lipid metabolism, membrane trafficking, and cell signaling. Storing excess lipids in the LD protects the cell against lipotoxicity [38]. The LD core is composed of neutral lipids, most commonly TAGs and CEs. The lipid core is surrounded by a phospholipid/cholesterol monolayer, which separates the hydrophobic lipids from the aqueous surroundings of the cytosol [39]. The monolayer is mostly composed of phospholipids, which stabilize the droplet and serve as an interface with other cellular compartments. Phosphatidylcholines (PC) is the most common lipid class in the LD membrane. Other lipid classes on the LD envelope include phosphatidylethanolamines (PE) and phosphatidylinositol (PI), albeit their levels are lower than that of PC [40,41]. Also, free cholesterol is a component of the LD lipid envelope, but present in smaller quantities than on lipid bilayers. Specific proteins of the perilipin-ADRP-TIP47 (PAT) family are embedded in the lipid monolayer [20]. The LDs envelope has an unexpected enrichment in sphingolipids (about 20% of total), compared to the 10% found in whole cell membranes [41,42]. Especially some ceramides (CER) are abundant in LDs, whereas sphingomyelin (SM), which is the dominant sphingolipid in other cell membranes, is lower in LD monolayer [41]. The lipid classes and molecular species differ between the LD phospholipid envelope and the total cellular phospholipid bilayers. These differences suggest that the phospholipids surrounding each droplet are specialized to carry out specific metabolic and lipid-trafficking functions of the adiposome [40]. Nutritional status affects the LD lipid profile [43].
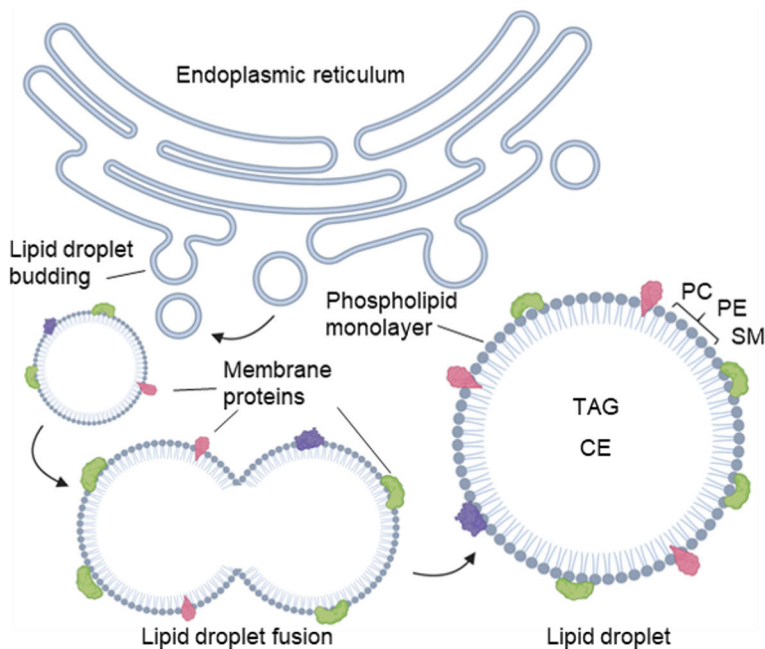
Figure 5. Lipid droplet (LD) synthesis. The LD consist of hydrophobic core surrounded by a phospholipid monolayer. The core contains neutral lipids, such as TAG and CE. The phospholipid monolayer is made of PC and PE, also small amounts of SM are present. Embedded in the phospholipid layer are many proteins. The LD formation begins at the endoplasmic reticulum (ER), where lipids are synthesized between the membranes, forming a growing lens, which can leave the ER by buddying. LDs can grow by lipid synthesizing enzyme activity on the membrane, or by fusing with each other. Created with BioRender.com. Modified from [39].

LDs form at the ER, where the enzymes for FA esterification and CE synthesis are located (Fig 5). The mechanisms are still poorly understood, but it is thought that the process begins with accumulation of neutral lipids between the two ER membrane sheets [44]. This will lead to the formation of a lipid lens, which would grow and bud off from the ER as a LD. Some proteins, such as fat storage-inducing transmembrane protein 2, seem to be required, likely to induce disruptions in the ER membrane morphology [45]. In addition, Seipin is crucial for LD formation, and it is believed to promote lipid transfer inside the LD [46].

Large LDs form by fusion of smaller vesicles or by a larger LD "swallowing" a smaller one. Growing LD size decreases the surface to volume ratio and liberates excess membrane lipids for the cells to utilize elsewhere. However, when lipids are accumulating within the hepatocytes, the LD formation can be so rapid that LD growth does not release enough membrane lipids to compensate for the increased demand needed in *de novo* LD synthesis [47].

A study found that in the brown adipose tissue LDs, 37.3% of the associated proteins were involved lipid metabolism and energy production proteins, 13.6% in other metabolism proteins, 17.8% in trafficking and transport, 5.9% in oxidation or reduction, 4.7% were chaperones, 3% in transcription and translation and 1.2% in cytoskeleton [48]. The rest (16.6%) were categorized as being involved in "other functions".

Perilipins (1-5) are quite well-known proteins located on the LD membrane. Plin1 and Plin4 have the highest expression in the adipose tissue [49,50], while Plin 5 is most common in oxidative tissues (heart). Plin 2 and 3 are expressed widely [51,52]. *Plin 5* is expressed in various tissues, and it has been found to regulate LD accumulation and may play a role as a scaffold protein in LD hydrolysis [53,54].

The function of LD is to store fats for fast usage if needed for energy of cell growth. Another function is to protect the cell against lipotoxicity. Free FAs can disrupt membrane integrity, or they can be incorporated into lipid species that are cytotoxic if they are accumulating at high concentrations (CER, acylcarnitine, diacylglycerol) [39].

2.1.2.2.6 Fatty acid export

Lipoproteins provide means for the organism to transport energy-dense but hydrophobic lipids in bloodstream to their target tissues. Lipoproteins include chylomicrons, VLDL, intermediate-density lipoprotein (IDL), low-density lipoprotein (LDL) and high-density lipoprotein (HDL). The density of apolipoprotein B- (ApoB) containing lipoproteins depends mainly on the ratio of cholesterol to TAG content in the core [55]. Lipoproteins are spherical structures made of lipids and proteins, and they are synthesized in the liver, intestines and, during fetal development, in the yolk sac [55,56]. On the outer surface of lipoproteins is composed of a single layer of phospholipids which surrounds a core made of neutral lipids, mainly CEs and TAGs [57]. The hydrophobic parts of the phospholipids face the hydrophobic core and hydrophilic portions point outwards to the hydrophilic environment. There are special proteins, called apolipoproteins, embedded in the surface of lipoproteins which stabilize the structure and give it its identity and destination [55]. The most important of them is ApoB. It is large in size, has unique amphipathic properties, and is required for the assembly of VLDL lipoprotein in the liver. Certain genetic variants in ApoB gene are associated with dyslipidemias, such as hypercholesterolemia and atherosclerotic disease [58]. Chylomicrons are produced in the intestines and enter the blood stream after first bypassing the liver. The liver later uptakes chylomicron remnants, after other tissues have absorbed most of the chylomicron cargo. Liver, in turn, produces VLDL and releases it into the blood circulation. The machinery responsible for assembling VLDL is located in the ER.

The process involves the translocation of ApoB protein from the cytoplasmic layer of the ER into the ER lumen and binding of lipid molecule to the emerging ApoB chain during the translocation [59]. Synthesized lipoproteins are secreted into blood stream where they will travel to target tissues. Peripheral tissues, mainly adipose and muscle tissues, are able to uptake the FAs and glycerol from VLDL, transforming the VLDL into IDL, which can be taken up by liver or hydrolyzed by hepatic lipase enzyme, turning IDL to LDL, which is high in cholesterol. HDL is synthetized mainly in the liver (to a lesser degree in the intestines), and it has an important role in carrying cholesterol from the periphery to the liver [55]. The key protein in HDL synthesis is ApoA, and increased expression of ApoA has been linked to reduced lipid accumulation in some mouse models of liver steatosis [60].

2.1.3   Liver metabolism during fasting

Liver is an organ, which can interconvert energy substrates, which helps the body to adapt to fasting. Fasting elevates DNL, so much that roughly 25% of all the FAs originate from 2-carbon precursors derived from glucose, fructose, and amino acids [31]. FAs can also be used for fatty acid oxidation and the energy from that can be used for gluconeogenesis. The rate of FA oxidation increases during fasting after carbohydrate stores are depleted.

Prolonged fasting induces a massive release of fatty acids from the adipose tissue by lipolysis and as a result, the blood fatty acid levels increase. Once the FAs reach the liver, they are taken up and metabolized into ketone-bodies. FAs can be re-esterified in TAG and incorporated into VLDL which is then secreted from the liver. Peroxisomal proliferator-activated receptors (PPAR) are the main switch in the liver's adaptation to the fasting state [61,62].

Plasma insulin concentrations decrease during fasting and initiate a lipolytic program in white adipose tissue [63]. This increases the plasma FA concentration that can be taken up by the liver. The liver can use FAs both for the production of ketone bodies and local energy supply [18].

2.1.4   The metabolism of toxic compounds

Most drugs and toxic compounds enter the body with food. Many of them are hydrophobic and cannot be eliminated by kidneys unless they are converted into hydrophilic form [64]. This process takes place in the liver, and it is composed of two steps or phases. In the phase 1, polar groups, like hydroxyl (OH) or carboxyl (COOH) are introduced into the compound to make it polar [64]. This often includes oxidation reaction, involves cytochrome 450 enzymes and takes place on ER. Phase 2 includes a conjugation reaction of the phase 1 product with another compound

(often glucuronic acid; also, glycine, taurine or sulfate are possible) to further increase hydrophilic properties of the compound [64].

2.1.5   Sexual dimorphism of the liver

Liver is a sexually dimorphic organ, meaning that female and male livers differ in gene expression, lipid and steroid metabolism and susceptibility to disease. There are four major liver diseases that show sex differences in the susceptibility: steatosis, hepatitis, cirrhosis, and HCC [65]. Liver function is regulated in a sexually dimorphic manner by neuroendocrine system and this dimorphism originates in the brain. It is regulated mostly by growth hormone (GH), which acts as a hormonal stimulus for growth from childhood onwards. GH is secreted in sexually dimorphic manner in many species, including rodents and human [66]. GH dependent regulation of sex-specific cytochrome P450 (CYP) genes has been found in many species, but in rodents the sex-differences are striking [67,68]. In mice, both males and females secrete GH in a fluctuating manner, but in males this is more regular. Males produce plasma GH peaks every 2.5h with stable baseline concentrations in between. In females the peaks occurred every 1.4 h on average [68]. The longer intervals in the GH peaks in males and the pause between the pulses allow resensitization of the GH receptors [69]. In females the secretion is more constant, consisting of lower and overlapping peaks. These differences can be reverted by giving estradiol to males or testosterone to females [70,71]. GH receptors are found in the liver and GH action regulates sex-specific expression of CYP enzymes [72,73]. CYPs are a large family of enzymes that catalyze the metabolism of various compounds, such as drug, steroid hormones and toxins. The sex-specific differences in the expression of these enzymes may lead to differences in the sensitivity to toxins and the adverse drug reactions [74]. Lack of GH receptors in the liver leads to IR, glucose intolerance, and increased circulating free FAs in mice [75].

Estradiol (E2) is the most potent female sex hormone in mouse and human. In premenopausal women E2 is produced mainly in the ovaries from cholesterol and secreted in the blood circulation, where it travels bound to albumin and crosses the cell membranes into the target tissues via passive diffusion [76]. In postmenopausal women and men, it is produced mainly in peripheral tissues from testosterone by aromatase. E2 exerts its effects through estrogen receptors in the target tissues. ER are found in various tissues throughout the body, including the liver. Estrogen receptor alpha is the predominant estrogen receptor in both sexes in both human and mouse liver [76]. The levels of the nuclear estrogen receptor in the liver are age-dependent (in rats) rather than sex-dependent [77].

The classical estrogen receptors are nuclear receptors estrogen receptor alpha and -beta, which form homo- or heterodimers upon ligand binding and translocate to

nucleus, where they bind to the estrogen response elements (ERE) which are often located in promoter and enhancer regions of genes regulated by estrogen [76]. In addition to the classical estrogen receptors, there are also membrane-associated variants of estrogen receptor alpha and -beta, which exert their effects through activation of intracellular second messenger system [76]. In addition, a membrane bound G protein-coupled estrogen receptor 1 (GPER, also known as GRP 30) which is structurally unrelated to estrogen receptor alpha and estrogen receptor beta, but similarly to them, mediates its effects through activating the intracellular second messenger system [78]. The second messenger system is faster than the genomic signaling mediated by nuclear receptors, albeit less direct. In the liver, estrogens are known to play a role in the development of fatty liver and cirrhosis and ER are involved in the regulation of lipid metabolism and to protect from NAFLD [78].

Both female and male livers also express androgen receptors. There are different forms of androgen receptors, the truncated form, and the short form [79]. Similarly, to estrogen receptors, there are the classical nuclear receptors and the membrane bound androgen receptors. Androgen receptor is involved in the regulation of liver energy metabolism and androgen receptor signaling can protect the liver from steatosis, although there is also evidence that androgens may promote NAFLD development in some cases [65]. The genes regulated by the nuclear androgen receptors include fat oxidation related genes and lipid synthesis related genes [65].

2.2 Liver disease

2.2.1 Non-alcoholic fatty liver disease

Non-alcoholic fatty liver disease (NAFLD) is characterized as fat accumulation in hepatocytes in the absence of alcohol abuse. It is heavily associated with type 2 diabetes and obesity and its prevalence continues to rise in the Western countries as incidences of metabolic diseases increase. Worldwide the prevalence is approximately 30%, but it varies from population to population [80]. It is more prevalent in men than in women (22-42% and 13-24% respectively) [81]. The prevalence in women is relatively low in premenopausal age (6-9%), but in post-menopausal women the prevalence is similar to that of men (19-31%) [81]. DNL and abnormal accumulation of LDs are characteristics of NAFLD [82]. NAFLD can mean plain fat accumulation without inflammation, but approximately 20% of the cases develop into NASH, which includes hepatic inflammation in addition to the fat accumulation. NAFLD increases the probability of developing fibrosis and cirrhosis and increases the risk for hepatocellular cancer. NAFDL is histologically diagnosed when more than 5% of hepatocytes accumulate lipids [83]. Lipid accumulation can be divided into mild (6-32%), moderate (33-66%) and severe (>66%) according to

Younossi *et al* [1]. The lipid accumulation affects mostly the liver zone 3, located near the central vein [84,85]. The most common accumulating lipid type is TAGs, but since TAGs are not toxic to the cell, the severity grade of steatosis may not reflect the presence of severe symptoms or serious hepatic injury [54,86]. Accumulation of other, more toxic lipids, such as free FAs, diacylglycerols, CERs, cholesterols and phospholipids, may be more crucial to the disease progression.

The LD size can vary greatly, and NAFLD can be divided into macrovesicular and microvesicular types. Macrovesicular steatosis is characterized by one or a few large fat droplets, which can fill almost the whole cell and push the cell nucleus against the cytoplasm. Microvesicular steatosis, in turn, is characterized by numerous small LDs scattered in the cytoplasm. Macrovesicular steatosis is the predominant form in IR related NAFLD [87], while microvesicular LDs are typical finding in toxicity-induced steatosis, and it correlates with more severe histological findings and more advanced liver injury [83].

The traditional view to the stepwise progression of NAFLD from a healthy liver via simple liver steatosis to more severe steatohepatitis has been the two-hit hypothesis [88]. In this hypothesis, the first hit was IR, second hit being increased oxidative stress caused by increased oxidation of FAs. According to a more recent "multiple parallel hits" -hypothesis, there are multiple cellular mechanisms affecting simultaneously to cause hepatic inflammation and eventually progression to NASH [89].

The pathophysiology of NAFLD is still unclear, but it is now thought that IR is one of the main factors in the development of NAFLD. IR and the commonly underlying obesity are both associated with low grade systemic inflammation [90–92]. In IR, the muscle tissue, the adipose tissue and the liver cannot respond normally to insulin i.e., uptake glucose from the blood circulation. IR leads to increase in *de novo* lipogenesis in hepatocytes and decreases the liver's ability to synthesize and export TAG [93]. An infiltration of macrophages and other immune cells is observed in the liver, adipose tissue and pancreas associated with a cell population shift from an anti-inflammatory to a pro-inflammatory profile. Various liver damage factors are summarized in Figure 6.
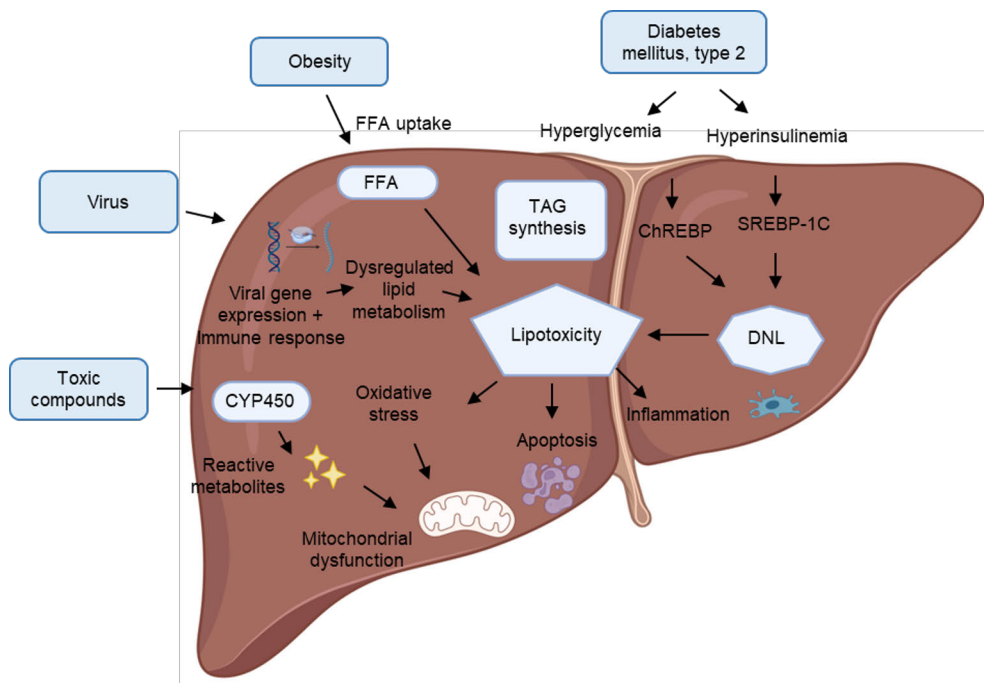
Figure 6. Summary of liver damage mechanisms including metabolic, viral and toxic stimuli. Many processes affect liver lipid metabolism indirectly and can lead to the development of steatosis. Created with BioRender.com. FFA=free fatty acid, TAG=triacylglycerol, ChREBP=carbohydrate-responsive element-binding protein, SREBP-1C=sterol regulatory element-binding protein, CYP450=cytochromes P450 enzyme, DNL=*de novo* lipogenesis.

Various genetic mutations have been associated with increased risk for NAFLD. PNPLA3 polymorphism rs738409 I148M was identified by Romeo and colleagues in 2008 and it has been found to be common in NAFLD cases without metabolic syndrome [94–97]. The variant causes a substitution of isoleucine by methionine in the amino acid position of 148 of PNPLA3 peptide and leads to loss of function [94,98]. This variant is associated with increased ALT & aspartate transferase (AST) levels [99,100], steatosis, inflammation [96,101], fibrosis and cirrhosis [100,101], and liver disease-associated mortality [102]. However, it is independent of body mass index and diabetes [97]. PNPLA3 has TAG lipase activity, and the variant leads to reduced TAG hydrolysis, FA remodeling in TAG and diminished VLDL secretion, causing accumulation of TAGs [98,103,104]. The rs738409 I148M may also affect the cellular localization of PNPLA3 protein, increasing its presence on LDs [104].

Transmembrane 6 superfamily 2 (TM6SF2) polymorphism rs58542926 is a guanine to adenine substitution and causes a glutamate to lysine substitution at amino acid position 167 of the TM6SF2 protein. This single nucleotide polymorphism (SNP) leads to loss of function and causes changes in the VLDL secretion pathway,

leading to TAG accumulation [105]. It is associated with steatosis, increased serum liver markers (ALT) and decreased VLDL secretion [106,107]. The carriers of this variant have increased risk of developing NASH and fibrosis [107,108]. In addition to fatty liver disease, TM6SF2 rs58542926 has been associated with cardiovascular disease [109].

GCKR polymorphisms are also associated with NAFLD and increases susceptibility to NASH [110,111]. GCKR functions as a fructose-6-phosphate-dependent inhibitor of glucokinase and regulates hepatic glucose metabolism and DNL via regulating glucokinase activation [111,112]. GCKR polymorphism *GCKR* P446L causes increase in hepatic glucose uptake and impairs FA oxidation [111].

MBOAT7 is a membrane-associated enzyme, and its function is to remodel the endomembrane phospholipids, especially PIs [113,114]. A loss of function rs641738 variant increases the risk of NAFLD and NASH [113]. MBOAT7 transfers polyunsaturated FAs to lysophospholipids, and it has high substrate specificity for arachidonoyl-CoA [115]. The MBOAT7 activity affects the availability of arachidonic acid (AA) for eicosanoid production, which regulates the eicosanoid biosynthesis [115,116]. Furthermore, the variants in the MBOAT7 locus are associated with altered ratios of AA metabolites in human plasma or serum [117]. Reduced MBOAT7 expression is associated with obesity [118]. and the loss of function rs641738 variant is associated with accumulation of lysophosphatidylinositol lipids [118], and increased lysophosphatidylinositol promotes transcription of genes involved in development of hepatic inflammation and fibrosis [118].

NAFLD may develop into NASH, and further into fibrosis and cirrhosis, and increases the risk for hepatocellular cancer (Fig. 7). Interestingly, many of the genetic variants that predispose to NAFLD and NASH (PNPLA3, TM6SF2, MBOAT7), also predispose to cirrhosis development in both the non-alcoholic and alcohol-induced fatty liver disease [119].

Figure 7. The progression of chronic liver disease can be divided into four stages. The first stage is the accumulation of fat in the hepatocytes (simple steatosis). This is reversible and often asymptomatic. The progression from simple steatosis to NASH involves hepatic inflammation and apoptosis. NASH increases the risk for fibrosis, in which the liver tissue is scarred. Fibrosis is a transitional stage and impairs the normal function of the hepatocytes. Fibrosis leads to cirrhosis, which increases the risk for hepatocellular carcinoma (HCC), which is associated by liver failure. Created with BioRender.com.

2.2.2   Non-alcoholic steatohepatitis

In addition to fat accumulation within hepatocytes, NASH presents with hepatic inflammation, hepatocellular ballooning, and necrosis. Hepatocellular ballooning refers to swollen cells which have rarefied cytoplasm, and it is often associated with Mallory-Denk bodies, which are irregular-shaped inclusions of hepatocytes, and found in various liver diseases [120]. They are composed of damaged intermediate filaments. Both lobular and portal inflammation can be present in NASH. Lobural inflammation refers to the presence of small aggregates of inflammatory cells within the hepatic parenchyma [85] and is often associated with altered chemokine and cytokine expression in the liver [14]. Mild forms of portal inflammation are common in NASH, and severe type, although relatively rare, may be a sign of more advanced disease [121]. Moreover, NASH may progress to liver fibrosis and even cirrhosis. Furthermore, it increases the risk for hepatocellular cancer. The proceeding from NAFLD to NASH is thought to involve many mechanisms which are linked to IR. These include altered adipokine and cytokine secretion due to dysfunctional adipose tissue [122]. Increased secretion of proinflammatory cytokines tumor necrosis factor alpha (TNFa) and interleukin 6 (IL-6) as well as activation of toll like receptor (TLR) and NLRP3 inflammasome are involved in the progression of NASH [123–126]. Hyperinsulinemia induces the generation of cytotoxic lipid species in the hepatocytes leading to mitochondrial dysfunction and the creation of reactive oxygen species [127]. NASH is commonly diagnosed with liver biopsy.

2.2.3   Toxic (acute) liver failure

Toxic liver injury or toxic liver failure is relatively rare condition, which can have several causes. It is characterized by rapid loss of functioning hepatocytes leading to compromised hepatic functions. Liver injury can be asymptomatic for a long time, until up to 70% of the hepatocytes are injured, but then the progression to fatality can be rapid [128]. Symptoms include jaundice, swelling of the abdomen, nausea as well as disorientation or confusion [129].

The common causes include toxin exposure, drug reaction, prolonged ischemia, neoplasia, metabolic disorders, and (viral) infections as well as immune-mediated processes [129]. In humans it is most often due to drug overdose, most commonly paracetamol. The hepatocytes in zone 1 (closest to the portal area) are most exposed to possible toxins in the circulation and are therefore often the most affected in toxicity induced acute liver failure [130]. Hepatocytes in zone 3 (closest to central vein), in turn, are responsible for most of the liver's synthesis activity and transforming functions and are more vulnerable to toxic metabolites of the cytochrome P450 systems [130]. Similarly, hepatocytes in zone 3 are more susceptible for hypoxia-induced injury.

2.2.4   Viral hepatitis

Viral hepatitis is an inflammation of the liver most often caused by infection by hepatitis virus A, B, C, D and E. In some cases, it can be caused also by some other viruses (for example yellow fever). Hepatitis A and E cause acute infection, they spread usually through contaminated food or water, occur in areas of poor sanitation, mainly developing countries. The symptoms of hepatitis A include nausea, vomiting, jaundice, fever, and abdominal pain, but it rarely causes acute liver failure. On the other hand, hepatitis A infection can also be asymptomatic. Hepatitis B, C and D spread through contact with infected person's blood. In addition, hepatitis B and D can spread through contact with body fluids, which may occur via used needles or unprotected sex. Hepatitis B can also be asymptomatic, but often causes symptoms like jaundice, tiredness, dark urine, and abdominal pain. Hepatitis B can also cause liver complications such as fibrosis and hepatic cancer. Hepatitis C virus (HCV) can cause chronic infection of the liver and its prevalence is estimated to be around 2.5 % worldwide, although the prevalence varies between regions [131]. In the beginning it can be asymptomatic, but after several years it can lead to liver fibrosis and predispose to liver fibrosis and end-stage liver complications, even liver cancer. Liver fibrosis refers to the accumulation of extracellular matrix proteins and leads to the formation of scar tissue within the liver. The process reminds of wound healing response and renders the tissue non-functional. HCV modifies metabolic pathways in the host cells to better suit its own need. The infection by the hepatitis virus induces the host antiviral immune response, which leads to the development of (chronic) inflammation. These together promote hepatic fibrogenesis [132]. Moreover, HCV produces proteins in the infected cells that can alter host pathways to favor tumor development (proliferation and survival) [133].

HCV infected cells contain a membranous web of vesicles that are thought to be the site of viral RNA replication [134]. This web is formed of double-membrane vesicles as protrusions of the ER toward the cytoplasm [135]. For this, the virus takes advantage of the lipid metabolism of the host, and in consequence, up to 70% of patients with chronic HCV develop liver disease [136]. HCV may directly cause the appearance of large LD in hepatocytes as it modifies the hepatocyte metabolism to favor its own replication and the production of virions. Both the life cycle and infectivity of HCV are dependent on host lipid metabolism. HCV virions exist as lipoviroparticles and hijacks the VLDL secretion pathway in host hepatocytes [137]. HCV circulates in the host blood stream incorporated in the host LDL and VLDL particles. It utilizes lipoprotein receptors to gain entry to hepatocytes [138], and alters cellular lipid homeostasis to promote its own replication and release from cells [139].

HCV affects the formation of the VLDL, by interfering with microsomal triglyceride transfer protein (MTTP). It has been demonstrated that synthesis of CE with C16 and C22/24 carbon chain is increased in the presence of HCV [41]. In

consequence, the increase in sphingolipid concentration may affect the size of LDs and increase the levels of both CEs and CER [41]. HCV utilizes LDs for assembly of the virions. Currently available data on HCV genotype 3a effect on CE synthesis suggests that metabolic steatosis and viral steatosis may follow distinct pathways [140]. About a 10-fold rise in liver TAGs and 2.5-fold rise in DAGs compared to controls (CTRL) was observed in patients presenting with NAFLD. Interestingly no change in CER was observed. To date, the exact mechanism by which HCV alters metabolic pathways leading to liver steatosis remains unclear, but it can induce IR and oxidative stress [41,140].

2.2.5   Cirrhosis and hepatocellular carcinoma

NAFLD and NASH both contribute to the progression of cirrhosis [141] and HCC, the two end stages of chronic liver disease. HCC is a cancer with one of the highest mortality rates worldwide [142]. Overall, there has been a recent increase in HCC mortality of Europe [143], and men are predisposed to the development of HCC [144]. HCC is currently it is the sixth most common cause of cancer in developed countries and the second most lethal cancer in men globally [145]. Cirrhosis refers to extensive extracellular matrix accumulation in the liver. It is preceded by hepatic inflammation and liver damage, which leads to the activation of stellate cells, which transdifferentiate into matrix protein-secreting myofibroblasts, the major player in fibrogenesis [146]. In addition to fibrotic changes, cirrhosis leads to vascular distortion, resulting in increased blood pressure in the portal vein [147].

2.2.6   Mouse models of fatty liver disease

Mouse models of fatty liver disease can be very useful tools in studying human liver disease. Basic liver functions and metabolisms have been highly conserved during evolution, but the natural environment (eg. diet) is different, and the results cannot always be translated from mouse to human. Because the fatty liver disease in humans is a complex disease, the optimal characteristics of the animal model depend on which aspect of the disease is under investigation. The models do not often reproduce the histological patterns typical in human disease. Fibrosis and hepatocellular ballooning are less common in mouse models. Other concerns are the metabolic pathways involved in the pathological process, which may not be the same in human and mouse models. For example, cholesterol is carried mainly in LDL in humans and in HDL in mice, leading to inherent resistance to atherosclerosis in the wild-type (WT) mice [148] . In addition, pathogenic factors, such as apoptosis, fibrosis, oxidative stress should be present in the model.

2.2.6.1 Diet-induced models

Diet-induced animal models are popular in fatty liver disease research because they mimic diet-induced obesity and IR, which is a common risk factor/cause in humans. These diets are usually high in fat and/or sugar, and therefore lead to long-term excessive caloric intake in the form of lipids, cholesterol, and carbohydrates.

Commonly used high-fat diets (HFD) usually broadly resemble human diets regarding macronutrient composition and contain 45% to 60% fat by calories [149]. The excessive energy intake leads to fat accumulation, increased inflammation and finally to the development of fibrosis, although this process is slow in mice, considering the relatively short life span of that species. The diet is usually continued for several weeks or months. In mice, a HFD for 12 to 16 weeks leads to IR, steatosis, hepatic ballooning and obesity [150,151] and increased ALT and AST levels after 34 weeks [152]. These diets mimic the aspects of the modern Western diet, and the animals are expected to develop IR with the associated systemic inflammation, obesity, and hepatic steatosis, and in the long term, they mimic the main metabolic changes and histological markers of human NAFLD, but the pathological outcome is often milder.

In addition to high fat content, high fructose content diets are also used to induce NAFLD in mice. Instead of animal feed, fructose is often added to the drinking water. It is metabolized in the liver and enhances DNL, induces hepatic fat accumulation and inhibits beta-oxidation [153]. It leads to increased body weight, plasma TAG and glucose levels. Steatosis (without clear NASH pathologies) can be observed in 10 to 15 weeks on high fructose diet [153]. High fructose diet can also be used together with HFD. These high-fat high-fructose diets (HFHFD) often produce more severe form of NAFLD, especially oxidative stress, macrophage aggregation and liver fibrosis were more common than in HFD fed mice after 16 weeks [154]. Although female rats showed higher degree of hepatic fat accumulation on HFHFD, male rats suffered from significant increase in liver injury, inflammation, and oxidative stress [155].

Atherogenic diets (AthD) are often used to model atherosclerosis, but they can be useful in studying NAFLD as well. They are high in cholesterol (1-1.25%) and often contain also cholic acid (0.5%), because cholic acid enhances the absorption of cholesterol and reduces the breakdown of cholesterol into bile acids, leading to impaired cholesterol removal [156–158]. Cholate promotes the expression of genes associated with extracellular matrix deposition in hepatic fibrosis [157]. Cholesterol, in turn, induces the expression of genes involved in inflammation [157]. AthD induces the development of liver steatosis, inflammation and increased serum ALT levels (after 6 weeks), as dietary and liver cholesterol accumulation induces symptoms of NASH, including steatosis and inflammation accompanied with moderate weight loss [159].

Hepatocellular ballooning (degenerative, swollen hepatocyte) and fibrosis develop after prolonged exposure (24 weeks) [157].

Table 1. The most common diet-induced and chemically-induced liver disease models in mice.

DIET	MECHANISM	BWT	IR	STEATOSIS	ALT	INFL.	FIBROSIS
HFD	excess fat intake	up [152]	yes [152]	yes [152]	yes, after extended exposure [152]	yes, mild [152]	yes, after extended exposure [152]
MCD	impaired b-oxidation	down [160]	no [160]	yes [161]	yes [161]	yes [161]	mild [160]
ATHD	increased cholesterol absorption, decreased bile acids	no [159,162]	no [162]	yes [159]	yes [163]	yes [159]	yes [159,162]
CCL₄	accumulation of toxic peroxidation products due to oxidative stress	no [164]	no [164]	yes [165]	yes [165,166]	yes [166]	yes [165]
DEN	oxidative stress, DNA mutations	no [167]	yes [167]	no [167]	yes [167]	yes [167]	yes [167]

BWT=body weight, IR=insulin resistance (systemic), ALT=alanine aminotransferase, INFL=inflammation, HFD=high-fat diet, MCD=methionine-choline-deficient diet. ATHD=atherogenic diet, CCL₄=carbon tetrachloride, DEN=diethylnitrosamide

One common diet used for inducing NASH is methionine- and choline-deficient diet (MCD). They usually have high sucrose content and moderate fat content (40% and 10% of calories, respectively), but they lack methionine and choline [168]. Methionine and choline are essential for beta-oxidation and are precursors to PC, the main phospholipid in biological membranes, including the one coating VLDL particles [169], and their depletion leads to steatosis (predominantly in the acinar zone 3) in two weeks [160,170] hepatocellular ballooning, inflammation and ROS-mediated liver damage in four weeks [160,171]. Fibrosis can set in as early as eight weeks after the initiation of MCD [170,172]. Steatosis development is caused by enhanced lipid uptake and decreased TAG export due to impaired VLDL formation [173] and suppression of SCD1 [174]. The main mechanism for disease development is thought to be lipotoxicity [168]. The mice lose body weight and do not develop IR and the changes in gene

expression do not reflect very well those seen in human NASH, even though the histological changes closely resemble human NASH [172,175–177]. MCD leads to accumulation of saturated, monounsaturated, and polyunsaturated FAs (especially monounsaturated FFAs) [168]. MCD diet causes suppression of lipogenesis and induction of TAG synthesis genes [168]. In some aspects MCD –induced models do not reflect the metabolic syndrome associated NAFLD pathogenesis. However, fat content in the diet does affect hepatic lipid peroxidation and the induction of inflammatory cytokines [178]. Commonly used diet-induced mouse models are summarized in Table 1.

2.2.6.2   Chemically-induced models

Various chemical compounds, for example streptozotocin or carbon tetrachloride (CCl$_4$) can be used alone or in combination with high-fat or high-sugar diet. Streptozotocin induces diabetes mellitus by causing DNA alkylation which leads to cell death in pancreatic islets [179] and inhibition of insulin synthesis. CCl$_4$ causes an oxidative stress reaction leading to accumulation of lipid and protein peroxidation products and later in severe necrosis and disruption of liver cell function [180]. However, CCl$_4$ is toxic to other organs as well, for example kidney and pancreas, and it may be challenging to distinguish between the effects of general toxicity and metabolic disturbances caused by liver damage [181]. These models produce steatosis relatively rapidly, but the pathogenesis differs from that of human NAFLD and may not model it well. In addition, these chemicals are highly toxic and may lead to animal deaths. Other chemical-induced models include diethylnitrosamine (DEN). It causes oxidative stress and DNA mutations and is often used to study the progression of fatty liver disease into HCC [167]. The most common chemically-induced mouse models for fatty liver are summarized in Table 1.

2.2.6.3   Genetically modified models

There are several genes that regulate the accumulation of lipids in the hepatocytes. Many of these have been knocked out in order to generate liver disease models. The best known are probably the leptin hormone deficient model (*ob/ob*) and defective leptin hormone receptor model (*db/db*), which are both results of spontaneous mutations in the laboratory mouse [182]. Leptin is a hormone produced in adipocytes by the fat tissue and by enterocytes in the small intestine. It binds to leptin receptor in the hypothalamus and is involved in the regulation of energy homeostasis by inhibiting hunger. This, in turn, reduces the amount of stored fat in the fat tissue. *Ob/ob* mice produce a truncated, inactive form of leptin, which is not able to bind the leptin receptor, which leads to hyperglycemia, hyperinsulinemia, and

dyslipidemia [183]. They have uncontrollable appetite and increased food intake and are therefore obese and they develop IR and hepatic steatosis [184,185]. *Db/db* mice have a dysfunctional leptin receptor due to natural mutation in the leptin receptor gene [182]. Both *ob/ob* and *db/db* mice develop obesity, IR and liver steatosis [184,186,187].

Other genetically modified mouse models of fatty liver include juvenile visceral fat (JVS) model. The mutation in the organic cation transporters gene occurred spontaneously and the mouse developed microvesicular steatosis within few days after birth [188–190]. The hepatocytes in these animals presented slightly swollen mitochondria, suggesting impairment in mitochondrial function [188]. Other symptoms included retarded growth and enlarged abdomen [188]. The JVS mice develop the fatty liver phenotype because of systemic carnitine deficiency [189]. Carnitine plays an important role in the mitochondrial FA oxidation as it transports FAs across the inner membrane of the mitochondria. Another mitochondrial beta oxidation related model is the mitochondrial trifunctional protein (MTP) KO mouse. MTP is involved in the LCFA oxidation in the mitochondria. The homozygous MTPKO animals develop hepatic steatosis but die within 36 hours after birth [191]. The heterozygous MTPKO animals develop fatty liver and IR [192].

Table 2. Commonly used genetically modified NAFLD mouse models.

MODEL	DEFECT	OBESITY	IR	STEATOSIS	FIBROSIS
OB/OB	Leptin deficiency [193]	yes [186]	yes [184]	yes [187]	no [187]
DB/DB	Leptin resistance [194]	yes [186]	yes [194]	yes [187]	no [187]
JVS	Carnitine transport defect [189]	no [188]	no [188]	yes [188]	not available
MTP KO	FA oxidation defect [192]	no [191]	yes [191]	yes [191,192]	not available
CD36 KO	lipid uptake defect [195]	no [196]	no [196]	no [195]	not available
AR KO	Lack of estrogen [197]	yes [198]	no [198]	yes [198]	not available

IR=insulin resistance (systemic). OB=obesity, DB=diabetes, JVS= juvenile visceral steatosis mouse, MTP= mitochondrial trifunctional protein, CD36=cluster of differentiation 36, AR=aromatase

CD36 is known to mediate LCFA uptake [199]. CD36 KO mouse shows a defect in lipid uptake in muscle and adipose tissue, and therefore they present with increased plasma LCFA and TAG levels [195,200], hepatic IR and increased hepatic gluconeogenesis [196]. These animals also have improved systemic insulin sensitivity and decreased body weight [196]. Interestingly, these mice show increased hepatic

TAG under fasting conditions, but not on fed state [195,196]. Furthermore, liver-specific defect in CD36 function has been shown to protect against fatty liver [201].

Aromatase catalyzes the final step in the biosynthesis of C18 estrogens, and therefore mice lacking functional aromatase enzyme (ArKO) cannot synthesize endogenous estrogens [197]. The adult ArKO female mice show drastically increased body weight from a young age, while male KO mice show lower body weight early in life, but at one year old they develop obesity [198]. In line with this, both males and females develop fatty liver by the time they are one year old [198]. Male mice develop glucose intolerance followed by hepatic steatosis due to their estrogen deficiency [202]. A summary of the commonly used mouse models of fatty liver disease is presented in Table 2.

2.2.6.4   Composite models

Diabetes mouse models, mainly *ob/ob* and *db/db* spontaneously develop hepatic steatosis [187]. In *ob/ob* mice the steatosis will progress into NASH when these mice are fed HFD, but not spontaneously [193]. Liver fibrosis can be induced in the *db/db* mice by feeding MCD for four weeks, but *ob/ob* fail to develop fibrosis on MCD or even when administered CCl$_4$ [203,204].

Genetically modified atherosclerosis models ApoE-/- and LDL receptor KO (Ldlr-/-) are useful models of NASH when challenged with HFD. Ldlr-/- mice develop hyperlipidemia after a short high cholesterol diet, which rapidly leads to hepatic steatosis associated with inflammation and accumulation of macrophages in the liver as well as bloated Kupffer cells [205,206].

Ppara KO mice develop liver steatosis after 24-hour fasting, even though hepatic lipid uptake seems decreased rather than increased in these mice [207]. Similarly, PparaKO mice fed HFD for several weeks also accumulate fat in the liver and are more sensitive to HFD than WT mice, due to dysfunction in FA oxidation [207].

Taken together, genetically modified models and composite models mimic certain aspects of the fatty liver disease, but translating the results to human disease requires careful approach as human and mouse genetics vary, and the natural diet is very different for mice and human.

2.2.7   Treatment of fatty liver disease

Fatty liver disease is associated with increased co-morbidity and mortality, and it is currently the leading cause for end-stage liver disease and liver transplantation [208]. Co-morbidities include metabolic disorders, including diabetes and obesity as well as liver cirrhosis and HCC, all of which increase mortality.

As metabolic disorders, including obesity and diabetes, increase the risk of developing fatty liver disease, weight loss and the treatment of diabetes are important in both the prevention and first line treatment of NAFLD and NASH. Currently, there are not many effective, specifically tailored pharmacological treatment options for fatty liver disease, and most commonly used treatments may support weight loss and diabetes management and therefore also reduce liver pathologies.

Vitamin E is often recommended for its antioxidant properties to reduce oxidative stress, which is often associated with NASH. It has been shown to reduce serum ALT and AST levels in NASH patients [209–211] and to reduce steatosis and inflammation [209,210], but its efficacy is still questionable and in long term use may not be safe [212,213].

Many therapeutics that are used to treat diabetes and dyslipidemia are also used to treat NAFLD, including pioglitazone, metformin, and statin. Pioglitazone is a peroxisome PPARs agonist, and it is used to treat diabetes. It improves insulin sensitivity by activating PPAR-γ in the liver, muscle, and adipose tissues as well as shows anti-tumor activity through the inhibition of proliferative activity [214,215]. Plioglitazone has been shown in some studies to reduce serum ALT levels and reduce steatosis and inflammation [209]. Controversially it may lead to weight gain [209], but at the same time it has been found to postpone or slower the development of fibrosis and HCC in some animal models of cirrhosis [216].

Another antidiabetic drug, called metformin, acts through AMP-activated protein kinase to improve hepatic glucose metabolism and FA oxidation as well as reduces (ACC) activity and the expression of lipogenic enzymes, including SREBP-1 [217]. Metformin may aid weight loss through lifestyle changes, but it has not been shown to help improve histological pathologies in NASH [218,219]. Statins are commonly used in the prevention of cardiovascular disease. They are effective in lowering the plasma cholesterol concentration, and because high plasma lipid levels are associated with NASH, statins can be used to prevent cardiovascular disease in NASH patients. However, their efficacy in the treatment of NASH has not been studied extensively. The few studies that have looked at statins and NASH, suggested that they could have potential in protecting from steatosis, steatohepatitis and fibrosis [220–222].

Currently a potential new lipid-altering drug Aramchol, which is a stearoyl-Coenzyme A desaturase 1 (SCD-1) inhibitor is being tested in patients with fatty liver disease. This is a liver targeted therapy. SCD-1 is the rate limiting step in the synthesis of monounsaturated FAs, and its inhibition is associated with reduction of steatosis and improved insulin sensitivity [223,224].

Obeticholic acid is a synthetic FXR agonist that has been recently studied in NASH patients [225]. FXR is an intracellular receptor, which negatively regulates bile acid synthesis leading to reduction in gluconeogenesis, lipogenesis, and steatosis [226].

OCA has been shown to improve glucose and lipid metabolism. Clinical trial studies are still ongoing.

To date, there are no pharmacological treatments available for NALFD or NASH. However, several promising drugs are under development. Currently, commonly recommended treatment plans encourage exercise and healthy diet to help weight loss and improve IR. In case of non-diabetic NAFLD patients, vitamin E and pioglitazone have been suggested as beneficial. Due to its powerful antioxidant nature vitamin E is believed to target oxidative stress components, whereas pioglitazone ameliorates IR and liver histology [209,227]. At present, a few drug candidates e.g., obeticholic acid, elafibranor and selonsertib are evaluated for their potential to combat NASH and liver fibrosis. The new drugs could be a game changer for many patients struggling with NASH.

2.3   HSD17B enzymes

HSD17B enzymes belong to the large enzyme family of short-chain dehydrogenases/reductases (SDR), except HSD17B5, which belongs to the aldo-keto reductase family (ARK) [228]. SDR enzymes are oxidoreductases that use nicotinamide adenine dinucleotide (NAD) or nicotinamide-adenine-dinucleotide phosphate (NADP) as cofactors. SDR is one of the oldest and largest family of enzymes and represent in all forms of life [229]. SDRs are a very diverse group, and they share only about 15-30% of pairwise sequence similarity [229]. The large substrate pool is possible due to a highly variable C-terminal segment, creating unique active sites and ligand binding properties [230].

HSD17Bs are enzymes that catalyze the oxidoreduction of hydroxyl and oxo-functions at the position of carbon 17 of androgens and estrogens or their precursors, but also other substrates such as FAs and bile acids are known [231]. There are 14 HSD17Bs discovered in mammals to date. HSD17B15 was very recently characterized in Japanese eel, and it's thought to be involved in the regulation of androgen activity [232]. HSD17B enzymes are encoded by different (non-homologous) genes, producing distinct amino acid sequences leading to different subcellular localizations, varying co-factor as well as substrate preferences and tissue expression patterns. Like many other SRDs, they share two conserved domains: N-terminal co-enzyme-binding motif and an active site sequence [229,233].

The classical role for HSD17B enzymes is the regulation of sex steroid activity. HSD17B1 converts estrone to estradiol and is highly expressed in estrogen producing tissue [234]. In addition, HSD17B1 enzyme is shown to be highly expressed also in various normal and neoplastic extra-gonadal tissues, enabling local activation of estrone to estradiol in the target tissues [235,236]. In turn, HSD17B2 converts testosterone to androstenedione, as well as estradiol to estrone [237]. HSD17B3

converts androstenedione and 5α-androstanedione to more potent forms, testosterone, and dihydrotestosterone [238,239]. HSD17B5 converts the conversion of androstenedione to testosterone [228]. HSD17B6 catalyzing the production of potent androgens such as 5α-dihydrotestosterone from 3α-androstanediol [240]. Besides the role in steroid hormone metabolism, several HSD17B enzymes are involved in other metabolic pathways. HSD17B4 plays a role in peroxisomal oxidation of FAs [241]. HSD17B7 is involved in *de novo* cholesterol synthesis [242]. HSD17B8 is thought to be involved in the mitochondrial synthesis of FAs [243,244]. HSD17B10 may have a broad substrate specificity and is capable for mitochondrial beta-oxidation of FAs [245,246]. HSD17B11 contains an ER/LD targeting motif suggesting a function in lipid metabolism [247], however, it has been proposed to be involved in androgen metabolism [248,249]. However, the *in vivo* role is still unclear for some HSD17Bs.

2.3.1   HSD17B12

HSD17B12 was characterized as a 3-ketoacyl-CoA reductase (KAR) involved in long-chain FA elongation (LCFA), converting palmitic acid to AA [6]. HSD17B12 is ubiquitously expressed in mammalian tissues. The highest expression has been found in the tissues linked to energy metabolism, such as liver and adipose tissue. In addition, the FA elongation by HSD17B12 has been shown to play a role in the development of inflammation and cancer [250–252]. Previous research with HSD17B12KO mice in Poutanen lab has also indicated a role for the enzyme in AA synthesis and prostaglandin production [252,253]. HSD17B12 expression is relatively high in preadipocytes, and it further increases after adipocyte differentiation [254], but its role in the adipose tissue physiology is still unclear. The enzyme expression is regulated by SREBP, which is a key regulator of several enzymes involved in lipid metabolism and FA and cholesterol biosynthesis [255].

In recent genome-wide association studies (GWA), HSD17B12 has been identified as a candidate gene for type two diabetes [256–258]. Several single nucleotide polymorphism (SNP) mutations in the *Hsd17b12* gene have been identified: rs2176598, rs1061810 and rs4573668 [258]. HSD17B12 expression is downregulated in the adipose tissue and pancreatic islets of insulin-resistant subjects [258]. Another SNP, rs2176598, was associated with increased body mass index [259]. In addition, SNPs in *Hsd17b12* have been associated with cancer survival. For example, several SNPs are linked with cutaneous melanoma disease-specific survival [260], strongly associated with neuroblastoma [261].

Recently HSD17B12 was shown to promote HCV replication by aiding the infectious lipid particle production in Huh7.5 cells [262]. Furthermore, the HSD17B12 knockdown reduced LDs in Huh7.5 cells [262]. A very recent study found HSD17B12 to be involved in drug metabolism in vitro [263].

2.3.2   HSD17B13

HSD17B13 is a LD-associated protein [264–266]. It's N-terminus contains a 35 aa LD targeting sequence [267] and the promoter region contains binding site for C/EBP family of transcription factors, which regulate gene expression to control many cellular processed, including proliferation, differentiation, inflammation and metabolism [268]. *Hsd17b13* expression can be induced by LXRα-SREBP-1c pathway [269], a pathway that is a key regulator of both cholesterol and FA metabolism. Furthermore, *Hsd17b13* is expressed independent of PPARa, another key regulator of lipid metabolism [267].

The highest expression of *Hsd17b13* is observed in the liver in both human and mouse [233,264,267], so much so that it is quite a liver specific protein. Low levels have been detected in intestine, ovary, kidney, brain, lung, skeletal muscle, testis, and uterus [264,267]. The function of HSD17B13 is still unclear, however, it has been proposed a role in androgen and retinol metabolism [265,270]. The localization of HSD17B13 to the LD could suggest a function in fat metabolism. This idea was supported by a recent WGA study which showed that HSD17B13 was associated with lipid changes in patients with type 2 diabetes [271]. However, other studies did not observe HSD17B13 effects on lipid content [10,265].

HSD17B13 shares 78 % sequence similarity with *Hsd17b11*, and they are located in the same chromosome in human, mouse and rat [247]. Both HSD17B11 and HSD17B13 contain ER- and LD-targeting signals [247]. A very recent study on HSD17B13 protein crystal structure suggested that HSD17B13 localizes to the LD early in the budding phase [272].

2.3.3   HSD17B12 and HSD17B13 in fatty liver disease

As described before, in fatty liver disease, lipids accumulate within hepatocytes and the condition is strongly associated with metabolic disorders, such as dyslipidemia and IR, which are major health concerns with increasing prevalence. Metabolic disorders, in turn, are associated with many serious health problems including cardiovascular diseases, diabetes and cancer.

HSD17B12 has been proposed a role in the synthesis of AA and other LCFAs. AA and its metabolites can both cause and resolve inflammation that is associated and often precedes with numerous adverse conditions. Recent studies have suggested that AA and its downstream metabolites mediate liver steatosis and inflammation [273,274]. In addition, AA is thought to promote inflammation in adipose tissue [275], and moreover, (nutritional) AA has been shown to regulate the expression of lipogenic genes in adipocytes [276]. However, the role of HSD17B12 in lipid metabolism in the adipose tissue and the liver is still unclear.

The function of HSD17B13 is still unclear, however, increased hepatic HSD17B13 expression has been observed in patients with NAFLD and NASH [264,265]. In a recent study, HSD17B13 was shown to protect the liver from fibrosis in HSD17B13 knockdown mice on choline deficient diet [277]. However, another recent study using HSD17B13 KO mice did not observe a protective effect against hepatic fat accumulation or liver injury on HFD [278].

Several single nucleotide polymorphism (SNP) mutations in the *Hsd17b13* have been identified. In a GWA study in humans in 2018, Abul-Husn et al. identified variant rs72613567, which produced two novel liver transcripts [10]. One of these transcripts lacked exon 6 by alternative splicing, resulting in a truncated version of the protein. The other transcript was a result of guanine insertion in exon 6 which caused a frame shift and premature truncation of the protein. Both of these rendered the gene product non-functional and were associated with a lower risk of NASH, cirrhosis and HCC [10,265,279,280]. Soon after discovering the rs72613567 variant, Kozlitina et al. identified a new HSD17B13 variant rs143404524 which introduces a frameshift at position 192, downstream of the active site, and leads to loss of function [106]. However, variant rs143404524 was not associated with TAG accumulation in the liver. Ma et al. identified a nonsynonymous mutation variant rs62305723 in exon 6, which substitutes the proline with serine at position 260. This variant was associated with decreased ballooning and inflammation, but not with steatosis [265]. Another SNP variant rs6834314 is located downstream of *Hsd17b13* gene, and it was associated with increased steatosis but decreased inflammation, ballooning, and Mallory-Denk bodies in hepatocytes [265,280].

2.3.4 HSD17B12 and HSD17B13 as candidate drug targets

Both HSD17B12 and HSD17B13 have been proposed as potential drug targets for various diseases, and their inhibition may offer therapeutic benefits. HSD17B12 inhibition has been proposed as a potential therapeutic strategy for breast cancer, ovarian cancer, and colorectal cancer [252,281–283]. Considering the high expression of HSD17B12 enzyme in the lipogenic tissues, and its capacity to catalyze reactions in lipid metabolism, it could be a promising target for novel therapies for metabolic diseases as well. In addition, the putative role of HSD17B12 in prostaglandin synthesis makes it also an interesting candidate for therapies aiming to alleviate inflammation response. The wide expression pattern of HSD17B12 covering many tissues of the body may lead to potential off-target effects when using inhibitors to target HSD17B12.

HSD17B13 has been suggested as a potential drug target for nonalcoholic fatty liver disease (NAFLD), hepatic fibrosis and other metabolic disorders [277,284,285]. The HSD17B13 variants which protect against liver disease make small molecule

HSD17B13 inhibitors an attractive therapeutic to liver disease. The liver specificity of HSD17B13 expression makes its inhibition relatively safe regarding off-target effects [233,264,267].

The existence of several HSD17B13 variants with protective effect gives a possibility of modulating the HSD17B13 activity to create therapeutics for fatty liver disease, either by altering the gene expression (i.e., by using antisense oligonucleotides) or by inhibiting its activity directly using small synthetic inhibitors.

Further research is needed to fully understand the role of these enzymes in disease pathogenesis and to develop safe and effective drugs that target them.

3   Aims

The aim of the study was to characterize the *in vivo* function of two HSD17B enzymes, HSD17B12 and HSD17B13 using genetically modified mouse models. Characterizing these functions is important, because both enzymes could be possible targets for pharmaceutical therapies, especially in diseases related to metabolic disorders.

The specific aims of the study

To characterize the *Hsd17b12* function in lipid and energy metabolism.

To investigate the role of *Hsd17b12* and *Hsd17b13* in liver steatosis.

To explore the effects of *Hsd17b13* in reproduction.

4   Materials and Methods

4.1   Animals

The HSD17B13 knockout (HSD17B13KO) mice were acquired from Mutant Mouse Regional Resource Centers (https://www.mmrrc.org/). This mouse model was generated by replacing exons 1 and 2 of *Hsd17b13* gene with lacZ expressing cassette by homologous recombination in embryonic stem cells. Genotyping of the mice was performed by PCR with primer pairs for WT and mutated allele. For HSD17B13KO studies, three- and nine-month-old mice with age-matched WT litter mates as control animals. Both WT and KO animals had a hybrid genetic background (C57Bl/6N and SV129, 1:1).

The targeting vector for HSD17B12 (PGS00030_C_C05) was purchased from the European Conditional Mouse Mutagenesis Program (EUCOMM). In the construct, exon 2 of *Hsd17b12* gene was flanked by *loxP* sites, and a *lacZ* as well as neo cassette was flanked by FRT sites. The vector was linearized, and electroporated into G4 hybrid mouse embryonic stem cells (G4, 129S6B6F1) for homologous recombination with standard procedures. The colonies were screened with specific primers for the WT and the mutated allele (**II**, Table 1) to identify the properly targeted clones. The proper homologous recombination was then verified by sequencing. Thereafter, the lacZ-neo cassette was deleted from the selected ES cell clones by Flp recombination, and the cells were injected into C57BL/6N mouse blastocysts. The blastocysts were then surgically transferred into pseudopregnant foster mothers (NMRI strain). The resulting chimeric offspring were genotyped and mated with WT C57BL/6NCrl mice to produce the F1 generation to test the germ line transmission. Heterozygous littermates were used as breeding animals for mouse colony maintenance. The presence of the WT and/or mutated gene was analyzed by PCR (**II**, Table 1).

Rosa26CreERT strain was used together with the floxed strain to generate a Tam-inducible conditional KO mouse strain (HSD17B12cKO, **II**, Supplemental Fig. S1C). The primer pair used to identify the presence of Rosa26Cre-ERT alleles is listed in Table 1 (**II**). The adipocyte-specific, Tam-inducible conditional KO mouse strain (aHSD17B12cKO) was generated by breeding the HSD17B12-loxP with

AdipoqCreERT2 mice. The primers used for genotyping the presence of Cre-ERT2 gene in these mice are shown in (**II**, Table 1).

Daily intraperitoneal injections of 1.5 mg Tam (Sigma-Aldrich, Saint Louis, MO, USA) for five consecutive days were administered to induce gene disruptions in both inducible KO models at the age of eight weeks. Tam was dissolved in ethanol and then diluted 1:10 in rapeseed oil. Ethanol diluted in rapeseed oil was used as a vehicle.

The *Hsd17b12* floxed mice were crossbred with heterozygous Albumin-Cre mice [286] to generate a liver specific KO mouse strain LiB12cKO. The albumin promoter directs the Cre recombination in hepatocytes, from the time when hepatocytes begin to replace hematopoietic cells in the fetal liver (embryonic day 10) [287,288] and continues until the postnatal age of six weeks [289]. The pups were earmarked and genotyped with PCR at the age of approximately 14 days. The genotyping was performed using PCR, with primer pairs for the WT and mutated allele (**III**, Table 1).

All animal handlings were conducted under the animal license number 10605/04.10.07/2016 and 41729/2019, granted by the Animal Experiment Board in Finland, and were carried out in accordance with the institutional animal care policies that fully meet the requirements defined in the National Institutes of Health (Bethesda, MD, USA) guidelines on animal experimentation. Animals were housed at the Central Animal Laboratory at the University of Turku, Finland, in individually ventilated cages (IVC, Techniplast, Buguggiate, Italy) with approximately 70 air changes per hour, and with constant temperature at $21 \pm 3°C$ and humidity at $55 \pm 15\%$. A 12:12h light:dark cycle was applied, with a light change at 7 am and 7 pm. Autoclaved aspen chips were used as bedding (Tapvei Ltd, Harjumaa, Estonia). The animals were individually identified with ear marks. Littermates of the same sex were kept together in the same cage, 1 to 6 animals per cage, regardless of their genotypes. The animals were provided with soy-free natural ingredient feed to avoid the effects of phytoestrogens on the potential reproductive phenotype (Special Diets Services, Witham, UK). Both chow pellets and tap water were available *ad libitum*. Every cage had a nest-box and tissue paper was provided for nest building. Animals were sacrificed with CO_2 asphyxiation and cervical dislocation.

4.2   Histology

Liver and adipose tissue samples were fixed in 10% buffered formalin solution at room temperature (RT) for 16-20 hours, dehydrated and embedded in paraffin. for microscopic analysis 5 µm thick sections were stained with hematoxylin/eosin (HE) or Periodic acid–Schiff (PAS).

Ki-67 (Ki-67 Monoclonal Antibody, SolA15, eBioscience™, Thermo Fisher Scientific, Waltham, MA, USA) immunohistochemical staining was performed on four µm thick sections using Labvision™ autostainer (Thermo Fisher Scientific). For antigen retrieval, the sections were immersed in citrate buffer (pH 6) (Genemed Biotechnologies, Torrance, CA, USA) and placed in pressure cooker for 20 minutes. Sections were then washed by 0.05 M Tris-HCl (Reagena, Toivala, Finland) with 0.05% Tween 20 added. The antibody was diluted 1:2000 and incubated at room temperature (RT) for 60 minutes. The sections were incubated with the secondary antibody, rat on mouse HRP-polymer (Biocare Medical, Pacheco, CA, USA), at RT for 30 minutes and counter stained with Mayer's hematoxylin (Histolab Products AB, Västra Frölunda, Sweden). Pertex mounting medium (Histolab Products AB) was used for mounting.

TUNEL staining was performed on 4 µm thick tissue sections, which were then deparaffinized and rehydrated Antigen retrieval was performed in citrate buffer in microwave followed by blocking the endogenous peroxidase activity by 3% H_2O_2. TUNEL reaction mixture containing TdT and biotin-16-dUTP (Roche Diagnostics GmbH) was applied on the sections and incubated at 37°C for one hour. After that, the reaction was stopped by adding 300 mM NaCl. The sections were blocked with 3% BSA and incubated in ExtrAvidine (Sigma-Aldrich, diluted 1:500 in 1% BSA) for 30 min at 37°C, followed by staining with 3,3' diaminobenzidine (Dako Liquid DAB+ Substrate Choromogen System; Dako North America, Carpinteria, CA, USA). Finally, the sections were counterstained with Mayer's hematoxylin, dehydrated and mounted.

For Oil Red O (ORO) staining, the tissue samples were embedded in Tissue-Tek® O.C.T.TM (Sakura Finetek USA, Inc., Torrance, CA, USA) and frozen in 2-methylbutane cooled with dry ice. Then 8 µm thick sections were cut and stained with ORO (Sigma-Aldrich) according to standard procedures. Shortly, tissue sections were fixed in buffered formalin solution and then washed with water and with isopropanol. Oil red O solution was was used for staining, followed by washing with isopropanol and water, and then by mounted with Aquatex® (Merck, Darmstadt, Germany).

4.2.1   Image analysis

Microscope slides were scanned using Pannoramic 250 Flash digital slide scanner (3DHISTECH Ltd., Budapest, Hungary). For quantification of apoptotic and proliferating cells, digital slide images were then imported into QuPath, Version 0.2.0, an open-source software platform [290]. Apoptotic or proliferating cells were identified using the positive cell detection feature of QuPath, which detects the nuclei and classifies them as positive (apoptotic cells) or negative with QuPath's built-in

cell segmentation algorithms. The analysis was performed on one sagittal section of the left lateral liver lobe per animal (mean area 52.2 mm^2). A total of three outliers were excluded by ROUT method in GraphPad Prism (GraphPad Software, La Jolla, CA, USA) with coefficient Q=1% from male CTRL, male KO and female CTRL groups, one from each group. The mean percentage of positive nuclei of all detected nuclei was compared between the CTRL and KO groups.

To measure adipocyte size, PAS-stained adipose tissue slides were scanned for further analysis with Pannoramic 250 Flash series digital slide scanner (3DHISTECH Ltd). Three to four 10x magnified images were taken with the 3DHISTECH CaseViewer version 2.3. AdipoCount software [291] was used to measure the average adipocyte size in the images for each animal.

Micro- and macrovesicular steatosis was quantified from HE stained images with the deep learning model created in the Aiforia Create (version 5.3, Aiforia Technologies, Helsinki, Finland). The model can detect liver parenchyma, including normal hepatocytes, hepatocytes with macrovesicular and microvesicular fat accumulation. The tissue background consisting of tissue artefacts, blood vessels and other features that do not belong to the liver parenchyma can be excluded from the analysis. Inside parenchyma the model detects and quantifies the tissue area containing micro- and macrovesicular steatosis [292].

Transmission electron microscopy was carried out at the Institute of Biomedicine, at the University of Turku. For that, approximately a 1 mm^3 pieces of left lateral liver lobe of nine-month-old HSD17B13KO male mice were fixed with 5% glutaraldehyde in s-collidine buffer, dehydrated with ethanol, and embedded in Fluka Epoxy Embedding Medium kit (Sigma-Aldrich). Thin sections were cut using a Leica EM UC7 ultramicrotome (Leica Microsystems, Wetzlar, Germany) to thickness of 70 nm. The sections were stained using uranyl acetate and lead citrate. The sections were examined using a JEOL JEM-1400 Plus transmission electron microscope (JEOL Ltd., Tokyo, Japan) operated at 80 kV acceleration voltage.

4.3   Gene expression analysis

Total RNA was isolated from frozen liver tissues using TRIsure™ reagent (Bioline, Bioline reagents Ltd., London, UK) according to the manufacturer's instructions. Three micrograms of total RNA per sample were treated with deoxyribonuclease I using DNase I Amplification Grade Kit (Invitrogen Life Technologies, Paisley, UK or Sigma-Aldrich).

4.3.1   qPCR

For quantitative reverse transcription PCR (qRT-PCR), 500 ng of DNase I treated RNA was reverse-transcribed using the DyNAmo cDNA synthesis kit (Thermo Scientific, Waltham, MA, USA) or SensiFAST™ cDNA Synthesis Kit (Bioline). qRT-PCR were performed using the DyNAmo Flash SYBR Green qRT-PCR Kit (Thermo Scientific) and CFX96 Real-Time C1000 thermal cycler (Bio-Rad Laboratories, Hercules, CA, USA). Standards were run in duplicates, and all the genes of interest as well as endogenous control genes [ribosomal protein L19 (L19) and peptidylprolyl isomerase A (Ppia)] used for normalization were analyzed in triplicates. Primer sequences and qRT-PCR conditions for analyzing the expression of various genes are described in (**I**, Table 1 and **II**, Table 1).

4.3.2   RNAseq

For HSD17B13KO mouse model, total RNA was extracted from the livers of 3-month-old HSD17B13KO (n=6) and WT males (n=6), and purified using the NucleoSpin® RNA XS kit (Marcherey-Nagel GmbH, Düren, Germany). The samples were sequenced using HiSeq2500 sequencing instrument according to the protocols provided by the manufacturer (Illumina, Essex, U.K.) at the Finnish DNA Microarray and Sequencing Centre (Turku Centre for Biotechnology, University of Turku). Raw reads were quality controlled using the FastQC tool and the reads were aligned to the mouse reference genome version mm10 available at UCSC database (downloaded from Illumina iGenomes website (http://support.illumina.com/sequencing/sequencing_software/igenome.html)) using the default settings of Tophat software v2.0.10 [293]. HTSeq v0.6.1 [294] was used to count the uniquely mapped reads associated with each RefSeq annotated gene. The downstream analysis was performed using R version 3.1.0 [295] and Bioconductor version 2.14 [296]. The data were normalized using the Trimmed Mean of M-values (TMM) approach of the edgeR package [297]. Statistical testing between sample groups (KO vs. WT) was carried out using the Limma package [298] after having applied voom transformation. The cutoff for differential expression was set at false discovery rate (FDR) < 0.25, absolute fold change above 1.5 and mean RPKM expression level in at least one of the groups > 0.125. Heatmaps were produced based on RPKM expression values using Euclidean distance and the average linkage method for clustering.

For LiB12cKO mice, RNA samples were extracted from 10 KO and 10 WT males at the age of two months. RNA-sequensing of total RNA was performed using Illumina Novaseq sequencer (Illumina, San Diego, CA, USA) at Novogene (Cambridge, UK). The sequencing length was 150 base pairs from both ends and sequencing depth was 20 million reads per sample. The read quality was checked with FastQC (v.0.11.14) [299], and the reads were aligned to mm10 and assigned to

genes with Rsubread (v.2.0.0) [300]. EdgeR(v.3.28.0) [297] calcNormFactors was used for normalization to counts per million (CPM) and ROTS (v.1.14.0) [301] for differential expression (DE) analysis. DE genes with FDR < 0.05 and fold change > 2.0 were selected for functional enrichment analysis using Metascape metascape.org with default functional categories from GO Biological Processes (GO), KEGG (K) and Reactome (R). Additional enrichment analysis was done using DisGeNet database. The individual specific visualization of selected gene sets was conducted using pheatmap in R using RPKM (reads per kilobase pre million mapped reads).

4.3.3   Western blotting

Tissues were lysed in ice-cold RIPA buffer supplemented with a cocktail of protease inhibitors (Roche, Rotkreuz, Switzerland) using Tissue Lyser II (Qiagen, Düsseldorf, Germany) with 5 mm stainless steel beads at 50 Hz for two minutes. Lysates were centrifuged at 14,000 x g for 20 min at 4°C before collecting the supernatants containing the protein pool. Protein extracts were resolved by 5-20% gradient SDS-PAGE and blotted onto nitrocellulose membranes (Amersham, GE Healthcare, Buckinghamshire, UK). Detection of proteins was done with specific primary antibodies and HRP-conjugated secondary antibody using chemiluminescence (**I**, Table 2). The PXi/PXi Touch from SYNGENE (SYNOPTICS group, Cambridge, UK) and the GeneTools Software 4.03.00 were used to detect and quantify the signals. Signal strengths were normalized to the expression of either Actin (FAS, PEPCK, PPARA and SCD1) or ERM (ACC, pACC, AMPK, pAMPK, CD36, CPT1A, G6pase, PLIN2 and PLIN3).

4.3.4   In silico analysis

The relative mRNA/protein expression of HSD17B13 was investigated in a set of 11 different human studies and 41 mouse models of hepatic steatosis from the Gene Expression Omnibus database and in liver of Ob/Ob, Db/Db and liver-specific PTEN KO mice (http://www.ncbi.nlm.nih.gov/ gds/?term=hCC). A keyword-based searching was applied with "Steatosis" and "Fatty Liver". Only the series performed on tissues at the mRNA and protein levels (MPSS, RT-PCR, SAGE, array, high throughput sequencing, Mass Spec, protein array) and analyzed with the GEO2R algorithm were selected. Each study is reported referenced with its specific GEO dataset ID (GSE). Differences are expressed in Log2 fold changes. When the genes are detected several times in a dataset, the different values are represented in the tables. Adjusted p values were calculated by the Benjamini and Hochberg method. P-values < 0.05 (*) were considered statistically significant. The absence of

HSD17B13 in some studies is reported as undetected. The means of Log2 fold change values and the adjusted p-values are shown.

4.4   Lipidomic analysis

For lipidomic analysis in inducible HSD17B12cKO, blood was collected from five CTRL (Cre-, lox/lox) and five inducible HSD17B12cKO (Cre+, lox/lox) males, six days post Tam induction via heart puncture, allowed to coagulate overnight at +4°C and spun down to extract serum. For LiB12cKO mice, livers of 10 control males and 10 hHSD17B12cKO males were dissected and about 20 mg piece from the lateral lobe was snap frozen in liquid N_2. Thereafter, quantitative lipidomic analysis was carried out as described earlier [302]. Shortly, ethyl acetate and methanol extraction were performed to extract lipids from the samples. To a 100 µl serum sample 1 ml methanol, 1 ml water and 100 µl of labelled internal lipid standards were added, and lipids were extracted by adding 3.5 ml of ethyl acetate. Dried samples were reconstituted with 250 µl of mobile phase (dichloromethane:methanol; 50:50, containing 10 mM ammonium acetate) for injection. Lipid separation and quantitation was performed on the SCIEX Lipidyzer™ platform using a SCIEX 5500 QTRAP® mass spectrometer (SCIEX, Framingham, MA, USA) with SelexION® Differential ion mobility (DMS) technology. The lipid molecular species were measured using MRM strategy in both positive and negative polarities. Positive ion mode was used for the detection of lipid classes dihydroceramides (DCER), hexosylceramides (HCER), lactosylceramides (LCER), SM, diacylglycerols (DAG), CE, CER, TAGs (TAG), and negative ion mode was used for the detection of lipid classes lysophosphatidylethanolamines (LPE), lysophosphatidylcholines (LPC), PCs, PEs, and FFAs. Lipidomics Workflow Manager software (SCIEX) was used for acquisition of samples, automated data-processing, signal detection and lipid species concentration calculations. Data analysis was performed with MetaboAnalyst 4.0 [303]. For Tam-inducible HSD17B12cKO mice, a total of 856 lipids were analyzed, of which 222 lipids contained missing values. Of these, 137 lipids were found to have missing values in at least 40% of samples (2 samples) in both KO and CTRL mice and were, therefore, discarded prior to the statistical analysis. Missing values from the remaining 85 lipids were imputed using MissForest package [304]. Values were log-transformed, and no outliers were observed. For the LiB12cKO mice, a total of 943 lipids were analyzed. One outlier was identified in the CTRL group and excluded from the analysis.

4.5 Serum analysis

4.5.1 Clinical chemistry

Various clinical chemistry parameters were analyzed in the inducible HSD17B12cKO animals. On day six after the Tam induction. whole blood (roughly 110 µl) was collected via saphenous vein in BD Microtainer® lithium-heparin blood collection tubes from seven CTRL (Cre- lox/lox) and six HSD17B12cKO (Cre+ lox/lox) male mice as well as in five CTRL (Cre- lox/lox) and five (Cre+ lox/lox) female mice (Becton, Dickinson and Company, Franklin Lakes, NJ, USA) and analyzed for albumin, alkaline phosphatase, alanine aminotransferase (ALT), amylase, blood urea nitrogen, total calcium, creatinine, globulin, glucose, potassium, sodium, phosphate, total bilirubin and total protein concentrations using Comprehensive Diagnostic Profile rotor (Abaxis, Inc., Union City, CA, USA) Vetscan VS2 analyzer (Abaxis, Inc.).

Serum markers for liver function were analyzed in the LiB12cKO mice. At the age of 10 weeks, 100 µl blood was collected via saphenous vein from eight CTRL and eight LiB12cKO males and ten CTRL and ten LiB12cKO females in lithium-heparin tubes (Becton, Dickinson and Company, Franklin Lakes, NJ, USA). The samples were then analyzed using VetScan® Mammalian Liver Profile reagent rotor (Abaxis, Inc., Union City, CA, USA), which measured the following parameter: total bilirubin (TBIL), blood urea nitrogen (BUN), alkaline phosphatase (ALP), ALT, gamma-glutamyl transferase (GGT), bile acids (BA), albumin (ALB) and total cholesterol (CHOL). The analysis was run by using the VetScan Chemistry Analyzer (Abaxis, Inc. Union City, CA, USA) in the Central Animal Laboratory at the University of Turku

4.5.2 Metabolic analysis

AbsoluteIDQTM p150 kit (BIOCRATES Life Sciences AG, Innsbruck, Austria) was used to measure metabolites in liver samples of seven WT and nine HSD17B13KO male mice at the ages of three and nine months. Measurements were performed by BIOCRATES Life Sciences AG (Innsbruck, Austria) using an AB SCIEX 4000 QTrap™ mass spectrometer (AB SCIEX, Darmstadt, Germany) with electrospray ionization. The statistical computing environment R was used for all calculations and the R-package Limma was applied for statistical tests.

4.5.3   Triacylglycerol and cholesterol measurement

For HSD17B13KO mouse model, blood was collected by cardiac puncture and was allowed to coagulate at +4 °C for 15-20 h before serum was separated by centrifugation. Serum concentrations of TAG, cholesterol, high- (HDL) and low-density (LDL/VLDL) lipoprotein and glucose were determined by an automated Abott Architect analyzer (Abott Architect, Paris, France). Lipids were extracted from cryo-preserved liver samples of three- and nine-month-old HSD17B13KO and WT males by chloroform/methanol extraction [305], and TAGs (GPO-PAP kit, Roche/Hitachi, Rotkreuz, Switzerland), cholesterol and CE (Cholesterol/Cholesteryl Ester Quantitation Kit, Merck Millipore, Billerica, USA) were then measured).

For the Tam-inducible HSD17B12cKO mice, frozen liver samples were homogenized in PBS containing 0.1% Nonidet P-40 (Roche Diagnostics GmbH) with TissueLyser LT (Qiagen, Hilden, Germany) using 5 mm stainless steel beads at 50 Hz for two minutes. Samples were then incubated on ice for 30 min and spun down for 2 min at 12,000 relative centrifugal force (RCF). Serum Triglyceride Determination Kit (Sigma-Aldrich) was utilized according to the manufacturer's instructions to measure TAG concentration in the supernatants but scaled down for 96-well plates. The absorbance was measured with an EnSight multimode plate reader (PerkinElmer, Waltham, MA).

4.5.4   Glucose and pyruvate tolerance tests

Glucose tolerance test (GTT) was performed in mice fasted for either four hours (four- to five-month-old males) or six hours (seven- to nine-month-old males). The animals were fasted for 6 hours prior to pyruvate tolerance test (PTT). Glycemia was measured from tail blood with FreeStyle Lite blood glucose monitoring system (Abbott Diabetes Inc., Alameda, USA) immediately before glucose (GTT) or pyruvate (PTT) administration (time point 0). Glucose (1g/kg body weight) or pyruvate (2g/kg body weight) was administered intraperitoneally and blood glucose concentration was measured again 20, 40, 60 and 90 minutes after the administration.

4.5.5   Cytokine measurement

Serum cytokines were measured in ten CTRL (Cre-, lox/lox) and ten HSD17B12cKO (Cre+, lox/lox) males as well as nine CTRL (Cre-, lox/lox) and ten HSD17B12cKO (Cre+, lox/lox) females on day six post Tam induction in Tam-inducible HSD17B12cKO mice. Blood was collected via heart puncture and serum was separated after blood was allowed to coagulate overnight at +4ºC and spun down. Cytokine levels were measured using Luminex 200 with xPONENT 3.1. software (Luminex, Austin, TX, USA) and MILLIPLEX MAP Mouse

Cytokine/Chemokine Magnetic Bead Panel, MCYTOMAG-70K-PMX (Merck Millipore, Billerica,MA, USA) according to manufacturer's protocol. The cytokines measured included granulocyte-colony stimulating factor (G-CSF), Granulocyte-macrophage colony stimulating factor (GM-CSF), interferon gamma (IFN-y), IL-1, IL-1B, IL-2, IL-4, IL-5, IL-6, IL-7, IL-9, IL-10, IL-12 (p40), IL-12 (p70), IL-13, IL-15, IL-17, interferon gamma-induced protein 10 (IP-10), keratinocyte chemoattractant (KC), monocyte chemoattractant protein 1 (MCP-1), macrophage inflammatory protein 1-alpha (MIP-1a), MIP-1B, MIP-2, RANTES and TNFa. The minimum detectable concentrations were 3.2 pg/ml for all the cytokines except 12.8 pg/ml for IL-13.

4.6   Metabolic studies

4.6.1   Body weight and composition

HSD17B13KO: Body composition of nine-month-old male mice was analyzed using an EchoMRI-700TM (Echo Medical Systems, Houston, USA).

HSD17B12cKO: The body weight of the mice was monitored for seven days by weighing the mice once a day, starting at the time of the last Tam injection (day zero). The body composition (lean mass, fat mass, free water) was measured using the EchoMRI-700™ device (Echo Medical Systems, Houston, TX, USA) in live mice on day six after the last Tam injection. At the time of necropsy (six days after the last Tam injection) the weight of the various white adipose tissue (WAT) depots (subcutaneous, gonadal, perirenal), brown adipose tissue (BAT) as well as various organs (liver, spleen, kidneys, adrenals, pancreas, pituitary, heart) were measured and the tissues were collected in liquid nitrogen and formalin.

aHSD17B12cKO: The body weight and composition of the mice were monitored for three months by weighing the mice and performing the EchoMRI analyses once a month. The mice were sacrificed at the age of five months and interscapular BAT, subcutaneous, gonadal and perirenal adipose tissue as well as liver were collected in liquid nitrogen and formalin.

LiB12cKO: Mouse body weight was recorded at the ages of two, six and eight months. Body composition was measured with EchoMRI-700™ device (Echo Medical Systems, Houston, TX, USA) in live animals at the ages of six and eight months.

4.6.2   Monitoring food consumption

Food consumption was monitored in three CTRL (Cre- lox/lox) and five Tam-inducible HSD17B12cKO males housed in individual cages. To determine the

amount of consumed food, food pellets were weighed before the measuring period in the morning of day zero (after the last Tam injection) and then every 24 hours until day five post Tam induction.

4.6.3   Indirect calorimetry

Indirect calorimetry was analyzed in six CTRL (Cre- lox/lox) and six HSD17B12cKO (Cre+ lox/lox) males, placed (one mouse per cage) in OxyletPro™ indirect calorimetry cages (Panlab, S.L.U., Barcelona, Spain) three days after the first Tam-injection. The system analyzes changes in O_2 and CO_2 concentrations and its high precision extensiometric weight transducer measures water consumption. In addition, the sensor platform records spontaneous activity and rearing events to determine activity levels. The measurement (three days) was conducted between days three and five post Tam-induction.

4.6.4   PET-studies

Mice were fasted for 3 h with ad libitum access to water to standardize blood glucose level prior to 2-[18F]fluoro-2-deoxy-D-glucose ([18F]FDG) injection and the blood glucose concentrations were measured using a glucometer (Bayer Contour, Bayer, Leverkusen, Germany) before and after [18F]FDG PET/computed tomography (CT) imaging. For PET/CT imaging, the mice were anesthetized using isoflurane (3-4% induction and 1-2% maintenance) and the tail vein was cannulated. The mice were intravenously injected with 5.1 ± 0.1 MBq of [18F]FDG and scanned using a small-animal PET/CT (Inveon Multimodality, Siemens Medical Solutions, Knoxville, TN, USA) for 60 minutes starting from the time of the injection. The PET data acquired in a list mode was iteratively reconstructed with an ordered subset expectation maximization 3D algorithm, followed by maximum a posteriori reconstruction. Quantitative PET image analysis was performed using Carimas 2.9 software (Turku PET Centre). The regions of interest were defined in brain, heart, kidney, liver, lung, muscle and urinary bladder using CT as the anatomical reference. The uptake of [18F]FDG was reported as a standardized uptake value (SUV) which takes into account animal weight and injected radioactivity dose. Blood was collected via cardiac puncture under terminal isoflurane anesthesia and mice were sacrificed by cervical dislocation immediately after PET/CT. Various tissues were excised and weighted, and their total radioactivity was measured using a gamma counter (Triathler 3", Hidex Oy, Turku, Finland). The results were expressed as standard uptake value , which refers to the ratio of tissue radioactivity concentration at a point in time C(T) and the injected dose of radioactivity per kilogram of the patient's body weight.

4.6.5 Hepatic malonyl and glycogen quantification

For both malonyl and glycogen quantification measurements in HSD17B13KO males, approximately a 100 mg liver tissue was lysed using Tissue Lyser II (Qiagen), with 5 mm stainless steel beads at 50 Hz for two minutes. Lysates were centrifuged at 14,000 x g for five min at 4°C and the supernatants were then collected for analysis. For malonyl quantification, the tissue was homogenized in sterile phosphate buffered saline (PBS). For glycogen measurement, the liver tissue was homogenized in 25 mM citrate buffer (pH 4.2) containing sodium fluoride 2.5g/l. Hepatic Malonyl-CoA content was measured using an ELISA Kit for Malonyl-CoA (MyBioSource, San Diego, USA) according to the manufacturer's instructions. Victor x4 (Perkin Elmer) plate reader was used to measure optical density at 450 nm and malonyl concentrations were derived using a standard curve.

The glycogen concentration was measured by using quantitative colorimetric EnzyChromTM Glycogen Assay Kit (BioAssay Systems, Hayward, USA), according to the manufacturer's instructions. The optical density was read using Victor x4 (Perkin Elmer) plate reader at 570 nm and glycogen concentrations were obtained from a standard curve.

4.7 Reproductive phenotyping

Both male and female reproductive functions were analyzed. At first, the onset of puberty of at least five HSD17B13KO and WT animals starting at postnatal day 20 was analyzed by recording the age of balanopreputial separation in males and the vaginal opening of females. Subsequently, the estrus cycle and its regularity in 10 HSD17B13KO and 10 WT females were analyzed at the age of eight weeks. For this, vaginal smears were taken for a continuous period of 21 days. Dried smears were stained with Mayer's hematoxylin, and the cycle phase was defined based on the cell types present. Furthermore, mating behavior of four HSD17B13KO females and males at the age of three to four months and WT litter mates was analyzed by recording mating plugs, pregnancies, litter size and sex ratio. Additionally, the weight and macroscopic anatomy of the reproductive organs of nine-month-old male and female mice were analyzed. We also determined the serum concentrations of luteinizing hormone and follicle-stimulating hormone by using time-resolved immunofluorometric assays as previously described [306,307] and serum testosterone levels were measured in the male mice using an in house RIA.

4.8 Statistics

In the case of HSD17B13KO study, statistical analyses, except for the metabolomics, micro array data and in silico analyses, were carried out using GraphPad Prism 5

software (GraphPad Software, Inc., La Jolla, CA, USA). Unpaired t-test was used to determine statistical significance, which was set at P<0.05, and mean values ± standard deviation (SD) are presented. In the case of HSD17B12cKO studies, statistical analyses were carried out using GraphPad Prism 8.1.2 software (GraphPad Software, La Jolla, CA, USA), if not otherwise indicated. Outliers were identified using ROUT method in Prism with coefficient Q=1%. Shapiro-Wilk test was used to test for normal distribution. The statistical tests were chosen depending on the results of the Shapiro-Wilk tests of data normality. If not otherwise indicated, unpaired t test or nonparametric Mann-Whitney test was used to determine the statistical significance between two groups at single time point and two-way ANOVA for multiple time points. For adipocyte size and *Hsd17b12* mRNA expression, the statistical significance was analyzed by one-way ANOVA. The threshold for statistical significance was set at p<0.05. Results were expressed as mean ± SD, unless otherwise indicated.

5　Results

5.1　Validation of the mouse models

In this thesis project, four different genetically modified mouse models were used: HSD17B13KO, HSD17B12cKO, aHSD17B12cKO, LiB12cKO. As these mouse models have not been utilized in research previously, the proper gene disruption had to be validated.

In the constitutive KO mouse of HSD17B13, the gene disruption was confirmed in the liver tissue by qRT-PCR, and these results showed that the *Hsd17b13* gene expression was below the detection limit in the KO mice (**I**, Fig. 1D). Analyses of homozygous KO mice further indicated that *Hsd17b13* is not essential for embryonic development, as the pups were born with expected Mendelian ratio for all genotypes from the heterozygous breeding (data not shown).

In the inducible HSD17B12cKO mouse model, the exon 2 deletion was initiated at the age of eight weeks by 1.5 mg of Tam injections per day for five consecutive days. This led to a significant reduction in *Hsd17b12* mRNA levels in the various tissues measured six days after Tam injection, while the vehicle injection did not result in changes in the mRNA expression (**II**, Fig. 1A), confirming the Tam-dependency of the gene deletion. The most notable decrease in the mRNA level was observed in the liver with a drop of 94%, followed by the colon (85%), the WAT (77%) and BAT (76%). In addition, significant reduction was observed in the kidney (50%) and spleen (56%). In the different brain regions and adrenals, the mRNA levels were not affected significantly six days after completing the Tam treatment (**II**, Fig. 1A), despite the confirmed expression of Cre-recombinase (data not shown).

Similarly, the adipocyte-specific *Hsd17b12* KO mouse model (aHSD17B12cKO) was also induced by a five-day-long Tam treatment at the age of eight weeks, and the gene deletion was confirmed by qRT-PCR (**II**, Fig. 3A) in three different fat deposits: brown fat (BAT), gonadal fat and renal fat. Liver served as a CTRL tissue. The *Hsd17b12* expression was significantly lower in all three fat deposits compared with the CTRL groups, while there was no change in the expression in the liver.

To study the role of HSD17B12 specifically in the liver, we generated a hepatocyte-specific HSD17B12 knockout mouse model (LiB12cKO) in which Cre-

activity begins during embryogenesis. The *Hsd17b12* expression was very low in the LiB12cKO animals compared with the CTRL groups (**III**, Supplemental Fig. 1C). All genotypes were born in expected ratios, and they were viable (data not shown).

5.2   HSD17B13 in reproduction

Given the potential role of *Hsd17b13* in sex steroid metabolism, reproductive functions of HSD17B13KO mice were characterized at the age of three months. We did not observe differences in body and endocrine organ (pituitary, adrenal, testis, ovary) weights and morphology, puberty onsets in male and female, the length of the estrous cycle and fertility of female, as well as the litter sizes and the number of pregnancies (**I**, Supplemental Table 1 or data not shown) when we compared HSD17B13KO and WT mice up to the age of 3 months. Furthermore, there were no differences in the serum LH, FSH and testosterone concentrations in male and female HSD17B13KO mice compared with their WT littermate mice (**I**, Supplemental Table 1). Thus, we concluded that HSD17B13 is not significantly involved in the metabolism of sex steroids and the regulation of reproductive functions.

We did not study the HSD17B12cKO reproductive phenotype. However, we did not observe any anomalies while breeding the animals for the studies.

5.3   HSD17B12, HSD17B13 and well-being

The development of liver steatosis is often associated with increased body adiposity and impaired glucose tolerance. Total body and liver weights did not significantly differ between nine-month-old HSD17B13KO and WT male mice (**I**, Fig. 5A). Furthermore, body composition measurement indicated that HSD17B13KO and WT male mice displayed similar percentages of lean mass (64% +/- 4 in HSD17B13KO, 65% +/- 3 in WT, p=0.6022) and fat mass (31% +/- 5 in HSD17B13KO, 30% +/- 4 for WT, p=0.4077) (**I**, Fig. 5A). Moreover, glucose tolerance tests showed that deletion of *Hsd17b13* did not lead to a significant glucose intolerance in four- to five-month-old male mice (p=0.602) and in seven- to nine-month-old male mice (p= 0.261) (**I**, Fig. 5C). In line with this, analyses of the key factors involved in glycolysis, which are transcriptionally regulated, did not show significant differences between either three- or nine-month-old HSD17B13KO mice and the WT mice, except for pyruvate kinase (*Pkrl*), which was upregulated at the nine-month-old HSD17B13KO mice. (**I**, Fig. 5B). However, although mRNA expression of the key gluconeogenesis-regulating enzymes was similar in both age groups of WT and HSD17B13KO mice (**I**, Fig. 5D), protein expression of the glucose 6-phosphatase (G6Pase) was significantly reduced in nine-month-old HSD17B13KO mice compared with WT mice (**I**, Fig. 5E). However, hepatic glucose output, as

assessed by pyruvate tolerance test, was not affected by HSD17B13 deficiency in seven- to nine-month-old-male mice, and nor was the hepatic glycogen content (**I**, Supplemental Fig. 4).

Both the male and female HSD17B12cKO mice went through a dramatic loss of body weight during the first six days after the last Tam injection (**II**, Fig. 1B), and by day 6, the weight had decreased 17% in males (KO day zero, 30.3 g ± 1.45 g; KO day six, 25.1 ± 3.17 g) and 24% in females (KO day zero, 23.2 g ± 0.95 g; KO day six, 18.1 g ± 1.59 g). The Tam-treated CTRL mice lacking the Cre or expressing one WT allele did not show reduction in body weight during the study period. In the HSD17B12cKO, the weight loss was especially severe from day four to day six. The physical appearance and behavior of the HSD17B12cKO mice seemed normal for the first five days, while on day six the HSD17B12cKO mice showed signs of chronic pain with distress, which presented with piloerection, social isolation, partially closed eyelids, unresponsiveness, and snout grooming, and thus, the study period had to be limited to six days after the fifth Tam injection. EchoMRI analysis showed that the weight loss was associated with drastically lower body fat content in the HSD17B12cKO mice compared with the Tam-treated CTRL mice in both females and males (56% and 66% lower, respectively, **II**, Fig. 1C). The reduced fat mass was further confirmed by lower *ex vivo* weights of the different adipose tissue depots (**II**, Supplemental Fig. S2). In addition, the decreased amount of fat in the HSD17B12cKO mice displayed as smaller LDs in both the WAT and BAT in HSD17B12cKO mice compared with CTRL mice (**II**, Fig. 1D). The loss of fat tissue was accompanied by a significant loss of the lean mass (23% in females and 25% in males).

The LiB12cKO mice appeared normal and healthy. At the age of 2 months, their body weight did not differ from that of the CTRL mice (**II**, Fig. 1A). However, at the age of six to eight months, the body weight of the KO mice was significantly reduced compared to the CTRL mice (6-month-old males 11,9% p=0.002; 6-month-old females 12.8% p=0.004 and eight-month-old males 10.7% p=0.003; eight-month-old females 16.8% p=0.005), the difference being greater in the female mice. Also, the 6 months old male mice showed better glucose tolerance than the CTRL animals, but in females the glucose tolerance did not differ between the groups (**III**, Fig. 1D). We also tested their tolerance to insulin to see whether the change observed in males was due to insulin sensitivity, but there were no significant differences between the study groups in either sex (**III**, Fig. 1E).

Adipocyte-specific HSD17B12cKO mice appeared healthy throughout the follow up time of three months after the induction of gene disruption. Their body weights and body composition did not differ between the genotypes (**II**, Fig. 3B-C). In addition, the LDs within the adipocyte-specific HSD17B12cKO adipocytes did not appear smaller than in the CTRL mice (**II**, Fig. 3E). These results indicated that

the loss of HSD17B12 activity in the adipocytes in adult mice does not lead to the severe metabolic alteration and starvation that was observed in the HSD17B12cKO mice.

5.4 The effects of HSD17B13 and HSD17B12 deletion on liver morphology

5.4.1 Macroscopic morphology

In the HSD17B13KO animals the color of the liver was often pale or yellowish, but the HSD17B13KO mice liver size did not differ from that of the WT mice (**I**, Fig. 5A). In the Tam-induced HSD17B12cKO the liver size was smaller in the cKO animals compared to the WT littermates. In the LiB12cKO animals the livers were significantly larger in size compared to WT livers, and often appeared pale in color. The adipocyte specific HSD17B12cKO did not show any difference in the liver morphology.

Both male and female LiB12cKO mice showed significantly larger livers than the CTRL animals in all age groups studied (**III**, Fig. 1F). This difference was very notable already in two-month-old animals (males, FC=2.11 p=<0.001; females, FC=1.57 p=0.001). In six-month-old mice, the difference was even greater (males, FC=2.31 p=<0.001; females, FC=1.65 p=0.002), and at the age of eight months, the difference was still significant (males, FC=1.51 p=0.001; females, FC=1.64 p=<0.001). In addition, the color of KO livers was pale, which often indicates fatty liver (**III**, Fig. 1G).

5.4.2 Microscopic morphology

5.4.2.1 Liver steatosis

The development of hepatic steatosis was the most noticeable phenotype in HSD17B13KO. At the age of 3 months, microvesicular steatosis was observed in approximately 20% of HSD17B13KO males, while none of the WT males showed steatosis at this age (**I**, Fig. 2A). By the age of nine months, the LD size had increased dramatically, and both micro- and macrovesicular steatosis was observed in more than 80% of the livers of male HSD17B13KO mice (10 out of 12), while only mild microvesicular steatosis was observed in the livers of 3 out of 9 WT mice (**I**, Fig. 2A). In nine-month-old HSD17B13KO males, steatosis was characterized by a portocentral gradient with increasing number of large LDs (macrovesicular steatosis) from the central vein towards the portal region. Oil red O staining further confirmed

hepatic lipid accumulation at the age of nine months, demonstrated by an increased LD size in the HSD17B13KO liver compared with that observed in WT liver (**I**, Fig. 2A). Transmission electron microscopy confirmed the presence of various size LDs in the HSD17B13KO mice at nine months of age (Fig. 8). No changes in the mitochondria or other organelles were observed in the KO animals.
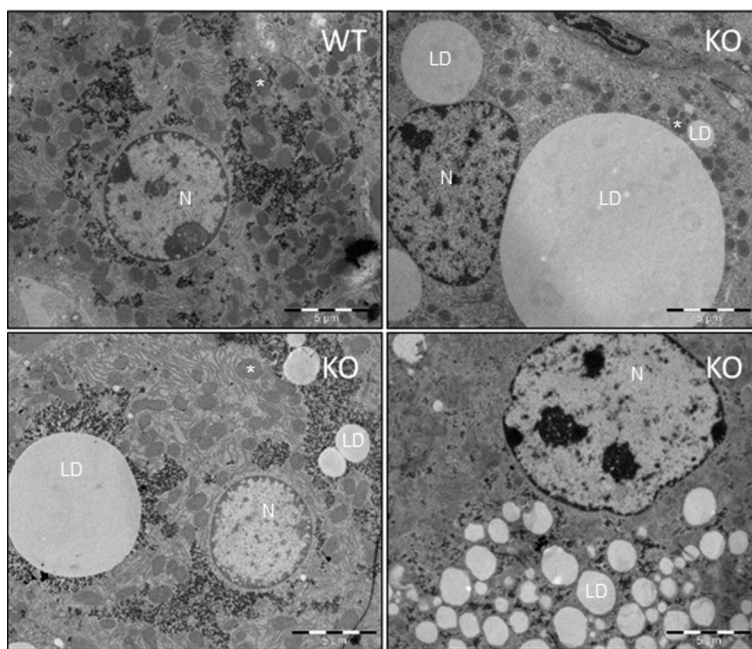
Figure 8. Transmission electron microscopy images of nine-month-old male livers. Various sizes of LDs were present in hepatocytes of the HSD17B13KO animals. LD=lipid droplet, N=nucleus, *=mitochondrion. Scale bar 5 µm.

A significant fat accumulation was observed in the livers of female HSD17B12cKO mice six days after the Tam injection (**II**, Fig. 5A,C). Fat accumulation was present in some HSD17B12cKO male mice as well, but the difference in the hepatic TAG level between the CTRL and HSD17B12cKO males was not statistically significant. In females, in addition to microvesicular steatosis, a trend of increasing percentage of apoptotic cells was present in the HSD17B12cKO livers, indicating lipotoxic hepatocellular injury (**II**, Fig. 5D).

The Lib12cKO mice showed accumulation of LDs in the KO livers (**III**, Fig. 2A). Micro- and macrovesicular steatosis was quantified using deep learning model image analysis, and the results showed increased macrovesicular steatosis in two-month-old males (macro, FC=2.46 p=<0.0239), but not in older age groups (**III**, Fig. 2B). Microvesicular steatosis was significantly higher in two- and six-month-old

males (FC=7.60 p=0.0015; FC=18.74 p=<0,0012, respectively). In females, the differences between the LiB12cKO and the CTRL mice were not statistically significant, except in eight-month-old group, which showed increased microvesicular steatosis (FC=4.25 p=0,0007). Together these data show that despite of the increased steatosis in the LiB12cKO mice, the LDs are smaller and more numerous in the LiB12cKO mice compared with the CTRL mice.

5.4.2.2   Other signs of liver damage

In addition to steatosis, histopathological analysis of liver sections from WT and HSD17B13KO mice indicated an increased occurrence of inflammatory cells in the liver of HSD17B13KO males. At the age of three months, microgranulomas (Kupffer cell aggregations) were present in approximately 60% (in seven out of 12) of the liver specimens from HSD17B13KO mice, while only 25% of their WT littermates (two out of eight) presented with microgranuloma aggregation (**I**, Fig. 6A). Furthermore, portal inflammation and ductular proliferation in the portal tracts were present in the HSD17B13KO males (**I**, Fig. 6A). This indicated, that in addition to steatosis, HSD17B13KO males showed signs of increased inflammation, which is in parallel with the known features of NASH**.** While lipid accumulation was the most pronounced finding in the nine-month-old males, some of them also showed signs of hepatic inflammation (**I**, Fig. 6A).

The LiB12cKO mice showed increased apoptosis in the liver. The quantification of TUNEL stained apoptotic cells by image analysis showed a significantly higher percentage of apoptotic cells in LiB12cKO males than in the CTRL males (FC 2.70, p=0.04) (**III**, Fig. 4A). In females, the difference was not significant. We then quantified the proliferative cells by Ki-67 staining and image analysis. The results showed significantly higher percentage of proliferative cells in the KO livers compared with the CTRL livers (males, FC=2.64 p=<0.001; females, FC=1.86 p=0.008) (**III**, Fig. 4C).

5.5   HSD17B12 and HSD17B13 and metabolic phenotype

5.5.1   Food intake and hypothalamic regulation

As described earlier, the inducible HSD17B12cKO lost up to 20% of their body weight within six days after the last Tam dose and this weight loss was accompanied by a drastic loss of body fat content and lean mass in both females and males. This led us to observe the food and water intake in these mice. These results showed that the HSD17B12cKO mice considerably reduced both water and food consumption

during the days three to five after Tam induction (**II**, Fig. 2A), as well as the caloric intake was markedly reduced during the days two to five after induction (**II**, Fig. 2B). The CTRL males consumed 3.7-4.0 g of chow per day while the HSD17B12cKO males consumed only 0.4-1.4 g per day, leading to significantly reduced food intake over the study period (p< 0.004). In line with this, KO mice showed lower serum glucose levels compared to CTRL mice(**II**, Table 2). The lipid contents in the feces of KO mice did not differ from that of the CTRL mice, suggesting that the reduced body weight was not due to impaired fat absorption in the KO mice (**II**, Fig. 2C). These results urged us to assess the expression levels of the genes mediating the satiety and hunger signals in the hypothalamus. Gene expression for major hunger-inducing signaling factors, such as neuropeptide Y and agouti-related peptide were upregulated, while for those regulating satiety, proopiomelanocortin was downregulated and corticotropin releasing hormone, was upregulated in the HSD17B12cKO mice compared with the CTRL mice (**II**, Fig. 2D).

5.5.2   Energy consumption

To clarify the cause of the rapid reduction of adipose tissue in HSD17B12cKO mice, we assessed the overall energy consumption in males. The results showed that energy consumption of the HSD17B12cKO did not differ from that of the CTRL mice when normalized to the lean mass (**II**, Supplemental Fig. S3A). Therefore, the results indicate that the weight loss was not caused by a change in the metabolic rate of the HSD17B12cKO mice. Furthermore, there was no difference in the locomotor activity (**II**, Supplemental Fig. S3B) or in the number of rearing events (**II**, Supplemental Fig. S3C) between the HSD17B12cKO and the CTRL mice. However, HSD17B12cKO males show a reduced respiratory exchange ratio during day four, indicating that the mice move from using carbohydrates as the fuel source towards burning more fat (**II**, Supplemental Fig. S3D). Both *in vivo* and *ex vivo* results from [$_{18}$F]FDG PET imaging, (**II**, Supplemental Fig. S4) showed no change, or a slight increase, in the uptake of glucose in the brain of HSD17B12cKO mice compared with the CTRL mice. These results suggest that the weight loss in the HSD17B12cKO mice is related to reduced food intake rather than changes in energy consumption.

5.5.3   Serum markers of metabolic dysfunction

No differences in serum concentrations of HDL, LDL, and cholesterol were observed between WT and HSD17B13KO mice in both three- and nine-month-old mice. Serum TAG levels seemed lower in HSD17B13KO mice, even though this decrease

was not statistically significant (**I**, Supplemental Table 2). Decreased serum TAG levels are in line with the abnormal storage of lipids in the hepatocytes.

The presence of liver injury in Tam-inducible HSD17B12cKO mice was supported by an 8-fold (p< 0.005) and a 5-fold increase in serum ALT levels in HSD17B12cKO females and males, respectively, compared with CTRL mice (**II**, Fig. 5B). Similarly, LiB12cKO mice showed increased ALT and ALP levels in both male and female mice (**III**, Table 2).

As the HSD17B12cKO mice presented with signs of general indisposition on day six post Tam-induction, we measured serum cytokine levels to evaluate their general inflammatory status. The results showed a marked increase in IL-6, IL-17 and G-CSF levels in both male and female KO mice compared to the CTRL mice (**II**, Table 3.). Furthermore, the data revealed a slight reduction in the levels of interferon gamma-induced protein 10 (IP-10), IL-1a and IL-5 in males, and of macrophage inflammatory protein 1 alpha (, interferon gamma (IFN-g) and KC in females. These results confirmed that the HSD17B12cKO mice suffered from systemic inflammation. In addition, the inducible HSD17B12cKO mice showed increased levels of serum albumin and total proteins compared with the CTRL group, measured on *day 6* post induction. This could indicate severe dehydration and is in line with the reduced water intake in HSD17BcKO mice (**II**, Table 2).

5.6 HSD17B12 and HSD17B13 effects on molecular pathways in the liver

5.6.1 Transcriptomics

The global hepatic transcriptome of 3-month-old HSD17B13KO and WT mice was analyzed by RNAseq to investigate which mechanisms were involved in development of fatty liver in the HSD17B13KO mice. Our goal was to characterize the potential changes in the gene expression at the onset of early signs of steatosis. The two genotypes clearly clustered separately by the hierarchal clustering analysis of the RNAseq data (**I**, Supplemental Fig. 1), with a total of 74 differentially expressed genes (50 up and 24 down). Gene ontology analysis revealed significantly altered expressions in several key regulators of the lipid metabolism in the HSD17B13KO liver (**I**, Supplemental Table 3). This prompted us to further evaluate the changes in key effectors in lipid metabolism in the liver tissues of three- and nine-month-old WT and HSD17B13KO mice.

We used qRT-PCR and WB to analyze the changes in both RNA and protein levels for the major players in the hepatic energy metabolism. Of the two important FA transporters, i.e. *Cd36* and *Fatp2*, only *Cd36* mRNA showed a minor increase in the in nine-month-old KO mice (**I**, Fig. 3A), and this result was not reflected in a

similar change at the protein level (**I**, Fig. 3B), suggesting that FA uptake is not responsible for steatosis development in HSD17B13KO mice, even though the mRNA levels of the rate-limiting genes of DNL, i.e. *Fasn*, *Acc* and *Scd1*, did not show significant changes in the RNAseq analysis (FC=-1.271; FC=1.006; FC=-1.382, respectively), or by qRT-PCR, (**I**, Fig. 3C). Protein expressions of FAS, SCD1 and ACC were significantly higher in the nine-month-old HSD17B13KO mice, while only ACC was upregulated at the age of three months. The results also indicated that the relative amount of the phosphorylated ACC over the total amount of ACC protein did not differ between the HSD17B13KO mice and their WT littermates (**I**, Fig. 3D). These results show that HSD17B13 deficiency leads to post-transcriptional upregulation of key enzymes promoting DNL leading to increase in FA production. In line with the upregulated lipogenesis and TAG content in the of HSD17B13KO liver, the expression of *Gpat3*, a gene coding for an enzyme catalyzing the first step of FA esterification in TAG synthesis, showed a marked upregulation in the RNAseq analysis (5.7-fold upregulation in the KO as compared with WT, p<0.001). This result was confirmed by qRT-PCR at the age of three months (8-fold upregulation, p<0.01) and at nine months (3-fold upregulation, p<0.001) (**I**, Fig. 3E). Other major genes involved in FA esterification, e.g., *Dgat1* and *Dgat2*, were not significantly changed in HSD17B13KO liver (**I**, Fig. 3E) suggesting a specific upregulation of *Gpat3* expression in the absence of HSD17B13.

As HSD17B13 has been previously reported to associate with LDs, we investigated whether there was compensatory expression of proteins involved in LD formation in the HSD17B13KO mice. The clustering analysis of the mRNA expression for the various LD proteins described earlier by Su et al. 2014 (Su 2014), did not result in separate clusters for the two genotypes (**I**, Supplemental Fig. 2). Furthermore, the classical LD proteins, such as perilipins (*Plin1*, *Plin2*, *Plin3*), were not altered in the RNAseq or qRT-PCR analyses (**I**, Fig. 3F). The only significant change was the increased protein expression of PLIN2 in the liver of nine-month-old HSD17B13KO mice (**I**, Fig. 3G), although some variability was present between individual mice. However, it is unclear whether the upregulation of PLIN2 is indirectly induced by the increased LD biogenesis or is the result of HSD17B13 deficiency.

Furthermore, RNAseq results revealed that 14 genes involved in the immune response were altered between the WT and HSD17B13KO livers, with a p-value of 4.4×10^{-7} for the GO term "immune response". The changes between these genes were also demonstrated by hierarchical clustering (**I**, Fig. 6B). These data confirm that in addition to steatosis, HSD17B13 deficiency promotes inflammation of hepatic tissue.

In the LiB12cKO liver transcriptomics, the functional enrichment analysis using differentially expressed genes and DisGeNet database shows which human diseases

show similar gene expression changes compared to LiB12cKO (**III**, 3A). Among the most similar were fatty liver disease, hyperlipidemia, NASH, and dyslipidemias. Furthermore, functional enrichment analysis with default functional categories from GO Biological Processes (GO), KEGG (K) and Reactome (R), revealed that the most affected pathways the LiB12cKO liver included monocarboxylic acid metabolic process, toxicity related pathways, such as response to toxic substance and drug catabolic process. In addition, damage response related pathways were affected, such as response to wounding, response to extracellular stimulus and mitotic cell cycle. The most upregulated gene in the LiB12cKO liver transcriptomics was Lymphocyte Antigen 6D *(Ly6d)*, involved in lymphocyte differentiation (**III**, Supplemental table1). However, even more interesting was the second highest gene *Cyp4a14*, a member of *Cyp4a*-group, which was increased almost 40-fold. Other upregulated genes in the same Cyp4a-group, which code for enzymes involved in the AA metabolism, were *Cyp4a31*, *Cyp4a10* and *Cyp4a12b* (**III**, 3C). The most decreased expression was found in the major urinary proteins 7 (*Mup7*) with 72.7-fold decrease (**III**, Supplemental table1). Many other Mup genes were among the most decreased expression genes. The second most decreased expression showed the *Hsd3b5* gene, which was more than 65.8-fold reduced. In addition, several *Cyp2c* genes were downregulated, including *Cyp2c37* (FC -14,2), *Cyp2c54* (FC -7,6), *Cyp2c50* (FC -6,0), *Cyp2c69* (FC -5,4), *Cyp2c40* (FC -5,1), *Cyp2c29* (FC -3,8) *Cyp2c23* (FC -2,4), *Cyp2c67* (FC -2,4), *Cyp2c68* (FC -2,1). The *Cyp2C*-genes encode enzymes that are involved in the AA metabolism. Together these data indicate that hepatic HSD17B12 deficiency leads to alterations in AA metabolism.

Comparing the differentially expressed genes between the HSD17B13KO and LiB12cKO models revealed that these models shared only 11 genes that were deregulated in both (Fig. 9A). Furthermore, five of these genes were upregulated and two downregulated in both models (Fig. 9B). The upregulated genes included *Cyp4a10*, keratin 23 (*Krt23*), phosphatidylcholine transfer protein (*Pctp*), sulfatase 2 (*Sulf2*) and acyl-Coenzyme A dehydrogenase family, member 12 (*Acad12*) and downregulated genes were UDP glucuronosyltransferase 2 family, polypeptide B38 (*Ugt2b38*) and family with sequence similarity 47, member E (*Fam47e*). There were also two genes upregulated in HSD17B13KO livers and downregulated in LiB12cKO. These were phospholysine phosphohistidine inorganic pyrophosphate phosphatase (*Lhpp*) and ornithine aminotransferase (*Oat*). In addition, two genes were upregulated in LiB12cKO livers and downregulated in HSD17B13KO livers. These were methylenetetrahydrofolate dehydrogenase (NAD+ dependent), methenyltetrahydrofolate cyclohydrolase (*Mthfd2*) and RIKEN cDNA 4933431E20 gene (*4933431E20Rik*). This indicates that mostly the disruption of *Hsd17b12* and *Hsd17b13* affect different genes.
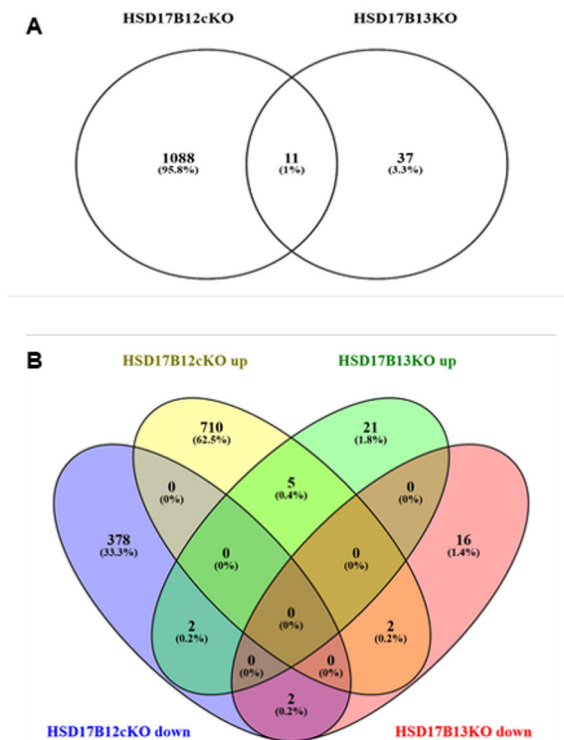
Figure 9. Comparison of differentially expressed genes in LiB12cKO male livers and HSD17B13KO male livers. (A) A Venn diagram showing the overlap in all differentially expressed genes in the two mouse models. Each circle represents differentially expressed genes between the KO and CTRL livers in one model. These models share only 11 genes with altered expressions. (B) A Venn diagram where up and down regulated genes have been separated in both models. These models share five upregulated and two downregulated genes.

5.6.2   Lipidomics

We performed serum lipidomic analysis to obtain a more detailed understanding of the consequences of the *Hsd17b12* disruption on circulating lipids in HSD17B12cKO mice. As expected, the majority of the 872 metabolites of 13 different lipid classes measured were at markedly lower levels in the HSD17B12cKO mice, while some lipid species accumulating in the KO mice were identified as well. The genotypes completely segregated into separate clusters according to the phenotype, shown by the heat map (**II**, Fig. 4A). TAG was the most severely decreased lipid class, but also CER, LPE, LPC, PC, SM and LCER were significantly lower in HSD17B12cKO serum than in the CTRL mice (**II**, Fig. 4B). Interestingly, the HSD17B12cKO showed a 1.39-fold higher concentration of DCER $(\log2(1.39) = 0.48)$ **II**, Fig. 4B) compared to CTRL group, being the only lipid class

found to accumulate during the weight loss. Even though the total amount of CER was markedly reduced, the DCER/CER ratio was increased by 2.6-fold (CTRL, DCER/CER = 0.16; KO, DCER/CER =0.42), with highest increase in the concentration of DCER (FA16:0). All classes of ceramides (CER, DCER, LCER and HCER), also presented with an increased relative amount of FAs with chain length of 14 and 16 carbon atoms (FA 14:0 and FA16:0), and a reduced amount of FAs with longer chain lengths (FA 18:0 and FA20:0, FA22:0 and 22:1, FA24:0 and 24:1, **II**, Fig. 4C). This suggests a defect in the FA elongation in the HSD17B12cKO. However, to our surprise, we did not observe any specific changes in the AA levels as a free FA, or as a component of the various lipid classes.

In the lipidomics analysis in two-month-old LiB12cKO male livers, the CTRL and KO mice separated in different clusters based on the composition of lipid species (**III**, Supplemental Fig. 3). Interestingly, only SM class of lipids showed increased concentrations (FC=-1.45, p=<0.001) in the KO livers (**III**, Fig. 2C). The proposed role for HSD17B12 is in the elongation of long chain FAs, especially AA (. However, the liver lipidomic results did not show a decrease in the carbon side chains of 18 to 20 carbons (**III**, Fig. 3D-E). Instead, we observed a moderate increase or no change in the concentration of the FA20:4 containing lipid species. Interestingly, there was a decrease in the saturated FAs with carbon side chains of 18 and 20 that were incorporated in the phospholipids LPC, LPE, PC, PE, and SM. These results do not suggest that HSD17B12 would be involved in the elongation of AA or other FAs with similar chain length.

5.6.3   Metabolomics

In the HSD17B13KO mice the concentration of C16 and C18:1 acylcarnitines were upregulated by 2-fold (p=0.01) compared to the WT mice (**I**, Fig. 4A), suggesting a defect in transferring LCFAs into mitochondria for beta-oxidation. Mitochondrial beta-oxidation of FAs is an important pathway for lipid catabolism and one possible cause for the development of fatty liver is impaired fat oxidation. We measured the concentration of Malonyl CoA, one of the most potent inhibitors of acyl carnitine uptake by mitochondria, but no difference was observed between the HSD17B13KO and WT liver (**I**, Supplemental Fig. 3C). While the ACC enzyme, responsible for malonyl CoA formation was increased, no change was detected in the relative amount of the phosphorylated form, regulated by the AMPK. Parallel to this, no change in the AMPK expression on mRNA or protein level, or in its phosphorylation status, was found in the HSD17B13KO compared with WT mice (**I**, Supplemental Fig. 3A, B). PPARa is an important transcriptional activator of beta-oxidation, however, its expression was not affected in the absence of HSD17B13 (**I**, Fig. 4B, C). Despite this, RNAseq and qRT-PCR analyses indicated that mRNA expression

of proteins related to mitochondrial beta-oxidation, such as *Cpt1a*, *Acad10* and *Acox1* were either significantly increased, or displayed a trend towards an increase in the liver tissues of HSD17B13KO mice (**I**, Fig. 4B), which was in line with the increased levels of the acylcarnitines. However, the increased *Cpt1a* expression in the KO mice was not reflected on the protein level (**I**, Fig. 4C). Finally, mRNA expression of key regulators of FA export from the liver, e.g., *Apob* and *Mttp*, was unaltered, which suggests that this process was not impaired in the absence of HSD17B13 (**I**, Fig. 4D). Phospholipids, such as PCs, lysophosphatidylcholines and SMs showed a trend of increased levels in the HSD17B13KO liver compared to WT, while the levels of amino acids showed a tendency for decreased levels in the KO mouse liver (**I**, Fig. 4A, Supplemental Table 4).

6　　Discussion

The current understanding of the *in vivo* roles of HSD17B12 and HSD17B13 is still limited. Even though they both belong to the same group of enzymes, they do not share significant sequence similarity and their function, substrate specificity, intracellular location and tissue distribution are likely to be different. They both have been suggested a role in the liver lipid metabolism, however, their *in vivo* function is still unclear. HSD17B13 is located on the LD surface and could be involved for example in LD fusion or function as a scaffold protein [308,309]. HSD17B12 is located on ER and is thought to be involved in the elongation of very-long-chain FAs, especially in the synthesis of AA [6].

In this work, we have used KO animal models to study the role of HSD17B12 and HSD17B13 in lipid metabolism. HSD17B13KO model was developed by replacing exons 2 and 3 with lacZ-expressing cassette by homologous recombination. In HSD17B12 KO models we utilized the Cre-Lox system, and crossbred the floxed HSD17B12 mouse strain with Rosa26-CreERT, Adipoq-CreERT2 and Albumin-Cre mouse strains to create mouse models with an inducible gene disruption in a wide array of tissues, an inducible disruption in adipose tissue and a non-inducible disruption in hepatocytes, respectively. Based on the results obtained from these KO mouse models, the common effect that the disruption of either of these two genes, globally or in the liver, causes is a fatty liver. As the development of NAFLD is affected by the interactions of genes and environmental factors, there are several ways that NAFLD can develop and it can be associated by various other pathologies ranging from IR, infections, toxicity and autoimmune conditions. The common factors in the HSD17B13KO and HSD17B12cKO liver phenotype were increased TAG and CE accumulation, a typical change seen also in NAFLD and NASH patients [310]. In addition, phospholipids were slightly increased and there were changes in SM concentrations in all of the models. Signs of inflammation was also observed in both gene KOs (HSD17B13KO, inducible HSD17B12cKO and LiB12cKO). None of the mouse models showed increased body weight or impaired glucose tolerance, which are strongly associated with the epidemics of NAFLD especially in the developed countries. Quite the contrary, the inducible HSD17B12cKO and LiB12cKO both lost body weight and the latter also

showed improved glucose tolerance (males). The KO of *Hsd17b13* did not seem to affect body weight.

The TAG accumulation in the liver of the HSD17B13KO mice is associated with the marked up-regulation of the FA esterification related gene *Gpat3*. Deficiency of GPAT3 enzyme has been shown to prevent diet-induced fat accumulation in white adipose tissues and to reduce fat absorption from the intestines [311,312], but its effects in the liver are less clear. GPAT3 knockdown in mice was also associated with an improved glucose tolerance that was likely promoted by an increased energy expenditure [313]. GPAT3 is closely related to GPAT4, which is located on the LD membrane [314,315], and regulates LD size. GPAT3 is known to be associated with ER and its upregulation has been shown to increase TAG accumulation (but not phospholipid accumulation) in mammalian cells [316], and furthermore, a recent study linked increased *Gpat3* expression to increased LD size in Kupffer cells [317]. Taken together, the up-regulation of *Gpat3* in HSD17B13KO mice could represent a potential mechanism contributing to the accumulation of LDs. Other mechanism that promotes lipid accumulation within the hepatocytes in HSD17B13KO mice was the overexpression of genes in the DNL pathway, such as *Fas, Acc,* and *Scd1* [318]. The mechanisms behind the specific up-regulation of GPAT3 and the FAS, ACC, SCD1 in the absence of HSD17B13 are unknown.

In the LiB12cKO model, there were several upregulated genes that are related to lipid metabolism, including the DNL related *Scd1*, *Fasn* and *Acc* (not shown), as well as the rate limiting step of TAG esterification gene *Gpat3*. At the same time other TAG esterification genes *Dgat1* and *Dgat2* were downregulated in the KO males. The more striking result in the liver transcriptomics analysis was the changes in the expression of many genes that are involved in the synthesis of prostaglandins and eicosanoids. The most notable change was the increase in the expression of several *Cyp4a* genes, which code for enzymes that are known to catalyze the ω-hydroxylation of AA to 20-hydroxyeicosatetraenoic acid (20-HETE) [319,320]. *Cyp4a14* showed the most increased expression. Another group of enzymes using AA as a substrate are the CYP2C enzymes [321], and many of them were downregulated in the LiB12cKO livers. These results suggest that there has been a shift from converting AA to EET towards converting AA to 20-HETE. 20-HETE has been associated with vasoconstriction [322], while EET has been implicated in vasodilation and protection against inflammation [323,324]. However, we did not observe any clear change in the AA concentrations in the liver that could explain the changes in the gene expression. However, these changes could at least partly explain the liver phenotype in these mice, because a recent study found a link between reduced serum EET concentration and NAFLD in human, in addition, a connection between decreased CYP epoxygenase activity and progression of NASH was found [325]. 20-HETE may also

have mitogenic properties, which could explain the increased hepatocyte proliferation [326].

The comparison of hepatic gene expression between HSD17B13KO and the Lib12cKO mice showed that these two liver phenotypes share only 11 genes with altered expression in both models, and of these genes, only seven were changed in the same direction (up- or downregulated). This indicates that despite many similarities in the phenotype, the molecular mechanisms behind the pathogenesis are not the same in these models. The upregulated genes *Ptcp* and *Acad12* are involved in the mitochondrial FA beta-oxidation [327–329]. *Ptcp* has been associated with hepatic steatosis in mice [330]. Shared upregulated genes also included *Cyp4a10*, which is involved in AA metabolism, but also in FA omega-oxidation on the ER [319,320,331,332]. This suggests that FA oxidation is affected in both HSD17B13KO and LiB12cKO mouse models.

Both HSD17B13 and HSD17B12 seem to play a role in the formation or regulation of LD size. HSD17B13 deficiency led to increased number and increased size of LDs in nine-month-old animals. In addition, the macrovesicular steatosis was concentrated around the portal region in the HSD17B13KO males, while the disruption of *Hsd17b12* did not cause any spatial gradient regarding LD size. *Hsd17b12* disruption in the hepatocytes caused increased LD formation, but this was mainly microvesicular steatosis, while there was a trend of declining macrovesicular steatosis in older animals. In inducible HSD17B12cKO, the steatosis was mainly microvesicular.

Hepatic zone 1, located around the portal vein is the area where the functions that require oxygen take place, such as beta oxidation of FAs. Interestingly, there was a gradient of increasing LD size from central vein towards portal area. This could indicate a fault in the FA oxidation in the absence of *Hsd17b13*, which is also supported by the increased levels of C16 and C18 acylcarnitines in the KO animals. Acylcarnitines are key players in the transport of FAs across the mitochondrial membrane for beta oxidation [333]. Similarly, the increase in the gene expression of some genes involved in the lipid oxidation (*Cpt1a* and *Acad10*) supports the idea that HSD17B13 deficiency leads to decreased FA oxidation. Impaired FA oxidation could explain the TAG accumulation, at least in part, as decreased FA oxidation is present in patients with NAFLD [334]. HSD17B13 is a LD-associated protein and localizes on the LD surface. Its function is unknown, but the LDs associate and interact with mitochondria (and peroxisomes) in energy producing tissues, including brown adipose tissue, heart, and skeletal muscle [48,335,336]. Perhaps counterintuitively, the interaction between LD and mitochondria decreases beta-oxidation and improves ATP-production, which, in turn, supports lipid synthesis [337]. Reduced interaction between LDs and mitochondria may protect against HFD-induced IR and liver steatosis [338]. It is also known that some proteins (PLIN5) on the LD surface facilitate

the docking of LDs to the mitochondria [339,340]. In addition to mitochondria, LDs are associated also with the ER, endosomes, and peroxisomes [341]. As a LD-associated protein *Hsd17b13* could play a role in the association of LDs with mitochondria or some other organelles, including other LDs.

LiB12cKO mice showed an increase in microvesicular steatosis, while there was a trend of decreasing macrovesicular steatosis with age. HSD17B12 is located on the ER surface, where both FA elongation and LD biogenesis take place. LDs arise from the ER as a result of increased TAG and CE synthesis. These neutral lipids are deposited between the ER membranes and the forming lens grows to form an LD, which finally emerges in the cytosol. There are many proteins that regulate LD formation and later contact with other cellular membrane bound organelles. Cell death-inducing DFF45-like effector C (*CIDEC)* was significantly increased in the LiB12cKO livers. CIDEC has been shown to localize on both the ER and the LDs in adipocytes and it is known to promote TAG storage and LD formation [86,342,343]. *CIDEC* expression has been shown to increase in both NAFLD and alcoholic steatohepatitis, but not in a healthy liver [344–346]. CIDEC expression increases also in obesity and fasting [347]. More interestingly, in brown and white adipocytes CIDEC isoforms determine the development of either one large LD (white fat) or several small LDs (brown fat) [348]. Increased expression of CIDEC could be responsible for increased microvesicular steatosis in the LiB12cKO mice.

Flotillin 1 (FLOT1) is a LD associated protein [349,350]. FLOT1 has been shown to facilitate the interactions between LDs and ER, and its expression and recruitment to LDs increases in the fed state and decreases in the fasted state [351]. *Flotillin 1* gene expression was significantly increased in the LiB12cKO livers, which supports the idea, that HSD17B12 is involved in the formation of LDs. On the other interactions with LDs with other membrane containing organelles, synaptosomal-associated protein of 23 kDa (SNAP23) facilitates LD and mitochondrion interaction [351,352]. SNAP23 expression increases in the fasted state when there is an increased need for energy by oxidation [351]. *Snap23* gene expression is not significantly changed in the LiB12cKO livers, which could indicate that the beta-oxidation is unaffected in the LiB12cKO livers. SNAP23 is part of SNARE protein complex, other proteins in the complex are N-ethylmaleimide-sensitive-factor (NSF), N-ethylmaleimide sensitive fusion protein attachment protein alpha (NAPA), syntaxin-5 (STX5) and vesicle-associated membrane protein 4 (VAMP4) [353]. However, none of these were affected in the LiB12cKO livers. SNARE complex is involved in the LD fusion [353]. These results suggest that the increase in the small LDs observed in the older LiB12cKO livers is not due to impaired LD fusion. HSD17B12 as an ER localized protein may be affecting the LD growth on ER or the budding of new LDs from the ER.

In HSD17B13KO mice the liver phenotype was more evident in male mice. In females there was no difference between KO and the WT groups. In humans, men

are known to be more susceptible than (premenopausal) women to liver steatosis and related liver injury while in postmenopausal women the prevalence is similar or higher than in men [354–357]. The protection against NAFLD in pre-menopausal women is thought to be mediated by estrogen [354,355]. Several mouse models of NAFLD also support the higher susceptibility of males in developing fatty liver [175,358]. Estrogen is thought to mediate the protective effects against liver diseases in women as premenopausal women are less susceptible to liver diseases and as postmenopausal women receiving hormonal replacement therapy show protection against liver fibrosis [359,360]. Whether the protective effects in female HSD17B13KO were mediated through estradiol is unclear.

Females are known to be more sensitive to toxicity and acute liver failure [361,362], likely due to underlying sex differences in toxic compound- and energy metabolism, as well as disruption of GH and estrogen receptor signaling [363]. This could explain the slightly more severe liver phenotype in the female inducible HSD17B12cKO mice, if the drastic body weight loss and liver phenotype of the inducible HSD17B12cKO mice was caused by toxicity. In the LiB12cKO phenotype, the picture was more complicated regarding sex differences. Reduction in body fat percentage was more noticeable in females, even though liver steatosis was observed to a similar degree in both sexes. Furthermore, LiB12cKO male mice showed more pronounced liver damage. This could at least partly be explained by different sensitivity to toxicity between sexes [363] and estrogen signaling [175,358].

HSD17B13KO animals did not gain weight and their body composition did not differ from the WT animals. Also, their glucose tolerance was not changed compared to the WT mice. Inducible HSD17B12cKO mice lost weight drastically after gene disruption within six days, and on day six their health and well-being deteriorate rapidly, and they have to be euthanized for ethical reasons. With the weight-loss, they lose a lot of their adipose tissue. Interestingly, the adipocyte-specific HSD17B12cKO mice did not present with any visible phenotype, as they did not lose or gain adipose tissue weight, and the adipocyte size did not differ between the KO and the CTRL animals. LiB12cKO mice also had a bit lower body weight at older age, but not at the age of eight weeks. The male mice also showed improved glucose tolerance. This is not typical for the most common type of NAFLD, which is associated with increased body adiposity and impaired glucose tolerance. However, globally up to 20% of the patients with NAFLD are non-obese or lean [364]. A recent meta-analysis found, that similarly to obese NAFLD, also lean NAFLD is more prevalent in men than in women and in higher middle-aged subjects compared to other age groups [365]. Earlier studies have linked lean or non-obese NAFLD with increased fructose and dietary fat consumption [366]. Hepatic steatosis can be caused by impaired VLDL secretion, as in the case of liver-specific Mttp knockout mice [367]. In these mice the glucose tolerance and peripheral fat storages remain unaffected.

However, the liver specific MttpKO mice do not show signs of hepatic inflammation [368].

HSD17B13KO male mice showed increased levels of hepatic TAGs as well as phospholipids and lysophosphatidylcholines. In addition, SMs were also slightly increased. The results suggest that HSD17B13 causes changes in several pathways, which may play a role in developing liver steatosis. These pathways include increased lipogenesis and FA esterification as well as a deficiency in transporting FAs into mitochondria for beta-oxidation.

In the inducible HSD17B12cKO animals, all lipid classes were decreased in serum, except DCER. There was an accumulation of sphingolipid species, especially CER and DCER with carbon chain length of 16 atoms and a decrease in the carbon chain length of 18 or more atoms. This could suggest that HSD17B12 plays a role in sphingolipid metabolism. However, this could be a secondary effect as sphingolipids are important signaling molecules [369]. This could support the role of HSD17B12 in chain elongation even though it suggests that HSD17B12 functions at earlier step than previously believed or that its role in FA elongation is indirect.

There was an increase in all of the lipid classes, except SM in the LiB12cKO livers (lipidomics). Interestingly, there was an increase in the polyunsaturated FA. We did not see an overall decrease in the concentrations of FAs with carbon chain length of 18 or 20. The only decreased species of this length was seen in the saturated FAs that were incorporated in the phospholipid species (LPC, LPE, PC, PE and SM). These data do not directly support the idea that HSD17B12 plays a role in the elongation of long chain FAs, however, it is possible that there are compensatory mechanisms, for example FA synthesis from other tissues. That would make FAs available for uptake by the liver and mask the impaired FA elongation in the hepatocytes. On the other hand, some studies suggest that NAFLD may affect lipid chain length, for example, NAFLD and NADH patients may have decreased γ-linoleic acid (18:3n-6), AA (20:4n-6), eicosapentanoic acid (20:5n-3) and docosahexanoic acid (22:6n-3) [310,370]. This suggests that changes in the lipid chain lengths observed in the LiB12cKO could be secondary effects from the fatty liver.

We identified signs of inflammation in all three mouse models presenting with fatty liver. In the HSD17B13KO males, inflammation was evident by the accumulation of microgranulomas (localized aggregates of inflammatory cells, macrophages) and the changes in the expression of immune response genes. Microgranulomas have been observed in various (bacterial) infections [371–373], but they are usually a nonspecific reaction to liver injury [374–376] and a common finding in NASH [376]. In the inducible HSD17B12cKO animals, we observed increased serum cytokines in both sexes, including granulocyte colony-stimulating factor (G-CSF), Il-6 and IL-17. Cytokines form a loose category of small proteins, which are important in cell signaling. They are produced by various cells, including immune

cells and endothelial cells as well as fibroblasts, and important to the regulation of immune response. Increased serum cytokines have been linked to many pathological conditions [377] and IL-6 is known to induce cachexia [378–380]. IL-17 induces the production of G-CSF and they have been linked to inflammatory autoimmune diseases [381].

Support for inflammation in the LiB12cKO came from lipidomics results, which showed that SMs was the only lipid class that was decreased in the LiB12cKO livers. On the other hand, DCER was the only lipid class that was increased in the inducible HSD17B12cKO serum. Both SM and DCER can be converted to CER, which acts as a second messenger and mediates apoptotic signaling [382]. Inflammatory cytokines are known to increase CER [383,384]. In addition to cytokines, also toxic compounds can increase CER [385–387]. At the same time, SM metabolism and CER may play a role in the regulation of inflammatory cytokines [388]. Taken together, in all models, we see signs of inflammation, but it manifests in different ways.

The here analyzed models can be used to study NAFLD, as they present with many of the same pathologies as NAFLD. They can model various aspects of the disease that are not linked to obesity and IR. Overall, these results support the idea that the HSD17B12cKO and HSD17B13 liver phenotypes present a different molecular basis for development of NAFLD pathologies, as they share only 11 genes that were affected in both models.

7 Summary/Conclusions

The scope of this study was to characterize the role of HSD17B enzymes in lipid metabolism and lipid disorder. Classically HSD17B enzymes are recognized for their role in the regulation of sex steroid hormone activity, however, some of them have alternative role in the metabolism of other lipids. HSD17B13 is an LD-associated protein, and our results suggest that it could have protective effects against fatty liver disease and propose a role for HSD17B12 in the LD formation. The results do not directly support the earlier proposed role for HSD17B12 in the elongation of VLCFAs but cannot exclude that either. Using KO mouse models gave the advantage of observing systemic effects of gene disruption, which cannot be achieved with *in vitro* methods.

The main findings of the studies conducted herein are as follows:

- The HSD17B13KO mouse model revealed liver steatosis associated with liver inflammation. This phenotype was more pronounced with male mice. Reproductive impairment was not observed in HSD17B13KO mice.

- The disruption of *Hsd17b12* in adult mice led to rapid weight loss and microvesicular liver steatosis. In addition, there was also accumulation of CER with carbon chain length of 16 and shorter and a decrease in the CER with carbon chain length of 18 and longer in the inducible HSD17B12cKO mice.

- Inducing the *Hsd17b12* gene deletion in the adipose tissue of adult mice did not reveal any clear phenotype, therefore HSD17B12 does not play a crucial role in adipocyte metabolism.

- Liver-specific disruption of *Hsd17b12* led to liver microvesicular steatosis. The formation of LDs seemed to be impaired in the LiB12cKO mice.

Finally, although these two enzymes are not closely structurally related, the KO mice of either enzyme led to liver steatosis and other liver injury. However, the molecular pathways were distinct between the models. The hepatic effects of disrupting the *Hsd17b12* and *Hsd17b13* are illustrated in Fig. 10. Glucose tolerance was not impaired in either of these models, and they were not obese, therefore the

metabolic phenotype in these models did not closely resemble the metabolic NAFLD, which is becoming a health burden in the developed countries. Importantly, these models do mimic some aspects of the NAFLD, for example micro- and macrovesicular steatosis, and therefore they could be good targets for drug development. Yet, more studies are needed for finding the *in vivo* function of these enzymes.
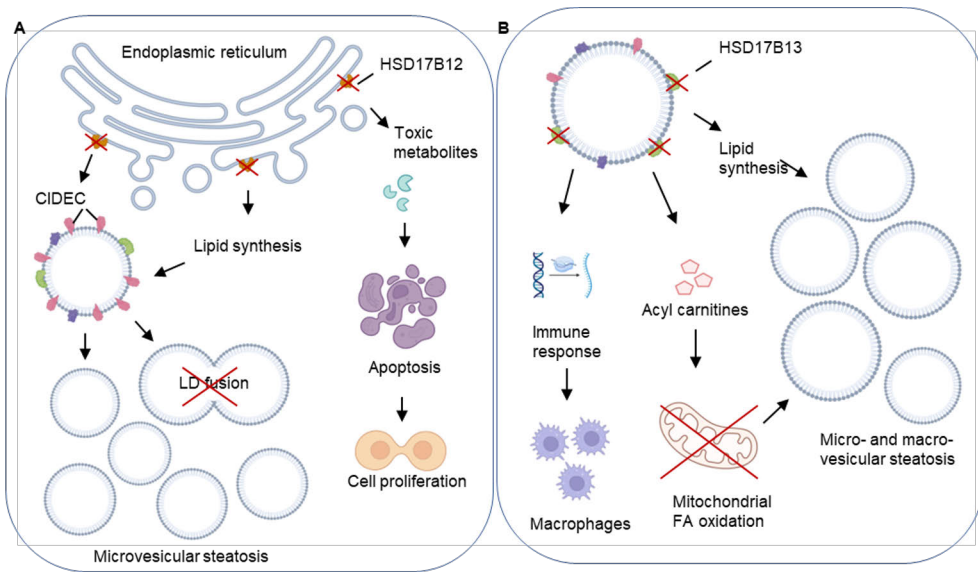
Figure 10. Summary of the hepatic effects of disrupting A) *Hsd17b12* and B) *Hsd17b13*. The ablation of the enzyme function leads to LD accumulation, but at least in part by a different mechanism. Created with BioRender.com.

Acknowledgements

Lehtiniemi, Heidi Elamo, Mari Vähä-Mäkilä, Mehrad Mahmoudian, Saori Itoshima, Sara Simonen, Leena Karlsson, Rilla Ritakallio, Sheila Cisneros Montalvo, Oana Grigoras, Jonna Palmu, Mona Niiranen. I am missing you, Tuula Hämäläinen and Minna Lindroth. You held everything together in the labs and knew all the answers. Pirjo Pakarinen, thank you for being a great mentor for me when I was involved in teaching *in vivo* imaging.

I would like to thank the personnel of the Central Animal Laboratory for the good care and help with animal work.

I got a great opportunity to be a part of collaboration projects with Professor Artur Mayerhofer's research group at Ludwig-Maximilian-University. I would like to express my gratitude to the whole group and especially to Annika Missel and Katja Eubler for hosting me during my visit to your lab.

Gabriela Martínez Chacón and Raul, thank you for your friendship. I have always had a great time with you. Thank you, Gaby, for being a great travel company, those trips I will always remember.

I will be eternally grateful to Justina Zdrojewska. I got to know you already before I started my Ph.D work. Over the years, you have become a close friend. Thank you for all the support, long phone calls, and frequent messages. Thank you also for sharing your cat, it's great to have him around every now and then.

Most importantly, my loving thanks goes to my family. My parents Risto and Henna, you have supported me throughout my life and you have always been willing to listen and encourage me. My brothers Jussi and Jaakko and my sister Saana, thank you for being there for me. Thank you Sille, Teemu, Annis, Julius, Noel, Artturi, Anette, Riitta, Raimo, Lotta, Arto, Emilia, Ulla-Maija and Teuvo. I am lucky that I have a large extended family that is so supportive.

10.10.2023
Hanna Heikelä

References

1. Younossi, Z. M. *et al.* Pathologic criteria for nonalcoholic steatohepatitis: Interprotocol agreement and ability to predict liver-related mortality. *Hepatology* **53**, 1874–1882 (2011).
2. Armstrong, M. J., Adams, L. A., Canbay, A. & Syn, W. K. Extrahepatic complications of nonalcoholic fatty liver disease. *Hepatology* **59**, 1174–1197 (2014).
3. Eslam, M., Valenti, L. & Romeo, S. Genetics and epigenetics of NAFLD and NASH: Clinical impact. *J Hepatol* **68**, 268–279 (2018).
4. Su, W. *et al.* Role of HSD17B13 in the liver physiology and pathophysiology. *Molecular and Cellular Endocrinology* vol. 489 119–125 Preprint at https://doi.org/10.1016/j.mce.2018.10.014 (2019).
5. Saloniemi, T., Jokela, H., Strauss, L., Pakarinen, P. & Poutanen, M. The diversity of sex steroid action: Novel functions of hydroxysteroid (17β) dehydrogenases as revealed by genetically modified mouse models. *Journal of Endocrinology* **212**, 27–40 (2012).
6. Moon, Y. A. & Horton, J. D. Identification of two mammalian reductases involved in the two-carbon fatty acyl elongation cascade. *Journal of Biological Chemistry* **278**, 7335–7343 (2003).
7. Rantakari, P. *et al.* Hydroxysteroid (17β) dehydrogenase 12 is essential for mouse organogenesis and embryonic survival. *Endocrinology* **151**, 1893–1901 (2010).
8. Horiguchi, Y., Araki, M. & Motojima, K. 17β-Hydroxysteroid dehydrogenase type 13 is a liver-specific lipid droplet-associated protein. *Biochem Biophys Res Commun* **370**, 235–238 (2008).
9. Su, W. *et al.* Comparative proteomic study reveals 17β-HSD13 as a pathogenic protein in nonalcoholic fatty liver disease. *Proc Natl Acad Sci U S A* **111**, 11437–11442 (2014).
10. Abul-Husn, N. S. *et al.* A Protein-Truncating HSD17B13 Variant and Protection from Chronic Liver Disease. *New England Journal of Medicine* **378**, 1096–1106 (2018).
11. Kruepunga, N., Hakvoort, T. B. M., Hikspoors, J. P. J. M., Köhler, S. E. & Lamers, W. H. Anatomy of rodent and human livers: What are the differences? *Biochim Biophys Acta Mol Basis Dis* **1865**, 869–878 (2019).
12. Trefts, E., Gannon, M. & Wasserman, D. H. The liver. *Current Biology* **27**, R1147–R1151 (2017).
13. Krishna, M. Microscopic anatomy of the liver. *Clin Liver Dis (Hoboken)* **2**, S4–S7 (2013).
14. Bilzer, M., Roggel, F. & Gerbes, A. L. Role of Kupffer cells in host defense and liver disease. *Liver International* **26**, 1175–1186 (2006).
15. Hrncir, H. R., Hantelys, F. & Gracz, A. D. Panic at the bile duct: how intrahepatic cholangiocytes respond to stress and injury. *Am J Pathol* **S0002-9440**, 63–69 (2023).
16. Gordillo, M., Evans, T. & Gouon-Evans, V. Orchestrating liver development. *Development* **142**, 2094–2108 (2015).
17. Rajas, F., Gautier-Stein, A. & Mithieux, G. Glucose-6 phosphate, A central hub for liver carbohydrate metabolism. *Metabolites* **9**, 282 (2019).
18. Rui, L. Energy metabolism in the liver. *Compr Physiol* **4**, 177–197 (2014).
19. Stayrook, K. R. *et al.* Regulation of carbohydrate metabolism by the farnesoid X receptor. *Endocrinology* **146**, 984–991 (2005).

20. Alves-Bezerra, M. & Cohen, D. E. Triglyceride metabolism in the liver. *Compr Physiol* **8**, 1–22 (2018).

21. Higuchi, N. *et al.* Liver X receptor in cooperation with SREBP-1c is a major lipid synthesis regulator in nonalcoholic fatty liver disease. *Hepatology Research* **38**, 1122–1129 (2008).

22. Chiang, J. Y. L. Regulation of bile acid synthesis: Pathways, nuclear receptors, and mechanisms. *J Hepatol* **40**, 539–551 (2004).

23. Lee, J. H. *et al.* The transcription factor cyclic AMP-responsive element-binding protein H regulates triglyceride metabolism. *Nat Med* **17**, 812–815 (2011).

24. Krammer, J. *et al.* Overexpression of CD36 and Acyl-CoA Synthetases FATP2, FATP4 and ACSL1 Increases Fatty Acid Uptake in Human Hepatoma Cells. *Int. J. Med. Sci* **8**, 599–614 (2011).

25. Miquilena-Colina, M. E. *et al.* Hepatic fatty acid translocase CD36 upregulation is associated with insulin resistance, hyperinsulinaemia and increased steatosis in non-alcoholic steatohepatitis and chronic hepatitis C. *Gut* **60**, 1394–1402 (2011).

26. Memon, R. A. *et al.* Regulation of Putative Fatty Acid Transporters and Acyl-CoA Synthetase in Liver and Adipose Tissue in o b/o b M i c e. *Diabetes* **48**, 121–127 (1999).

27. Grevengoed, T. J., Klett, E. L. & Coleman, R. A. Acyl-CoA metabolism and partitioning. *Annu Rev Nutr* **34**, 1–30 (2014).

28. Chabowski, A. *et al.* Fatty acid transporters involved in the palmitate and oleate induced insulin resistance in primary rat hepatocytes. *Acta Physiologica* **207**, 346–357 (2013).

29. Doege, H. *et al.* Targeted Deletion of FATP5 Reveals Multiple Functions in Liver Metabolism: Alterations in Hepatic Lipid Homeostasis. *Gastroenterology* **130**, 1245–1258 (2006).

30. Woudenberg, J. *et al.* Caveolin-1 is enriched in the peroxisomal membrane of rat hepatocytes. *Hepatology* **51**, 1744–1753 (2010).

31. Donnelly, K. L. *et al.* Sources of fatty acids stored in liver and secreted via lipoproteins in patients with nonalcoholic fatty liver disease. *Journal of Clinical Investigation* **115**, 1343–1351 (2005).

32. Kihara, A. Very long-chain fatty acids: Elongation, physiology and related disorders. *J Biochem* **152**, 387–395 (2012).

33. Leonard, A. E., Pereira, S. L., Sprecher, H. & Huang, Y. S. Elongation of long-chain fatty acids. *Prog Lipid Res* **43**, 36–54 (2004).

34. Horton, J. D., Goldstein, J. L. & Brown, M. S. SREBPs: activators of the complete program of cholesterol and fatty acid synthesis in the liver. *Journal of Clinical Investigation* **109**, 1125–1131 (2002).

35. Postic, C., Dentin, R., Denechaud, P. D. & Girard, J. ChREBP, a transcriptional regulator of glucose and lipid metabolism. *Annu Rev Nutr* **27**, 179–192 (2007).

36. Nowinski, S. M. *et al.* Mitochondrial fatty acid synthesis coordinates oxidative metabolism in mammalian mitochondria. *Elife* **9**, 1–35 (2020).

37. Schlaepfer, I. R. *et al.* Hypoxia induces triglycerides accumulation in prostate cancer cells and extracellular vesicles supporting growth and invasiveness following reoxygenation. *Oncotarget* **6**, 22836–22856 (2015).

38. Listenberger, L. L. *et al.* Triglyceride accumulation protects against fatty acid-induced lipotoxicity. *PNAS* **100**, 3077–3082 (2003).

39. Olzmann, J. A. & Carvalho, P. Dynamics and functions of lipid droplets. *Nat Rev Mol Cell Biol* **20**, 137–155 (2019).

40. Bartz, R. *et al.* Lipidomics reveals that adiposomes store ether lipids and mediate phospholipid traffic. *The Journal of Lipid Research* **48**, 837–847 (2007).

41. Loizides-Mangold, U. *et al.* HCV 3a Core Protein Increases Lipid Droplet Cholesteryl Ester Content via a Mechanism Dependent on Sphingolipid Biosynthesis. *PLoS One* **11**, (2014).

42. Walther, T. C. & Farese, R. V. Lipid droplets and cellular lipid metabolism. *Annu Rev Biochem* **81**, 687–714 (2012).

43. Chitraju, C. *et al.* Lipidomic analysis of lipid droplets from murine hepatocytes reveals distinct signatures for nutritional stress. *J Lipid Res* **53**, 2141–2152 (2012).

44. Chorlay, A. & Thiam, A. R. An Asymmetry in Monolayer Tension Regulates Lipid Droplet Budding Direction. *Biophys J* **114**, 631–640 (2018).

45. Chen, F. *et al.* FIT2 organizes lipid droplet biogenesis with ER tubule-forming proteins and septins. *Journal of Cell Biology* **220**, (2021).

46. Salo, V. T. *et al.* Seipin Facilitates Triglyceride Flow to Lipid Droplet and Counteracts Droplet Ripening via Endoplasmic Reticulum Contact. *Dev Cell* **50**, 478-493.e9 (2019).

47. la Fuente, F. P. de *et al.* Exercise regulates lipid droplet dynamics in normal and fatty liver. *Biochim Biophys Acta Mol Cell Biol Lipids* **1864**, (2019).

48. Yu, J. *et al.* Lipid droplet remodeling and interaction with mitochondria in mouse brown adipose tissue during cold treatment. *Biochim Biophys Acta Mol Cell Res* **1853**, 918–928 (2015).

49. Greenberg, A. S. *et al.* Perilipin, a Major Hormonally Regulated Adipocyte-specific Phosphoprotein Associated with the Periphery of Lipid Storage Droplets*. *J Biol Chem* **266**, 11341–11346 (1991).

50. Wolins, N. E. *et al.* S3-12, adipophilin, and TIP47 package lipid in adipocytes. *Journal of Biological Chemistry* **280**, 19146–19155 (2005).

51. Heid, H. W., Moll, R., Schwetlick, I., Rackwitz, H.-R. & Keenan, T. W. Adipophilin is a specific marker of lipid accumulation in diverse cell types and diseases. *Cell Tissue Res* **294**, 309–321 (1998).

52. Than, N. G., Sumegi, B., Than, G. N., Kispal, G. & Bohn, H. Cloning and sequence analysis of cDNAs encoding human placental tissue protein 17 (PP17) variants. *Eur J Biochem* **258**, 752–757 (1998).

53. Dalen, K. T. *et al.* LSDP5 is a PAT protein specifically expressed in fatty acid oxidizing tissues. *Biochim Biophys Acta Mol Cell Biol Lipids* **1771**, 210–227 (2007).

54. Yamaguchi, T., Matsushita, S., Motojima, K., Hirose, F. & Osumi, T. MLDP, a novel PAT family protein localized to lipid droplets and enriched in the heart, is regulated by peroxisome proliferator-activated receptorα. *Journal of Biological Chemistry* **281**, 14232–14240 (2006).

55. Feingold, K. R. *Introduction to Lipids and Lipoproteins*. *National Institutes of Health. Feingold KR* (MDText.com, Inc, 2000).

56. Farese, R. V. *et al.* A novel function for apolipoprotein B: Lipoprotein synthesis in the yolk sac is critical for maternal-fetal lipid transport in mice. *J Lipid Res* **37**, 347–360 (1996).

57. Davis, R. A., Mcneal, M. M. & Moses, R. L. Intrahepatic Assembly of Very Low Density Lipoprotein. *The Journal of Biological Chemistry* **257**, 2634–2640 (1982).

58. Berberich, A. J. & Hegele, R. A. The complex molecular genetics of familial hypercholesterolaemia. *Nat Rev Cardiol* **16**, 9–20 (2019).

59. Pease, R., Harrison, G. B. & Scott, J. Cotranslocational insertion of apolipoprotein B into the inner leaflet of the endoplasmic reticulum. *Nature* **353**, 448–450 (1991).

60. Ma, D., Liu, W. & Wang, Y. ApoA-I or ABCA1 expression suppresses fatty acid synthesis by reducing 27-hydroxycholesterol levels. *Biochimie* **103**, 101–108 (2014).

61. Hashimoto, T. *et al.* Defect in Peroxisome Proliferator-activated Receptor α-inducible Fatty Acid Oxidation Determines the Severity of Hepatic Steatosis in Response to Fasting. *Journal of Biological Chemistry* **275**, 28918–28928 (2000).

62. Leone, T. C., Weinheimer, C. J. & Kelly, D. P. A critical role for the peroxisome proliferator-activated receptor (PPAR) in the cellular fasting response: The PPAR-null mouse as a model of fatty acid oxidation disorders (nuclear hormone receptorslipid metabolismtranscriptional controldietary regulation). *Medical Sciences* **96**, 7473–7478 (1999).

63. Santoro, A., McGraw, T. E. & Kahn, B. B. Insulin action in adipocytes, adipose remodeling, and systemic effects. *Cell Metab* **33**, 748–757 (2021).

64. Furge, L. L. & Guengerich, F. P. Cytochrome P450 enzymes in drug metabolism and chemical toxicology: An introduction. *Biochemistry and Molecular Biology Education* **34**, 66–74 (2006).

65. Ma, W. L., Lai, H. C., Yeh, S., Cai, X. & Chang, C. Androgen receptor roles in hepatocellular carcinoma, fatty liver, cirrhosis and hepatitis. *Endocr Relat Cancer* **21**, (2014).

66. Addison, M. L. & Rissman, E. F. Sexual dimorphism of growth hormone in the hypothalamus: Regulation by estradiol. *Endocrinology* **153**, 1898–1907 (2012).

67. Robinson, I. C. A. F., Gevers, E. R. & Bennett, P. A. Sex differences in growth hormone secretion and action in the rat. *Growth Hormone & IGF Research* **8**, 39–47 (1998).

68. Waxman, D. J. & O'Connor, C. Growth hormone regulation of sex-dependent liver gene expression. *Molecular Endocrinology* **20**, 2613–2629 (2006).

69. Macleod, J. N., Pampori, N. A., Shapiro, B. H. & Macleod, S. A. (j N. Sex differences in the ultradian pattern of plasma growth hormone concentrations in mice. *Journal of Endocrinology* **131**, 395–399 (1991).

70. Painson, J.-C., Veldhuis, J. D. & Tannenbaum, G. S. Single exposure to testosterone in adulthood rapidly induces regularity in the growth hormone release process. *Am J Physiol Endocrinol Metab* **278**, 933–940 (2000).

71. Painson, J.-C., Thorner, M. 0, Krieg, R. J. & Tannenbaums, G. S. Short Term Adult Exposure to Estradiol Feminizes the Male Pattern of Spontaneous and Growth Hormone-Releasing Factor-Stimulated Growth Hormone Secretion in the Rat*. *Endocrinology* **130**, (1992).

72. Mcintosht, I. & Bishop, J. 0. Differential Expression in Male and Female Mouse Liver of Very Similar mRNAs Specified by Two Group 1 Major Urinary Protein Genes. *Mol Cell Biol* **9**, 2202–2207 (1989).

73. Sundseths, S. S., Alberta, J. A. & Waxmans, D. J. Sex-specific, Growth Hormone-regulated Transcription of the Cytochrome P450 2 C l l and 2 C 1 2 Genes*. *J Biol Chem* **267**, 3907–3914 (1992).

74. Renaud, H. J., Cui, J. Y., Khan, M. & Klaassen, C. D. Tissue distribution and gender-divergent expression of 78 cytochrome p450 mRNAs in mice. *Toxicological Sciences* **124**, 261–277 (2011).

75. Fan, Y. *et al.* Liver-specific deletion of the growth hormone receptor reveals essential role of growth hormone signaling in hepatic lipid metabolism. *Journal of Biological Chemistry* **284**, 19937–19944 (2009).

76. Palmisano, B. T., Zhu, L. & Stafford, J. M. Role of estrogens in the regulation of liver lipid metabolism. in *Advances in Experimental Medicine and Biology* vol. 1043 227–256 (Springer New York LLC, 2017).

77. Lax, E. R., Tamulevi~ius~, P., Miller, A. & Schriefers, H. Hepatic Nuclear Estrogen Receptor Concentration in the Rat - Influence of Age, Sex, Gestation, Lactation and Estrous Cycle. *J. steroid Biochem* **19**, 1083–1088 (1983).

78. Pedram, A. *et al.* Estrogen Reduces Lipid Content in the Liver Exclusively from Membrane Receptor Signaling. *Sci Signal* **6**, (2013).

79. Davey, R. A. & Grossmann, M. Androgen Receptor Structure, Function and Biology: From Bench to Bedside. *Androgen Receptor Biology Clin Biochem Rev* **37**, 3 (2016).

80. Younossi, Z. M. *et al.* The global epidemiology of nonalcoholic fatty liver disease (NAFLD) and nonalcoholic steatohepatitis (NASH): a systematic review. *Hepatology* **77**, 1335–1347 (2023).

81. Lonardo, A. & Suzuki, A. Sexual dimorphism of NAFLD in adults. Focus on clinical aspects and implications for practice and translational research. *J Clin Med* **9**, (2020).

82. Lee, A. Y. *et al.* Dihydroceramide is a key metabolite that regulates autophagy and promotes fibrosis in hepatic steatosis model. *Biochem Biophys Res Commun* **494**, 460–469 (2017).

83. Tandra, S. *et al.* Presence and significance of microvesicular steatosis in nonalcoholic fatty liver disease. *J Hepatol* **55**, 654–659 (2011).

84. Brunt, E. M., Neuschwander-Tetri, B. A., Oliver, D., Wehmeier, K. R. & Bacon, B. R. Nonalcoholic steatohepatitis: Histologic features and clinical correlations with 30 blinded biopsy specimens. *Hum Pathol* **35**, 1070–1082 (2004).

85. Bedossa, P. & Patel, K. Biopsy and Noninvasive Methods to Assess Progression of Nonalcoholic Fatty Liver Disease. *Gastroenterology* **150**, 1811-1822.e4 (2016).

86. Puri, V. *et al.* Fat-specific protein 27, a novel lipid droplet protein that enhances triglyceride storage. *Journal of Biological Chemistry* **282**, 34213–34218 (2007).

87. Germano, C. W. *et al.* Microvesicular Steatosis in Individuals with Obesity: a Histological Marker of Non-alcoholic Fatty Liver Disease Severity. *Obes Surg* **33**, 813–820 (2023).

88. Day, C. P. & James, O. F. W. Steatohepatitis, a tale of two hits. *Gastroenterology* **114**, 842–845 (1998).

89. Tilg, H. & Moschen, A. R. Evolution of inflammation in nonalcoholic fatty liver disease: The multiple parallel hits hypothesis. *Hepatology* **52**, 1836–1846 (2010).

90. Yudkin, J. S., Stehouwer, C. D. A., Emeis, J. J. & Coppack, S. W. C-Reactive Protein in Healthy Subjects: Associations With Obesity, Insulin Resistance, and Endothelial Dysfunction A Potential Role for Cytokines Originating From Adipose Tissue? *Arterioscler Thromb Vasc Biol.* **19**, 972–978 (1999).

91. Bastard, J.-P. *et al.* Elevated Levels of Interleukin 6 Are Reduced in Serum and Subcutaneous Adipose Tissue of Obese Women after Weight Loss*. *J Clin Endocrinol Metab* **85**, 3338–3342 (2000).

92. Vozarova, B. *et al.* High White Blood Cell Count Is Associated With a Worsening of Insulin Sensitivity and Predicts the Development of Type 2 Diabetes. *Diabetes* **51**, 455–461 (2002).

93. Smith, G. I. *et al.* Insulin resistance drives hepatic de novo lipogenesis in nonalcoholic fatty liver disease. *Journal of Clinical Investigation* **130**, 1453–1460 (2020).

94. Romeo, S. *et al.* Genetic variation in PNPLA3 confers susceptibility to nonalcoholic fatty liver disease. *Nat Genet* **40**, 1461–1465 (2008).

95. Käräjämäki, A. J. *et al.* Non-alcoholic fatty liver disease with and without metabolic syndrome: Different long-term outcomes. *Metabolism* **66**, 55–63 (2017).

96. Martínez, L. A., Larrieta, E., Calva, J. J., Kershenobich, D. & Torre, A. The expression of PNPLA3 polymorphism could be the key for severe liver disease in NAFLD in hispanic population. *Ann Hepatol* **16**, 909–915 (2017).

97. Trépo, E., Romeo, S. & Zucman-Rossi, J. PNPLA3 gene in liver diseases. *J Hepatol* **65**, 339–412 (2016).

98. Pingitore, P. *et al.* Recombinant PNPLA3 protein shows triglyceride hydrolase activity and its I148M mutation results in loss of function. *Biochim Biophys Acta Mol Cell Biol Lipids* **1841**, 574–580 (2014).

99. Li, Q. *et al.* PNPLA3 Polymorphisms and Liver Aminotransferase Levels in a Mexican American Population. *Clin Invest Med.* **35**, E237 (2012).

100. Roe, J. D., Garcia, L. A., Klimentidis, Y. C. & Coletta, D. K. Association of PNPLA3 I148M with Liver Disease Biomarkers in Latinos. *Hum Hered* **86**, 21–27 (2021).

101. Kawaguchi, T. *et al.* Genetic polymorphisms of the human PNPLA3 gene are strongly associated with severity of non-alcoholic fatty liver disease in Japanese. *PLoS One* **7**, (2012).

102. Meffert, P. J. *et al.* The PNPLA3 SNP rs738409:G allele is associated with increased liver disease-associated mortality but reduced overall mortality in a population-based cohort. *J Hepatol* **68**, 840–866 (2018).

103. Pirazzi, C. *et al.* Patatin-like phospholipase domain-containing 3 (PNPLA3) I148M (rs738409) affects hepatic VLDL secretion in humans and in vitro. *J Hepatol* **57**, 1276–1282 (2012).

104. Ruhanen, H. *et al.* PNPLA3 mediates hepatocyte triacylglycerol remodeling. *J Lipid Res* **55**, 739–746 (2014).

105. Mahdessian, H. *et al.* TM6SF2 is a regulator of liver fat metabolism influencing triglyceride secretion and hepatic lipid droplet content. *Proc Natl Acad Sci U S A* **111**, 8913–8918 (2014).

106. Kozlitina, J. *et al.* Exome-wide association study identifies a TM6SF2 variant that confers susceptibility to nonalcoholic fatty liver disease. *Nat Genet* **46**, 352–356 (2014).

107. Dongiovanni, P. *et al.* Transmembrane 6 Superfamily Member 2 Gene Variant Disentangles Nonalcoholic Steatohepatitis From Cardiovascular Disease. *Hepatology* **61**, 506–514 (2015).

108. Liu, Y. L. *et al.* TM6SF2 rs58542926 influences hepatic fibrosis progression in patients with non-alcoholic fatty liver disease. *Nat Commun* **5**, (2014).

109. Holmen, O. L. *et al.* Systematic evaluation of coding variation identifies a candidate causal variant in TM6SF2 influencing total cholesterol and myocardial infarction risk. *Nat Genet* **46**, 345–351 (2014).

110. Tan, H. L. *et al.* Association of glucokinase regulatory gene polymorphisms with risk and severity of non-alcoholic fatty liver disease: An interaction study with adiponutrin gene. *J Gastroenterol* **49**, 1056–1064 (2014).

111. Santoro, N. *et al.* Variant in the glucokinase regulatory protein (GCKR) gene is associated with fatty liver in obese children and adolescents. *Hepatology* **55**, 781–789 (2012).

112. Peter, A. *et al.* Hepatic glucokinase expression is associated with lipogenesis and fatty liver in humans. *Journal of Clinical Endocrinology and Metabolism* **96**, (2011).

113. Mancina, R. M. *et al.* The MBOAT7-TMC4 Variant rs641738 Increases Risk of Nonalcoholic Fatty Liver Disease in Individuals of European Descent. *Gastroenterology* **150**, 1219-1230.e6 (2016).

114. Caddeo, A. *et al.* MBOAT7 is anchored to endomembranes by six transmembrane domains. *J Struct Biol* **206**, 349–360 (2019).

115. Gijón, M. A., Riekhof, W. R., Zarini, S., Murphy, R. C. & Voelker, D. R. Lysophospholipid acyltransferases and arachidonate recycling in human neutrophils. *Journal of Biological Chemistry* **283**, 30235–30245 (2008).

116. Zarini, S., Gijón, M. A., Folco, G. & Murphy, R. C. Effect of arachidonic acid reacylation on leukotriene biosynthesis in human neutrophils stimulated with granulocyte-macrophage colony-stimulating factor and formyl-methionyl-leucyl-phenylalanine. *Journal of Biological Chemistry* **281**, 10134–10142 (2006).

117. Shin, S. Y. *et al.* An atlas of genetic influences on human blood metabolites. *Nat Genet* **46**, 543–550 (2014).

118. Helsley, R. N. *et al.* Obesity-linked suppression of membrane-bound o-acyltransferase 7 (MBOAT7) drives non-alcoholic fatty liver disease. *Elife* **8**, 1–69 (2019).

119. Buch, S. *et al.* A genome-wide association study confirms PNPLA3 and identifies TM6SF2 and MBOAT7 as risk loci for alcohol-related cirrhosis. *Nat Genet* **47**, 1443–1448 (2015).

120. Basaranoglu, M., Turhan, N., Sonsuz, A. & Basaranoglu, G. Mallory-Denk Bodies in chronic hepatitis. *World J Gastroenterol* **17**, 2172–2177 (2011).

121. Brunt, E. M. & Tiniakos, D. G. Histopathology of nonalcoholic fatty liver disease. *World J Gastroenterol* **16**, 5286–5296 (2010).

122. Guilherme, A., Virbasius, J. V., Puri, V. & Czech, M. P. Adipocyte dysfunctions linking obesity to insulin resistance and type 2 diabetes. *Nat Rev Mol Cell Biol* **9**, 367–377 (2008).

123. Chen, J., Zhou, H., Jin, H. & Liu, K. Role of Inflammatory Factors in Mediating the Effect of Lipids on Nonalcoholic Fatty Liver Disease: A Two-Step, Multivariable Mendelian Randomization Study. *Nutrients* **14**, (2022).

124. Wu, J. *et al.* Toll-like receptor-induced innate immune responses in non-parenchymal liver cells are cell type-specific. *Immunology* **129**, 363–374 (2010).

125. Shi, H. *et al.* TLR4 links innate immunity and fatty acid-induced insulin resistance. *Journal of Clinical Investigation* **116**, 3015–3025 (2006).

126. Mridha, A. R. *et al.* NLRP3 inflammasome blockade reduces liver inflammation and fibrosis in experimental NASH in mice. *J Hepatol* **66**, 1037–1046 (2017).

127. Buzzetti, E., Pinzani, M. & Tsochatzis, E. A. The multiple-hit pathogenesis of non-alcoholic fatty liver disease (NAFLD). *Metabolism* **65**, 1038–1048 (2016).

128. Hoofnagle, J. H. & Björnsson, E. S. Drug-Induced Liver Injury — Types and Phenotypes. *New England Journal of Medicine* **381**, 264–273 (2019).

129. Shah, N. J., Royer, A. & Savio, J. *Acute Liver Failure*. (StatPearls Publishing, 2023).
130. Sevior, D. K., Pelkonen, O. & Ahokas, J. T. Hepatocytes: The powerhouse of biotransformation. *International Journal of Biochemistry and Cell Biology* **44**, 257–261 (2012).
131. Petruzziello, A., Marigliano, S., Loquercio, G., Cozzolino, A. & Cacciapuoti, C. Global epidemiology of hepatitis C virus infection: An up-date of the distribution and circulation of hepatitis C virus genotypes. *World J Gastroenterol* **22**, 7824–7840 (2016).
132. Friedman, S. L. Evolving challenges in hepatic fibrosis. *Nat Rev Gastroenterol Hepatol* **7**, 425–436 (2010).
133. Goto, K., Andres Roca Suarez, A., Wrensch, F., Baumert, T. F. & Lupberger, J. Hepatitis c virus and hepatocellular carcinoma: When the host loses its grip. *Int J Mol Sci* **21**, (2020).
134. Miller, S. & Krijnse-Locker, J. Modification of intracellular membrane structures for virus replication. *Nat Rev Microbiol* **6**, 363–374 (2008).
135. Romero-Brey, I. *et al.* Three-Dimensional Architecture and Biogenesis of Membrane Structures Associated with Hepatitis C Virus Replication. *PLoS Pathog* **8**, (2012).
136. Machado, M. V., Oliveira, A. G. & Cortez-Pinto, H. Hepatic steatosis in hepatitis B virus infected patients: Meta-analysis of risk factors and comparison with hepatitis C infected patients. *J Gastroenterol Hepatol* **26**, 1361–1367 (2011).
137. Huang, H. *et al.* Hepatitis C virus production by human hepatocytes dependent on assembly and secretion of very low-density lipoproteins. *PNAS* **104**, 5848–5853 (2007).
138. Lyu, J. *et al.* Roles of lipoprotein receptors in the entry of hepatitis C virus. *World J Hepatol* **7**, 2535–2542 (2015).
139. Popescu, C. I. *et al.* Hepatitis C virus life cycle and lipid metabolism. *Biology (Basel)* **3**, 892–921 (2014).
140. Clément, S., Pascarella, S. & Negro, F. Hepatitis C virus infection: Molecular pathways to steatosis, insulin resistance and oxidative stress. *Viruses* **1**, 126–143 (2009).
141. Singh, S. *et al.* Fibrosis Progression in Nonalcoholic Fatty Liver vs Nonalcoholic Steatohepatitis: A Systematic Review and Meta-analysis of Paired-Biopsy Studies. *Clinical Gastroenterology and Hepatology* **13**, 643-654.e9 (2015).
142. Bray, F. *et al.* Global cancer statistics 2018: GLOBOCAN estimates of incidence and mortality worldwide for 36 cancers in 185 countries. *CA Cancer J Clin* **68**, 394–424 (2018).
143. Ascione, A., Fontanella, L., Imparato, M., Rinaldi, L. & De Luca, M. Mortality from cirrhosis and hepatocellular carcinoma in Western Europe over the last 40 years. *Liver International* **37**, 1193–1201 (2017).
144. Vilar-Gomez, E. *et al.* Fibrosis Severity as a Determinant of Cause-Specific Mortality in Patients With Advanced Nonalcoholic Fatty Liver Disease: A Multi-National Cohort Study. *Gastroenterology* **155**, 443-457.e17 (2018).
145. Torre, L. A. *et al.* Global cancer statistics, 2012. *CA Cancer J Clin* **65**, 87–108 (2015).
146. Higashi, T., Friedman, S. L. & Hoshida, Y. Hepatic stellate cells as key target in liver fibrosis. *Adv Drug Deliv Rev* **121**, 27–42 (2017).
147. Tsochatzis, E. A., Bosch, J. & Burroughs, A. K. Liver cirrhosis. *The Lancet* **383**, 1749–1761 (2014).
148. Gordon, S. M. *et al.* A comparison of the mouse and human lipoproteome: Suitability of the mouse model for studies of human lipoproteins. *J Proteome Res* **14**, 2686–2695 (2015).
149. Speakman, J. R. Use of high-fat diets to study rodent obesity as a model of human obesity. *Int J Obes* **43**, 1491–1492 (2019).
150. Jiang, M. *et al.* Pathogenesis of and major animal models used for nonalcoholic fatty liver disease. *Journal of International Medical Research* **47**, 1453–1466 (2019).
151. Eccleston, H. B. *et al.* Chronic Exposure to a High-Fat Diet Induces Hepatic Steatosis, Impairs Nitric Oxide Bioavailability, and Modifies the Mitochondrial Proteome in Mice. *Antioxid. Redox Signal.* **15**, 447–459 (2011).

152. Ito, M. *et al.* Longitudinal analysis of murine steatohepatitis model induced by chronic exposure to high-fat diet. *Hepatology Research* **37**, 50–57 (2007).

153. Lim, J. S., Mietus-Snyder, M., Valente, A., Schwarz, J. M. & Lustig, R. H. The role of fructose in the pathogenesis of NAFLD and the metabolic syndrome. *Nat Rev Gastroenterol Hepatol* **7**, 251–264 (2010).

154. Kohli, R. *et al.* High-fructose, medium chain trans fat diet induces liver fibrosis and elevates plasma coenzyme Q9 in a novel murine model of obesity and nonalcoholic steatohepatitis. *Hepatology* **52**, 934–944 (2010).

155. Chukijrungroat, N., Khamphaya, T., Weerachayaphorn, J., Songserm, T. & Saengsirisuwan, V. Hepatic FGF21 mediates sex differences in high-fat high-fructose diet-induced fatty liver. *Am J Physiol Endo-crinol Metab* **313**, 203–212 (2017).

156. Wang, D., Lammert, F., Cohen, D. E., Paigen, B. & Carey, M. C. Cholic acid aids absorption, biliary secretion, and phase transitions of cholesterol in murine cholelithogenesis. *Am. J. Physiol.* **276**, G751–G760 (1999).

157. Vergnes, L., Phan, J., Strauss, M., Tafuri, S. & Reue, K. Cholesterol and Cholate Components of an Atherogenic Diet Induce Distinct Stages of Hepatic Inflammatory Gene Expression. *Journal of Biological Chemistry* **278**, 42774–42784 (2003).

158. Woollett, L. A. *et al.* Cholic Acid Supplementation Enhances Cholesterol Absorption in Humans. *Gastroenterology* **126**, 724–731 (2004).

159. Kaminsky-Kolesnikov, Y. *et al.* Cholesterol Induces Nrf-2-and HIF-1 α-Dependent Hepatocyte Proliferation and Liver Regeneration to Ameliorate Bile Acid Toxicity in Mouse Models of NASH and Fibrosis. *Oxid Med Cell Longev* **2020**, (2020).

160. Veteläinen, R., Van Vliet, A. & Van Gulik, T. M. Essential pathogenic and metabolic differences in steatosis induced by choline or methione-choline deficient diets in a rat model. *J Gastroenterol Hepatol* **22**, 1526–1533 (2007).

161. Nakano, H. *et al.* The effects ofN-acetylcysteine and anti-intercellular adhesion molecule-1 monoclonal antibody against ischemia-reperfusion injury of the rat steatotic liver produced by a choline-methionine-deficient diet. *Hepatology* **26**, 670–678 (1997).

162. Matsuzawa, N. *et al.* Lipid-induced oxidative stress causes steatohepatitis in mice fed an atherogenic diet. *Hepatology* **46**, 1392–1403 (2007).

163. Daniels, S. J. *et al.* Addition of trans fat and alcohol has divergent effects on atherogenic diet-induced liver injury in rodent models of steatohepatitis. *Am J Physiol Gastrointest Liver Physiol* **318**, 410–418 (2020).

164. Liang, X., Wu, K., Liu, M. & Yang, B. Adverse impact of carbon tetrachloride on metabolic function in mice. *J Cell Biochem* **120**, 11973–11980 (2019).

165. Kanno, K., Tazuma, S. & Chayama, K. AT1A-deficient mice show less severe progression of liver fibrosis induced by CCl4. *Biochem Biophys Res Commun* **308**, 177–183 (2003).

166. Xie, Y. *et al.* Liver infiltration of multiple immune cells during the process of acute liver injury and repair. *World J Gastroenterol* **28**, 6537–6550 (2022).

167. Kishida, N. *et al.* Development of a novel mouse model of hepatocellular carcinoma with nonalcoholic steatohepatitis using a high-fat, choline-deficient diet and intraperitoneal injection of diethylnitrosamine. *BMC Gastroenterol* **16**, (2016).

168. Larter, C. Z. *et al.* Hepatic free fatty acids accumulate in experimental steatohepatitis: Role of adaptive pathways. *J Hepatol* **48**, 638–647 (2008).

169. Vance, D. E. Role of phosphatidylcholine biosynthesis in the regulation of lipoprotein homeostasis. *Curr Opin Lipidol* **19**, 229–234 (2008).

170. Weltman, M. D., Farrell, G. C. & Liddle, C. Increased hepatocyte CYP2E1 expression in a rat nutritional model of hepatic steatosis with inflammation. *Gastroenterology* **111**, 1645–1653 (1996).

171. Leclercq, I. A. *et al.* CYP2E1 and CYP4A as microsomal catalysts of lipid peroxides in murine nonalcoholic steatohepatitis. *J. Clin. Invest.* **105**, 1067–1075 (2000).

172. Sahai, A. *et al.* Upregulation of osteopontin expression is involved in the development of nonalcoholic steatohepatitis in a dietary murine model. *Am J Physiol Gastrointest Liver Physiol* **287**, 264–273 (2004).

173. Rinella, M. E. *et al.* Mechanisms of hepatic steatosis in mice fed a lipogenic methionine choline-deficient diet. in *Journal of Lipid Research* vol. 49 1068–1076 (2008).

174. Rizki, G. *et al.* Mice fed a lipogenic methionine-choline-deficient diet develop hypermetabolism coincident with hepatic suppression of SCD-1. *J Lipid Res* **47**, 2280–2290 (2006).

175. Kirsch, R. *et al.* Rodent nutritional model of non-alcoholic steatohepatitis: Species, strain and sex difference studies. *J Gastroenterol Hepatol* **18**, 1272–1282 (2003).

176. Raubenheimer, P. J., Nyirenda, M. J. & Walker, B. R. A choline-deficient diet exacerbates fatty liver but attenuates insulin resistance and glucose intolerance in mice fed a high-fat diet. *Diabetes* **55**, 2015–2020 (2006).

177. Han, J. H. *et al.* Metabolomic profiling distinction of human nonalcoholic fatty liver disease progression from a common rat model. *Obesity* **25**, 1069–1076 (2017).

178. Lee, G. S., Yan, J. S., Ng, R. K., Kakar, S. & Maher, J. J. Polyunsaturated fat in the methionine-choline-deficient diet influences hepatic inflammation but not hepatocellular injury. *J Lipid Res* **48**, 1885–1896 (2007).

179. Elsner, M., Guldbakke, B., Tiedge, M., Munday, R. & Lenzen, S. Relative importance of transport and alkylation for pancreatic beta-cell toxicity of streptozotocin. *Diabetologia* **43**, 1528–1533 (2000).

180. Weber, L., Boll, M. & Stampfl, A. Hepatoxicity and mechanism of action of haloalkanes: Carbon tetrachloride as a toxicological model. *Clinical Reviews in Toxicology* **33**, 105–136 (2003).

181. Mion, F., Géloën, A., Agosto, E. & Minaire, Y. Carbon tetrachloride-induced cirrhosis in rats: Influence of the acute effects of the toxin on glucose metabolism. *Hepatology* **23**, 582–588 (1996).

182. Suriano, F. *et al.* Novel insights into the genetically obese (ob/ob) and diabetic (db/db) mice: two sides of the same coin. *Microbiome* **9**, (2021).

183. Ritskes-Hoitinga, M., Tobin, G., Jensen, T. L. & Mikkelsen, L. F. Nutrition of the Laboratory Mouse. in *The Laboratory Mouse* 567–599 (Elsevier Ltd, 2012). doi:10.1016/B978-0-12-382008-2.00024-6.

184. Grasso, P., Leinung, M. C., Ingher, S. P. & Lee, D. W. In Vivo Effects of Leptin-Related Synthetic Peptides on Body Weight and Food Intake in Female ob/ob Mice: Localization of Leptin Activity to Domains Between Amino Acid Residues 106-140*. *Endocrinology* **138**, 1413–1418 (1997).

185. Perfield, J. W. *et al.* Altered hepatic lipid metabolism contributes to nonalcoholic fatty liver disease in leptin-deficient Ob/Ob Mice. *J Obes* **2013**, (2013).

186. Halaas, J. L. *et al.* Weight-Reducing Effects of the Plasma Protein Encoded by the obese Gene. *Science (1979)* **269**, 543–546 (1995).

187. Trak-Smayra, V. *et al.* Pathology of the liver in obese and diabetic ob/ob and db/db mice fed a standard or high-calorie diet. *Int J Exp Pathol* **92**, 413–421 (2011).

188. Koizumi I, T., Nikaido I, H., Hay Aka W A I, J., Nonomura, A. & Yoneda, & T. Infantile disease with microvesicular fatty infiltration of viscera spontaneously occurring in the C3H-H-2° strain of mouse with similarities to Reye's syndrome. *Lab Anim* **22**, 83–87 (1988).

189. Kuwajima, M. *et al.* Animal model of systemic carnitine deficiency: analysis in C3H-H-2 degrees strain of mouse associated with juvenile visceral steatosis. *Biochem Biophys Res Commun* **174**, 1090–1094 (1991).

190. Lu, K.-M., Nishimori, H., Nakamura, Y., Shima, K. & Kuwajima, M. A Missense Mutation of Mouse OCTN2, a Sodium-Dependent Carnitine Cotransporter, in the Juvenile Visceral Steatosis Mouse. *Biochem Biophys Res Commun.* **252**, 590–594 (1998).

191. Ibdah, J. A. *et al.* Lack of mitochondrial trifunctional protein in mice causes neonatal hypoglycemia and sudden death. *J. Clin. Invest.* **107**, 1403–1409 (2001).

192. Ibdah, J. A. *et al.* Mice heterozygous for a defect in mitochondrial trifunctional protein develop hepatic steatosis and insulin resistance. *Gastroenterology* **128**, 1381–1390 (2005).

193. Brix, A. E. *et al.* Evaluation of liver fatty acid oxidation in the leptin-deficient obese mouse. *Mol Genet Metab* **75**, 219–226 (2002).

194. Lee, G.-H. *et al.* Abnormal splicing of the leptin receptor in diabetic mice. *Nature* **379**, 632–634 (1996).

195. Coburn, C. T. *et al.* Defective uptake and utilization of long chain fatty acids in muscle and adipose tissues of CD36 knockout mice. *Journal of Biological Chemistry* **275**, 32523–32529 (2000).

196. Goudriaan, J. R. *et al.* CD36 deficiency increases insulin sensitivity in muscle, but induces insulin resistance in the liver in mice. *J Lipid Res* **44**, 2270–2277 (2003).

197. Fisher, C. R., Graves, K. H., Parlow, A. F. & Simpson, E. R. Characterization of mice deficient in aromatase (ArKO) because of targeted disruption of the cyp19 gene. *Proc. Natl. Acad. Sci.* **95**, 6965–6970 (1998).

198. Jones, M. E. E. *et al.* Aromatase-deficient (ArKO) mice have a phenotype of increased adiposity. *PNAS* **97**, 12735–12740 (2000).

199. Ibrahimi, A., Abumrad, N. A. & Abumrad, N. Role of CD36 in membrane transport of long-chain fatty acids. *Curr Opin Clin Nutr Metab Care* **5**, 139–145 (2002).

200. Febbraio, M. *et al.* A null mutation in murine CD36 reveals an important role in fatty acid and lipoprotein metabolism. *J Biol Chem* **274**, 19055–19062 (1999).

201. Wilson, C. G. *et al.* Hepatocyte-specific disruption of CD36 attenuates fatty liver and improves insulin sensitivity in HFD-fed mice. *Endocrinology* **157**, 570–585 (2016).

202. Van Sinderen, M. L. *et al.* Hepatic glucose intolerance precedes hepatic steatosis in the male aromatase knockout (ArKO) mouse. *PLoS One* **9**, (2014).

203. Sahai, A. *et al.* Obese and diabetic db/db mice develop marked liver fibrosis in a model of nonalcoholic steatohepatitis: role of short-form leptin receptors and osteopontin. *Am J Physiol Gastrointest Liver Physiol* **287**, 1035–1043 (2004).

204. Leclercq, I. A., Farrell, G. C., Schriemer, R. & Robertson, G. R. Leptin is essential for the hepatic fibrogenic response to chronic liver injury. *J Hepatol* **37**, 206–213 (2002).

205. Wouters, K. *et al.* Dietary cholesterol, rather than liver steatosis, leads to hepatic inflammation in hyperlipidemic mouse models of nonalcoholic steatohepatitis. *Hepatology* **48**, 474–486 (2008).

206. Bieghs, V. *et al.* Ldl receptor knock-out mice are a physiological model particularly vulnerable to study the onset of inflammation in non-alcoholic fatty liver disease. *PLoS One* **7**, (2012).

207. Kersten, S. *et al.* Peroxisome proliferator-activated receptor α mediates the adaptive response to fasting. *Journal of Clinical Investigation* **103**, 1489–1498 (1999).

208. Goldberg, D. *et al.* Changes in the Prevalence of Hepatitis C Virus Infection, Nonalcoholic Steatohepatitis, and Alcoholic Liver Disease Among Patients With Cirrhosis or Liver Failure on the Waitlist for Liver Transplantation. *Gastroenterology* **152**, 1090-1099.e1 (2017).

209. Sanyal, A. J. *et al.* Pioglitazone, Vitamin E, or Placebo for Nonalcoholic Steatohepatitis. *New England Journal of Medicine* **362**, 1675–1685 (2010).

210. Sato, K. *et al.* Vitamin E has a beneficial effect on nonalcoholic fatty liver disease: A meta-analysis of randomized controlled trials. *Nutrition* **31**, 923–930 (2015).

211. Ji, H. F., Sun, Y. & Shen, L. Effect of vitamin E supplementation on aminotransferase levels in patients with NAFLD, NASH, and CHC: Results from a meta-analysis. *Nutrition* **30**, 986–991 (2014).

212. Miller III, E. R. *et al.* Meta-Analysis: High-Dosage Vitamin E Supplementation May Increase All-Cause Mortality Background: Experimental models and observational studies. *Ann Intern Med.* **142**, 37–46 (2005).

213. Schürks, M., Glynn, R. J., Rist, P. M., Tzourio, C. & Kurth, T. Effects of vitamin E on stroke subtypes: Meta-analysis of randomised controlled trials. *BMJ (Online)* **341**, 1033 (2010).

214. Yang, Y. *et al.* Pioglitazone, a PPARγ agonist, inhibits growth and invasion of human hepatocellular carcinoma via blockade of the rage signaling. *Mol Carcinog* **54**, 1584–1595 (2015).

215. Ciaramella, V. *et al.* Activity and molecular targets of pioglitazone via blockade of proliferation, invasiveness and bioenergetics in human NSCLC. *Journal of Experimental and Clinical Cancer Research* **38**, (2019).

216. Li, S. *et al.* Pioglitazone Reduces Hepatocellular Carcinoma Development in Two Rodent Models of Cirrhosis. *Journal of Gastrointestinal Surgery* **23**, 101–111 (2019).

217. Zhou, G. *et al.* Role of AMP-activated protein kinase in mechanism of metformin action. *Journal of Clinical Investigation* **108**, 1167–1174 (2001).

218. Kazemi, R. *et al.* Metformin in Nonalcoholic Steatohepatitis: A Randomized Controlled Trial. *Middle East J Dig Dis* **4**, 16–22 (2012).

219. Li, Y., Liu, L., Wang, B., Wang, J. & Chen, D. Metformin in non-alcoholic fatty liver disease: A systematic review and meta-analysis. *Biomed Rep* **1**, 57–64 (2013).

220. Dongiovanni, P. *et al.* Statin use and non-alcoholic steatohepatitis in at risk individuals. *J Hepatol* **63**, 705–712 (2015).

221. Kargiotis, K. *et al.* Resolution of non-alcoholic steatohepatitis by rosuvastatin monotherapy in patients with metabolic syndrome. *World J Gastroenterol* **21**, 7860–7868 (2015).

222. Athyros, V. G. *et al.* The use of statins alone, or in combination with pioglitazone and other drugs, for the treatment of non-alcoholic fatty liver disease/non-alcoholic steatohepatitis and related cardiovascular risk. An Expert Panel Statement. *Metabolism* **71**, 17–32 (2017).

223. Miyazaki, M. *et al.* Stearoyl-CoA desaturase-1 deficiency attenuates obesity and insulin resistance in leptin-resistant obese mice. *Biochem Biophys Res Commun* **380**, 818–822 (2009).

224. Liu, X. L. *et al.* MiR-192-5p regulates lipid synthesis in non-Alcoholic fatty liver disease through SCD-1. *World J Gastroenterol* **23**, 8140–8151 (2017).

225. Younossi, Z. M. *et al.* Obeticholic acid for the treatment of non-alcoholic steatohepatitis: interim analysis from a multicentre, randomised, placebo-controlled phase 3 trial. *The Lancet* **394**, 2184–2196 (2019).

226. Watanabe, M. *et al.* Bile acids lower triglyceride levels via a pathway involving FXR, SHP, and SREBP-1c. *Journal of Clinical Investigation* **113**, 1408–1418 (2004).

227. Cusi, K. Treatment of patients with type 2 diabetes and non-alcoholic fatty liver disease: current approaches and future directions. *Diabetologia* **59**, 1112–1120 (2016).

228. Dufort, I., Rheault, P., Huang, X.-F., Soucy, P. & Luu-The, V. Characteristics of a Highly Labile Human Type 5 17-Hydroxysteroid Dehydrogenase. *Endocrinology* **140**, 568–574 (1999).

229. Jörnvall, H., Höög, J. O. & Persson, B. SDR and MDR: Completed genome sequences show these protein families to be large, of old origin, and of complex nature. *FEBS Lett* **445**, 261–264 (1999).

230. Wu, X., Lukacik, P., Kavanagh, K. L. & Oppermann, U. SDR-type human hydroxysteroid dehydrogenases involved in steroid hormone activation. *Mol Cell Endocrinol* **265–266**, 71–76 (2007).

231. Mindnich, R., Möller, G. & Adamski, J. The role of 17 beta-hydroxysteroid dehydrogenases. *Mol Cell Endocrinol* **218**, 7–20 (2004).

232. Suzuki, H., Ozaki, Y., Gen, K. & Kazeto, Y. Japanese eel retinol dehydrogenases 11/12-like are 17-ketosteroid reductases involved in sex steroid synthesis. *Gen Comp Endocrinol* **305**, (2021).

233. Liu, S. *et al.* Molecular cloning and expression analysis of a new gene for short- chain dehydrogenase/reductase 9. *Acta Biochim Pol* **54**, 213–218 (2007).

234. Poutanen, M., Miettinen, M. & Vihkot, R. Differential Estrogen Substrate Specificities for Transiently Expressed Human Placental 17& Hydroxysteroid Dehydrogenase and an Endogenous Enzyme Expressed in Cultured COS-m6 Cells*. *Endocrinology* **133**, 2639–2644 (1993).

235. Poutanen, M., Isomaa, V., Peltoketo, H. & Vihko, R. Role of 17fl-Hydroxysteroid Dehydrogenase Type 1 in Endocrine and Intracrine Estradiol Biosynthesis. *J. Steroid Biochem. 3dolec. Biol* **55**, 525–532 (1995).

236. Huhtinen, K., Ståhle, M., Perheentupa, A. & Poutanen, M. Estrogen biosynthesis and signaling in endometriosis. *Mol Cell Endocrinol* **358**, 146–154 (2012).

237. Wu, L. *et al.* Expression Cloning and Characterization of Human 178-Hydroxysteroid Dehydrogenase Type 2, a Microsomal Enzyme Possessing 20a-Hydroxysteroid Dehydrogenase Activity*. *J Biol Chem* **268**, 12964–12969 (1993).

238. Geissler, W. M. *et al.* Male pseudohermaphroditism caused by mutations of testicular 17b-hydroxysteroid dehydrogenase 3. *Nat Genet* **7**, 34–39 (1994).

239. O'shaughnessy, P. J. *et al.* Localization of 17-Hydroxysteroid Dehydrogenase/17-Ketosteroid Reductase Isoform Expression in the Developing Mouse Testis-Androstenedione Is the Major Androgen Secreted by Fetal/Neonatal Leydig Cells*. *Endocrinology* **141**, 2631–2637 (2000).

240. Biswas, M. G. & Russell, D. W. Expression Cloning and Characterization of Oxidative 17b-and 3a-Hydroxysteroid Dehydrogenases from Rat and Human Prostate. *J Biol Chem* **272**, 15959–15966 (1997).

241. Breitling, R., Marijanović, Z., Perović, D. & Adamski, J. Evolution of 17beta-HSD type 4, a multifunctional protein of beta-oxidation. *Mol Cell Endocrinol* **171**, 205–10 (2001).

242. Jokela, H. *et al.* Hydroxysteroid (17β) dehydrogenase 7 activity is essential for fetal de novo cholesterol synthesis and for neuroectodermal survival and cardiovascular differentiation in early mouse embryos. *Endocrinology* **151**, 1884–1892 (2010).

243. Chen, Z. *et al.* 17β-Hydroxysteroid dehydrogenase type 8 and carbonyl reductase type 4 assemble as a ketoacyl reductase of human mitochondrial FAS. *The FASEB Journal* **23**, 3682–3691 (2009).

244. Venkatesan, R. *et al.* Insights into mitochondrial fatty acid synthesis from the structure of heterotetrameric 3-ketoacyl-ACP reductase/3R-hydroxyacyl-CoA dehydrogenase. *Nat Commun* **5**, (2014).

245. He, X., Merz, G., Mehta, P., Schulz, H. & Yang, S. Human Brain Short Chain L -3-Hydroxyacyl Coenzyme A Dehydrogenase Is a Single-domain Multifunctional Enzyme. *Biochemistry* **274**, 15014–15019 (1999).

246. Shafqat, N. *et al.* Expanded substrate screenings of human and Drosophila type 10 17β-hydroxysteroid dehydrogenases (HSDs) reveal multiple specificities in bile acid and steroid hormone metabolism: characterization of multifunctional 3α/7α/7β/17β/20β/21-HSD. *Biochem. J* **376**, 49–60 (2003).

247. Horiguchi, Y., Araki, M. & Motojima, K. Identification and characterization of the ER/lipid droplet-targeting sequence in 17β-hydroxysteroid dehydrogenase type 11. *Arch Biochem Biophys* **479**, 121–130 (2008).

248. Brereton, P. *et al.* Pan1b (17bHSD11)-enzymatic activity and distribution in the lung. *Mol Cell Endocrinol* **171**, 111–117 (2001).

249. Chai, Z. *et al.* 17β-hydroxysteroid dehydrogenase type XI localizes to human steroidogenic cells. *Endocrinology* **114**, 2084–2091 (2003).

250. Nagasaki, S. *et al.* 17 -Hydroxysteroid Dehydrogenase Type 12 in Human Breast Carcinoma: A Prognostic Factor via Potential Regulation of Fatty Acid Synthesis. *Cancer Res* **69**, 1392–1399 (2009).

251. Visus, C. *et al.* Identification of Hydroxysteroid (17β) dehydrogenase type 12 (HSD17B12) as a CD8+ T-cell-defined human tumor antigen of human carcinomas. *Cancer Immunol Immunother* **60**, 919–29 (2011).

252. Kemiläinen, H. *et al.* The Expression of HSD17B12 Is Associated with COX-2 Expression and Is Increased in High-Grade Epithelial Ovarian Cancer. *Oncology* **94**, 233–242 (2018).

253. Rantakari, P. *et al.* Hydroxysteroid (17β) dehydrogenase 12 is essential for mouse organogenesis and embryonic survival. *Endocrinology* **151**, 1893–1901 (2010).

254. Bellemare, V., Laberge, P., Noël, S., Tchernof, A. & Luu-The, V. Differential estrogenic 17β-hydroxysteroid dehydrogenase activity and type 12 17β-hydroxysteroid dehydrogenase expression levels in preadipocytes and differentiated adipocytes. *Journal of Steroid Biochemistry and Molecular Biology* **114**, 129–134 (2009).

255. Nagasaki, S., Miki, Y., Akahira, J., Suzuki, T. & Sasano, H. Transcriptional regulation of 17beta-hydroxysteroid dehydrogenase type 12 by SREBP-1. *Mol Cell Endocrinol* **307**, 163–8 (2009).

256. Das, S. K. & Sharma, N. K. Expression quantitative trait analyses to identify causal genetic variants for type 2 diabetes susceptibility. *World J Diabetes* **5**, 97 (2014).

257. Scott, R. A. *et al.* An Expanded Genome-Wide Association Study of Type 2 Diabetes in Europeans. *Diabetes* **66**, 2888–2902 (2017).

258. Hachim, M. Y. *et al.* An integrative phenotype–genotype approach using phenotypic characteristics from the UAE national diabetes study identifies HSD17B12 as a candidate gene for obesity and type 2 diabetes. *Genes (Basel)* **11**, (2020).

259. Locke, A. E. *et al.* Genetic studies of body mass index yield new insights for obesity biology. *Nature* **518**, 197–206 (2015).

260. Dai, W. *et al.* Genetic variants in ELOVL2 and HSD17B12 predict melanoma-specific survival. *Int J Cancer* **145**, 2619–2628 (2019).

261. Capasso, M. *et al.* Common genetic variants in NEFL influence gene expression and Neuroblastoma risk. *Cancer Res* **74**, 6913–6924 (2014).

262. Mohamed, B. *et al.* Very-long-chain fatty acid metabolic capacity of 17-beta-hydroxysteroid dehydrogenase type 12 (HSD17B12) promotes replication of hepatitis C virus and related flaviviruses. *Sci Rep* **10**, (2020).

263. Ichida, H. *et al.* Identification of HSD17B12 as an enzyme catalyzing drug reduction reactions through investigation of nabumetone metabolism. *Arch Biochem Biophys* **736**, (2023).

264. Su, W. *et al.* Comparative proteomic study reveals 17 -HSD13 as a pathogenic protein in nonalcoholic fatty liver disease. *Proceedings of the National Academy of Sciences* **111**, 11437–11442 (2014).

265. Ma, Y. *et al.* 17-Beta Hydroxysteroid Dehydrogenase 13 Is a Hepatic Retinol Dehydrogenase Associated With Histological Features of Nonalcoholic Fatty Liver Disease. *Hepatology* **69**, 1504–1519 (2019).

266. Horiguchi, Y., Araki, M. & Motojima, K. 17β-Hydroxysteroid dehydrogenase type 13 is a liver-specific lipid droplet-associated protein. *Biochem Biophys Res Commun* **370**, 235–238 (2008).

267. Horiguchi, Y., Araki, M. & Motojima, K. 17β-Hydroxysteroid dehydrogenase type 13 is a liver-specific lipid droplet-associated protein. *Biochem Biophys Res Commun* **370**, 235–238 (2008).

268. Rotinen, M., Villar, J., Celay, J. & Encío, I. Type 10 17β-hydroxysteroid dehydrogenase expression is regulated by C/EBPβ in HepG2 cells. *Journal of Steroid Biochemistry and Molecular Biology* **122**, 164–171 (2010).

269. Su, W. *et al.* Liver X receptor α induces 17B-hydroxysteroid dehydrogenase-13 expression through SREBP-1c..pdf. *Am J Physiol Endocrinol Metab* **312**, E357–E367 (2017).

270. Moe, M. *et al.* Gene expression profiles in liver of pigs with extreme high and low levels of androstenone. *BMC Vet Res* **4**, 29 (2008).

271. Rotroff, D. M. *et al.* Genetic Variants in HSD17B3, SMAD3, and IPO11 Impact Circulating Lipids in Response to Fenofibrate in Individuals With Type 2 Diabetes. *Clin Pharmacol Ther* **103**, 712–721 (2018).

272. Liu, S. & Wang, Y. Crystal structures of 17-beta-hydroxysteroid dehydrogenase 13. *Nature Portfolio* (2023) doi:10.21203/rs.3.rs-2688507/v1.

273. Aslan, M., Özcan, F., Tuzcu, H., Kiraç, E. & Elpek, G. O. Inhibition of neutral sphingomyelinase decreases arachidonic acid mediated inflammation in liver ischemia-reperfusion injury. *Int J Clin Exp Pathol* **7**, 7814–7823 (2014).

274. Maciejewska, D. *et al.* Metabolites of arachidonic acid and linoleic acid in early stages of non-alcoholic fatty liver disease—A pilot study. *Prostaglandins Other Lipid Mediat* **121**, 184–189 (2015).

275. Cranmer-Byng, M. M., Liddle, D. M., De Boer, A. A., Monk, J. M. & Robinson, L. E. Proinflammatory effects of arachidonic acid in a lipopolysaccharide-induced inflammatory microenvironment in 3T3-L1 adipocytes in vitro. *Applied Physiology, Nutrition, and Metabolism* **40**, 142–154 (2015).

276. Vaidya, H. & Cheema, S. K. Arachidonic acid has a dominant effect to regulate lipogenic genes in 3T3-L1 adipocytes compared to omega-3 fatty acids. *Food Nutr Res* **59**, 1–6 (2015).

277. Luukkonen, P. K. *et al.* Inhibition of HSD17B13 protects against liver fibrosis by inhibition of pyrimidine catabolism in nonalcoholic steatohepatitis. *Proc Natl Acad Sci U S A* **120**, (2023).

278. Ma, Y. *et al.* 17-Beta Hydroxysteroid Dehydrogenase 13 Deficiency Does Not Protect Mice From Obesogenic Diet Injury. *Hepatology* **73**, 1701–1716 (2021).

279. Pirola, C. J. *et al.* Splice variant rs72613567 prevents worst histologic outcomes in patients with nonalcoholic fatty liver disease Running title: NASH and HSD17B13. *J Lipid Res* **60**, 176–185 (2018).

280. Ting, Y. W. *et al.* Loss-of-function hsd17b13 variants, non-alcoholic steatohepatitis and adverse liver outcomes: Results from a multi-ethnic asian cohort. *Clin Mol Hepatol* **27**, (2021).

281. Tsachaki, M. *et al.* Impact of 17β-HSD12, the 3-ketoacyl-CoA reductase of long-chain fatty acid synthesis, on breast cancer cell proliferation and migration. *Cellular and Molecular Life Sciences* **77**, 1153–1175 (2020).

282. Szajnik, M. *et al.* 17β hydroxysteroid dehydrogenase type 12 (HSD17B12) is a marker of poor prognosis in ovarian carcinoma. *Gynecol Oncol* **127**, 587–594 (2012).

283. Moon, Y. A. Emerging roles of polyunsaturated fatty acid synthesis pathway in colorectal cancer. *Anim Cells Syst (Seoul)* **27**, 61–71 (2023).

284. Wang, M. *et al.* Down-Regulating the High Level of 17-Beta-Hydroxysteroid Dehydrogenase 13 Plays a Therapeutic Role for Non-Alcoholic Fatty Liver Disease. *Int J Mol Sci* **23**, (2022).

285. Motomura, T. *et al.* Is hsd17b13 genetic variant a protector for liver dysfunction? Future perspective as a potential therapeutic target. *J Pers Med* **11**, (2021).

286. Postic, C. *et al.* Dual roles for glucokinase in glucose homeostasis as determined by lver and pancreatic b cell-specific gene knock-outs using crer recombinase. *Journal of Biological Chemistry* **274**, 305–315 (1999).

287. Mukarami T *et al.* Prealbumin gene expression during mouse development studied by in situ hybridization. *Cell differentiation and development* **22**, 1–9 (1987).

288. Weisend, C. M., Kundert, J. A., Suvorova, E. S., Prigge, J. R. & Schmidt, E. E. Cre activity in fetal albCre mouse hepatocytes: Utility for developmental studies. *Genesis* **47**, 789–92 (2009).

289. Postic, C. & Magnuson, M. A. DNA excision in liver by an albumin-Cre transgene occurs progressively with age. *Genesis* **26**, 149–150 (2000).

290. Bankhead, P. *et al.* QuPath: Open source software for digital pathology image analysis. *Sci Rep* **7**, 1–7 (2017).

291. Zhi, X. *et al.* AdipoCount: A new software for automatic adipocyte counting. *Front Physiol* **9**, (2018).

292. Mairinoja, L. *et al.* Deep learning based image analysis of liver steatosis in mouse models. *Am J Pathol* **193**, 1072–1080 (2023).

293. Kim, D. *et al.* TopHat2: accurate alignment of transcriptomes in the presence of insertions, deletions and gene fusions. *Genome Biol* **14**, R36 (2013).

294. Anders, S., Pyl, P. T. & Huber, W. HTSeq-A Python framework to work with high-throughput sequencing data. *Bioinformatics* **31**, 166–169 (2015).

295. R Development Core Team. R: A Language and Environment for Statistical Computing. *R Foundation for Statistical Computing* Preprint at https://www.r-project.org/. (2016).

296. Gentleman, R. C. *et al.* Bioconductor: open software development for computational biology and bioinformatics. *Genome Biol* **5**, R80 (2004).
297. Robinson, M. D., Mccarthy, D. J. & Smyth, G. K. edgeR: a Bioconductor package for differential expression analysis of digital gene expression data. *Bioinformatics* **26**, 139–40 (2010).
298. Ritchie, M. E. *et al.* limma powers differential expression analyses for RNA-sequencing and microarray studies. *Nucleic Acids Res* **43**, e47 (2015).
299. Andrews, S. FastQC: a quality control tool for high throughput sequence data. *http://www.bioinformatics.babraham.ac.uk/projects/fastqc.* (2019).
300. Liao, Y., Smyth, G. K. & Shi, W. The R package Rsubread is easier, faster, cheaper and better for alignment and quantification of RNA sequencing reads. *Nucleic Acids Res* **47**, (2019).
301. Suomi, T., Seyednasrollah, F., Jaakkola, M. K., Faux, T. & Elo, L. L. ROTS: An R package for reproducibility-optimized statistical testing. *PLoS Comput Biol* **13**, (2017).
302. Gaiser, R. A. *et al.* Integrated targeted metabolomic and lipidomic analysis: A novel approach to classifying early cystic precursors to invasive pancreatic cancer. *Sci Rep* **9**, 1–12 (2019).
303. Chong, J. *et al.* MetaboAnalyst 4.0: Towards more transparent and integrative metabolomics analysis. *Nucleic Acids Res* **46**, W486–W494 (2018).
304. Stekhoven, D. J. & Bühlmann, P. Missforest-Non-parametric missing value imputation for mixed-type data. *Bioinformatics* **28**, 112–118 (2012).
305. Folch, J., Lees, M. & Sloane Stanley, G. H. A simple method for the isolation and purification of total lipides from animal tissues. *J Biol Chem* **226**, 497–509 (1957).
306. Haavisto, A. M. *et al.* A supersensitive immunofluorometric assay for rat luteinizing hormone. *Endocrinology* **132**, 1687–1691 (1993).
307. Van Casteren, J. I. J., Schoonen, W. G. E. J. & Kloosterboer, H. J. Development of Time-Resolved Immunofluorometric Assays for Rat Follicle- Stimulating Hormone and Luteinizing Hormone and Application on Sera of Cycling Rats. *Biol Reprod* **62**, 886–894 (2000).
308. Zhang, H. B., Su, W., Xu, H., Zhang, X. Y. & Guan, Y. F. HSD17B13: A Potential Therapeutic Target for NAFLD. *Front Mol Biosci* **8**, (2022).
309. Ma, Y. *et al.* Characterization of essential domains in HSD17B13 for cellular localization and enzymatic activity. *J Lipid Res* **61**, 1400–1409 (2020).
310. Vvedenskaya, O. *et al.* Nonalcoholic fatty liver disease stratification by liver lipidomics. *J Lipid Res* **62**, (2021).
311. Ma, S. *et al.* Thyrotropin and Obesity: Increased Adipose Triglyceride Content Through Glycerol-3-Phosphate Acyltransferase 3. *Sci Rep* **5**, 7633 (2015).
312. Khatun, I. *et al.* Characterization of a novel intestinal glycerol-3-phosphate acyltransferase pathway and its role in lipid homeostasis. *Journal of Biological Chemistry* **291**, 2602–2615 (2016).
313. Cao, J. *et al.* Mice deleted for GPAT3 have reduced GPAT activity in white adipose tissue and altered energy and cholesterol homeostasis in diet-induced obesity. *Am J Physiol Endocrinol Metab* **306**, E1176-87 (2014).
314. Beigneux, A. P. *et al.* Agpat6 - A novel lipid biosynthetic gene required for triacylglycerol production in mammary epithelium. *J Lipid Res* **47**, 734–744 (2006).
315. Wilfling, F. *et al.* Triacylglycerol Synthesis Enzymes Mediate Lipid DropletGrowth by Relocalizing from the ER to Lipid Droplets. *Dev Cell* **24**, 384–399 (2013).
316. Cao, J., Li, J.-L., Li, D., Tobin, J. F. & Gimeno, R. E. Molecular identification of microsomal acyl-CoA:glycerol-3-phosphate acyltransferase, a key enzyme in de novo triacylglycerol synthesis. *Proceedings of the National Academy of Sciences* **103**, 19695–19700 (2006).
317. Fan, G. *et al.* GPAT3 regulates the synthesis of lipid intermediate LPA and exacerbates Kupffer cell inflammation mediated by the ERK signaling pathway. *Cell Death Dis* **14**, (2023).
318. Strable, M. S. & Ntambi, J. M. Genetic control of de novo lipogenesis: role in diet-induced obesity. *Crit Rev Biochem Mol Biol* **45**, 199–214 (2010).

319. Roman, L. *et al.* Expression of rabbit cytochromes P4504A which catalyze the omega-hydroxylation of arachidonic acid, fatty acids, and prostaglandins. *Arch Biochem Biophys* **307**, 57–65 (1993).

320. Capdevila, J. H. & Falck, J. R. Biochemical and molecular properties of the cytochrome P450 arachidonic acid monooxygenases. *Prostaglandins Other Lipid Mediat* **68–69**, 325–344 (2002).

321. Luo, G., Zeldin, D. C., Blaisdell, J. A., Hodgson, E. & Goldstein, J. A. Cloning and Expression of Murine CYP2Cs and Their Ability to Metabolize Arachidonic Acid 1. *Arch Biochem Biophys* **357**, 45–57 (1998).

322. Imig, J. D. Epoxyeicosatrienoic acids, 20-hydroxyeicosatetraenoic acid, and renal microvascular function. *Prostaglandins Other Lipid Mediat* **104–105**, 2–7 (2013).

323. Node, K. *et al.* Anti-inflammatory Properties of Cytochrome P450 Epoxygenase-Derived Eicosanoids. *Science (1979)* **285**, 1276–1279 (1999).

324. Zhang, Y. *et al.* EET homologs potently dilate coronary microvessels and activate BKCa channels. *Am J Physiol Heart Circ Physiol* **280**, 2430–2440 (2001).

325. Arvind, A., Osganian, S. A., Sjoquist, J. A., Corey, K. E. & Simon, T. G. Epoxygenase-Derived Epoxyeicosatrienoic Acid Mediators Are Associated With Nonalcoholic Fatty Liver Disease, Nonalcoholic Steatohepatitis, and Fibrosis. *Gastroenterology* **159**, 2232-2234.e4 (2020).

326. Lin, F. *et al.* 20-Hydroxyeicosatetraenoic acid is formed in response to EGF and is a mitogen in rat proximal tubule. *Am J Physiol* **269**, F806-816 (1995).

327. Li, X. *et al.* Integrative lipidomic and transcriptomic study unravels the therapeutic effects of saikosaponins A and D on non-alcoholic fatty liver disease. *Acta Pharm Sin B* **11**, 3527–3541 (2021).

328. Scapa, E. F. *et al.* Regulation of energy substrate utilization and hepatic insulin sensitivity by phosphatidylcholine transfer protein/StarD2. *The FASEB Journal* **22**, 2579–2590 (2008).

329. Kang, H. W. *et al.* Mice lacking Pctp/StarD2 exhibit increased adaptive thermogenesis and enlarged mitochondria in brown adipose tissue. *J Lipid Res* **50**, 2212–2221 (2009).

330. Druzak, S. A. *et al.* Ligand dependent interaction between PC-TP and PPARδ mitigates diet-induced hepatic steatosis in male mice. *Nat Commun* **14**, (2023).

331. Khalil, Y. *et al.* Tissue Proteome of 2-Hydroxyacyl-CoA Lyase Deficient Mice Reveals Peroxisome Proliferation and Activation of ω-Oxidation. *Int J Mol Sci* **23**, (2022).

332. Talley, J. & Mohiuddin, S. *Biochemistry, Fatty Acid Oxidation. StatPearls [Internet]* (StatPearls Publishing, 2023).

333. Longo, N., Frigeni, M. & Pasquali, M. Carnitine transport and fatty acid oxidation. *Biochim Biophys Acta Mol Cell Res* **1863**, 2422–2435 (2016).

334. Naguib, G. *et al.* Dietary fatty acid oxidation is decreased in non-alcoholic fatty liver disease: A palmitate breath test study. *Liver International* **40**, 590–597 (2020).

335. Wang, H. *et al.* Cardiomyocyte-specific perilipin 5 overexpression leads to myocardial steatosis and modest cardiac dysfunction. *J Lipid Res* **54**, 953–965 (2013).

336. Tarnopolsky, M. A. *et al.* Influence of endurance exercise training and sex on intramyocellular lipid and mitochondrial ultrastructure, substrate use, and mitochondrial enzyme activity. *Am J Physiol Regul Integr Comp Physiol* **292**, 1271–1278 (2007).

337. Benador, I. Y. *et al.* Mitochondria Bound to Lipid Droplets Have Unique Bioenergetics, Composition, and Dynamics that Support Lipid Droplet Expansion. *Cell Metab* **27**, 869-885.e6 (2018).

338. Boutant, M. *et al.* Mfn2 is critical for brown adipose tissue thermogenic function. *EMBO J* **36**, 1543–1558 (2017).

339. Wang, H. *et al.* Unique regulation of adipose triglyceride lipase (ATGL) by perilipin 5, a lipid droplet-associated protein. *Journal of Biological Chemistry* **286**, 15707–15715 (2011).

340. Gemmink, A. *et al.* Super-resolution microscopy localizes perilipin 5 at lipid droplet-mitochondria interaction sites and at lipid droplets juxtaposing to perilipin 2. *Biochim Biophys Acta Mol Cell Biol Lipids* **1863**, 1423–1432 (2018).

341. Pu, J. *et al.* Interactomic study on interaction between lipid droplets and mitochondria. *Protein Cell* **2**, 487–496 (2011).

342. Nian, Z. *et al.* Fat-specific protein 27 undergoes ubiquitin-dependent degradation regulated by triacylglycerol synthesis and lipid droplet formation. *Journal of Biological Chemistry* **285**, 9604–9615 (2010).

343. Lyu, X. *et al.* A gel-like condensation of Cidec generates lipid-permeable plates for lipid droplet fusion. *Dev Cell* **56**, 2592-2606.e7 (2021).

344. Matsusue, K. *et al.* Hepatic Steatosis in Leptin-Deficient Mice Is Promoted by the PPARγ Target Gene Fsp27. *Cell Metab* **7**, 302–311 (2008).

345. Aibara, D. *et al.* Expression of Hepatic Fat-Specific Protein 27 Depends on the Specific Etiology of Fatty Liver. *Biol. Pharm. Bull* **36**, 1766–1772 (2013).

346. Xu, X., Jiang, M., Zhang, Y., Bi, Y. & Han, M. Celecoxib attenuates cachectic events in mice by modulating the expression of vascular endothelial growth factor. *Mol Med Rep* **11**, 289–294 (2015).

347. Xu, W. *et al.* Differential roles of cell death-inducing DNA fragmentation factor-α-like effector (CIDE) proteins in promoting lipid droplet fusion and growth in subpopulations of hepatocytes. *Journal of Biological Chemistry* **291**, 4282–4293 (2016).

348. Nishimoto, Y. & Tamori, Y. CIDE family-mediated unique lipid droplet morphology in white adipose tissue and brown adipose tissue determines the adipocyte energy metabolism. *J Atheroscler Thromb* **24**, 989–998 (2017).

349. Liu, P. *et al.* Chinese Hamster Ovary K2 Cell Lipid Droplets Appear to be Metabolic Organelles Involved in Membrane Traffic. *Journal of Biological Chemistry* **279**, 3787–3792 (2004).

350. Rajendran, L., Le Lay, S. & Illges, H. Raft association and lipid droplet targeting of flotillins are independent of caveolin. *Biol Chem* **388**, 307–314 (2007).

351. Sadh, K., Rai, P. & Mallik, R. Feeding-fasting dependent recruitment of membrane microdomain proteins to lipid droplets purified from the liver. *PLoS One* **12**, (2017).

352. Jägerström, S. *et al.* Lipid droplets interact with mitochondria using SNAP23. *Cell Biol Int* **33**, 934–940 (2009).

353. Boström, P. *et al.* SNARE proteins mediate fusion between cytosolic lipid droplets and are implicated in insulin sensitivity. *Nat Cell Biol* **9**, 1286–1293 (2007).

354. Imhof, A. *et al.* Prevalence of non-alcoholic fatty liver and characteristics in overweight adolescents in the general population. *Eur J Epidemiol* **22**, 889–897 (2007).

355. Lonardo, A. *et al.* Sex Differences in Nonalcoholic Fatty Liver Disease: State of the Art and Identification of Research Gaps. *Hepatology* **70**, 1457–1469 (2019).

356. Long, M. T. *et al.* A simple clinical model predicts incident hepatic steatosis in a community-based cohort: The Framingham Heart Study. *Liver International* **38**, 1495–1503 (2018).

357. Yatsuji, S., Hashimoto, E., Tobari, M., Tokushige, K. & Shiratori, K. Influence of age and gender in Japanese patients with non-alcoholic steatohepatitis. *Hepatology Research* **37**, 1034–1043 (2007).

358. Hart-Unger, S. *et al.* Hormone signaling and fatty liver in females: Analysis of estrogen receptor α mutant mice. *Int J Obes* **41**, 945–954 (2017).

359. Codes, L. *et al.* Liver fibrosis in women with chronic hepatitis C: Evidence for the negative role of the menopause and steatosis and the potential benefit of hormone replacement therapy. *Gut* **56**, 390–395 (2007).

360. Di Martino, V. *et al.* Progression of liver fibrosis in women infected with hepatitis C: Long-term benefit of estrogen exposure. *Hepatology* **40**, 1426–1433 (2004).

361. Miller, M. A. Gender-Based Differences in the Toxicity of Pharmaceuticals-The Food and Drug Administration's Perspective. *Int J Toxicol* **20**, 149–152 (2001).

362. Ostapowicz, G. *et al.* Results of a Prospective Study of Acute Liver Failure at 17 Tertiary Care Centers in the United States. *Ann Intern Med* **137**, 947–954 (2002).

363. Wahlang, B. Sex Differences in Toxicant-Associated Fatty Liver Disease. *J Endocrinol* **258**, e220247 (2023).

364. Xu, R., Pan, J., Zhou, W., Ji, G. & Dang, Y. Recent advances in lean NAFLD. *Biomedicine and Pharmacotherapy* **153**, 113331 (2022).

365. Lu, F. Bin *et al.* Global epidemiology of lean non-alcoholic fatty liver disease: A systematic review and meta-analysis. *Journal of Gastroenterology and Hepatology (Australia)* **35**, 2041–2050 (2020).

366. Fan, J.-G., Kim, S.-U. & Wai-Sun Wong, V. New trends on obesity and NAFLD in Asia. *J Hepatol* **67**, 862–873 (2017).

367. Minehira, K. *et al.* Blocking VLDL secretion causes hepatic steatosis but does not affect peripheral lipid stores or insulin sensitivity in mice. *J Lipid Res* **49**, 2038–2044 (2008).

368. Björkegren, J., Beigneux, A., Bergo, M. O., Maher, J. J. & Young, S. G. Blocking the secretion of hepatic very low density lipoproteins renders the liver more susceptible to toxin-induced injury. *Journal of Biological Chemistry* **277**, 5476–5483 (2002).

369. Jiang, M., Li, C., Liu, Q., Wang, A. & Lei, M. Inhibiting ceramide synthesis attenuates hepatic steatosis and fibrosis in rats with non-alcoholic fatty liver disease. *Front Endocrinol (Lausanne)* **10**, (2019).

370. Puri, P. *et al.* A lipidomic analysis of nonalcoholic fatty liver disease. *Hepatology* **46**, 1081–1090 (2007).

371. Young, E. J., Hasanjani Roushan, M. R., Shafae, S., Genta, R. M. & Taylor, S. L. Liver histology of acute brucellosis caused by Brucella melitensis. *Hum Pathol* **45**, 2023–2028 (2014).

372. Huang, J., Lin, S., Wang, M., Wan, B. & Zhu, Y. Syphilitic hepatitis: A case report and review of the literature. *BMC Gastroenterol* **19**, (2019).

373. Smith, S. L. *et al.* Liver Biopsy Histopathology for Diagnosis of Johne's Disease in Sheep. *Vet Pathol* **51**, 915–918 (2014).

374. Firriolo, J. M. *et al.* Comparative 90-Day Feeding Study with Low-Viscosity White Mineral Oil in Fischer-344 and Sprague-Dawley-Derived CRL:CD Rats*. *Toxicol Pathol* **23**, 26–33 (1995).

375. Lamps, L. W. Hepatic granulomas: A review with emphasis on infectious causes. *Arch Pathol Lab Med* **139**, 867–875 (2015).

376. Lee, K. *et al.* A scoring system for the diagnosis of non-alcoholic steatohepatitis from liver biopsy. *J Pathol Transl Med* **54**, 228–236 (2020).

377. Kany, S., Vollrath, J. T. & Relja, B. Cytokines in inflammatory disease. *Int J Mol Sci* **20**, 6008 (2019).

378. Han, J., Meng, Q., Shen, L. & Wu, G. Interleukin-6 induces fat loss in cancer cachexia by promoting white adipose tissue lipolysis and browning. *Lipids Health Dis* **17**, 1–8 (2018).

379. Scott, H. R., McMillan, D. C., Crilly, A., McArdle, C. S. & Milroy, R. The relationship between weight loss and interleukin 6 in non-small-cell lung cancer. *Br J Cancer* **73**, 1560–1562 (1996).

380. Yao, X. *et al.* Targeting interleukin-6 in inflammatory autoimmune diseases and cancers. *Pharmacol Ther* **141**, 125–139 (2014).

381. Kuwabara, T., Ishikawa, F., Kondo, M. & Kakiuchi, T. The Role of IL-17 and Related Cytokines in Inflammatory Autoimmune Diseases. *Mediators Inflamm* **2017**, (2017).

382. Haimovitz-Friedman, A., Kolesnick, R. N. & Fuks, Z. Ceramide signaling in apoptosis. *Br Med Bull* **53**, 539–553 (1997).

383. Memon, R. A. *et al.* Endotoxin and Cytokines Increase Hepatic Sphingolipid Biosynthesis and Produce Lipoproteins Enriched in Ceramides and Sphingomyelin. *Medical and Dermatology Services* **18**, 1257 (1998).

384. De Mello, V. D. F. *et al.* Link between plasma ceramides, inflammation and insulin resistance: Association with serum IL-6 concentration in patients with coronary heart disease. *Diabetologia* **52**, 2612–2615 (2009).

385. Ichi, I., Nakahara, K., Fujii, K., Miyashita, Y. & Kojo, S. Increase of Ceramide in the Liver and Plasma after Carbon Tetrachloride Intoxication in the Rat. *J Nutr Sci Vitaminol* **53**, 53–56 (2007).

386. Chang, Z.-Q. *et al.* Endotoxin activates de novo sphingolipid biosynthesis via nuclear factor kappa B-mediated upregulation of Sptlc2. *Prostaglandins Other Lipid Mediat.* **94**, 44–52 (2011).
387. Ma, J. *et al.* Staphylococcus aureus α-Toxin Induces Inflammatory Cytokines via Lysosomal Acid Sphingomyelinase and Ceramides. *Cellular Physiology and Biochemistry* **43**, 2170–2184 (2017).
388. Dayong, W., Marko, M., Claycombe, K., Paulson, K. E. & Meydani, S. N. Ceramide-induced and age-associated increase in macrophage COX-2 expression is mediated through up-regulation of NF-κB activity. *Journal of Biological Chemistry* **278**, 10983–10992 (2003).

TURUN
YLIOPISTO
UNIVERSITY
OF TURKU